Tumor suppressor p16^{INK4a} and its potential regulator JunB in cytokine-induced senescence

Dissertation

der Mathematisch-Naturwissenschaftlichen Fakultät

der Eberhard Karls Universität Tübingen

zur Erlangung des Grades eines

Doktors der Naturwissenschaften

(Dr. rer. nat.)

vorgelegt von

M.Sc. Nadine Maria Simon

aus Neuwied

Tübingen

2020

Gedruckt mit Genehmigung der Mathematisch-Naturwissenschaftlichen Fakultät der Eberhard Karls Universität Tübingen.

Tag der mündlichen Qualifikation:	30.11.2020
Stellvertretender Dekan:	Prof. Dr. József Fortágh
1. Berichterstatter:	Prof. Dr. Hans-Georg Rammensee
2. Berichterstatter:	Prof. Dr. Jürgen Bauer

Abstract

In this work, the effect of cytokine-induced senescence (CIS) on genetic integrity and the way signal transduction of CIS occurs at the molecular level was studied. In the first part, the question was addressed whether the initiation of CIS leads to changes in chromosomal aberrations which might increase the malignancy of tumor cells.

Therefore, different murine RIP1-Tag2 (RT2) and RIP1-Tag2 x signal transducer and activator of transcription $1^{-/-}$ (RT2xStat$1^{-/-}$) cancer cell lines were treated with the $CD4^{+}$ T-helper cell 1 (T_h1) cytokines interferon gamma (IFNγ) and tumor necrosis factor (TNF) and it was investigated whether the chromosomal aberrations of the tumor cell lines were changed by this treatment. For this purpose, the genetic material of these cells was examined before starting the experiment, and after 96 h treatment with medium or T_h1 cytokines using array comparative genomic hybridization (CGH). The results of the experiments show that primary RT2 cancer cell lines are a heterogeneous population. If an equilibrium between the subpopulations has already been established at the time of the investigation, T_h1 cytokine treatment does not alter chromosomal aberrations. This applies to both RT2 and RT2xStat$1^{-/-}$ cancer cell lines. However, if the equilibrium has not been established at the time of the experiment, changes in chromosomal aberrations may occur after CIS induction. This phenomenon appeared in RT2 cancer cell line 3, which resulted in a specific selection of chromosome 4 and, respectively, cyclin-dependent kinase inhibitor 2A (Cdkn2a) loss subpopulation. An *in vivo* transfer of this cell line (referred to as mouse subcutaneous cell line (mSc)) with subsequent immune checkpoint blockade (ICB) treatment showed that these cells can no longer respond to ICB. A subsequent CGH analysis of the different mSc revealed that the cells have a selective Cdkn2a loss. A subsequent *in vitro* T_h1 cytokine treatment proved that the cells could no longer respond to CIS. In summary, it was demonstrated that the treatment with the T_h1 cytokines could alter the selection of chromosomal aberrations within a heterogeneous cell population. Moreover, it was shown that the absence of Cdkn2a prevents CIS induction.

The induction of CIS is particularly interesting as a potential treatment option for inaccessible or metastasized cancers, as it leads to cyclin-dependent kinase inhibitor 2A ($p16^{INK4a}$)-dependent growth arrest. Since TNF cannot be administered systemically due to its cytotoxic effect, identification of the signaling pathway is crucial to induce TNF-independent activation of the TNF signaling pathway. Therefore, it was investigated how $p16^{INK4a}$ expression is induced after IFNγ and TNF stimulation. A possible candidate for signal transduction is the activator protein 1 (AP-1) transcription factor

JunB proto-oncogene (JunB). As shown in the experiments, JunB expression is induced in CIS. This JunB expression is TNF-dependent. Further investigations showed that the TNF-dependent induction of JunB expression is mediated by nuclear factor kappa-light-chain-enhancer of activated B-cells (NF-κB). Different techniques were used to downregulate or knockout JunB. According to the hypothesis, this would lead to a reduced $p16^{INK4a}$ expression, which prevents the induction of CIS. Despite a reduced JunB expression, none of the approaches could prevent the induction of CIS. It remains unclear whether the remaining quantity of JunB is sufficient to induce a $p16^{INK4a}$ expression or whether other transcription factors are involved in the $p16^{INK4a}$ induction.

Zusammenfassung

In dieser Arbeit wurde der Einfluss der zytokininduzierten Seneszenz (CIS) auf die genetische Integrität untersucht und wie die Signalübertragung der CIS auf molekularer Ebene erfolgt. Im ersten Teil der Arbeit wurde der Frage nachgegangen, ob die Einleitung der CIS zu Veränderungen in den Chromosomenaberrationen führt, welche die Malignität der Tumorzellen verstärken könnte.

Dazu wurden verschiedene murine RT2 und RT2xStat1$^{-/-}$ Krebszelllinien mit den T_h1 Zytokinen (IFNγ und TNF) behandelt und untersucht, ob die Chromosomenaberrationen der Tumorzelllinien durch diese Behandlung verändert werden. Zu diesem Zweck wurde das genetische Material der Zellen vor Beginn des Experiments und nach 96 h Behandlung mit Medium oder T_h1 Zytokinen unter Verwendung der CGH untersucht. Die Ergebnisse der Experimente zeigen, dass es sich bei den primären RT2 Krebszelllinien um eine heterogene Population handelt. Wenn zum Zeitpunkt der Untersuchung bereits ein Gleichgewicht zwischen den Subpopulationen vorliegt, führt eine T_h1-Zytokinbehandlung nicht zu einer Veränderung der Chromosomenaberrationen. Dies gilt sowohl für RT2 als auch für RT2xStat1$^{-/-}$ Krebszelllinien. Wenn das Gleichgewicht zum Zeitpunkt des Experiments jedoch noch nicht hergestellt ist, können nach der CIS Induktion Veränderungen der Chromosomenaberrationen auftreten. Dies führte zu einer spezifischen Selektion von einer Chromosom 4 bzw. Cdkn2a deletierten Subpopulation der RT2 Krebszelllinie 3. Ein *in vivo* Transfer dieser Zelllinie (nachfolgend als mSc bezeichnet) mit anschließender Immuncheckpointtherapie (ICB) zeigte, dass das Wachstum dieser Zellen nicht mehr durch die ICB gestoppt werden konnte. Eine nachfolgende CGH Analyse der verschiedenen mSc ergab, dass die Zellen einen punktuellen Verlust des Cdkn2a Genes aufweisen. Eine anschliessende *in vitro* T_h1-Zytokinbehandlung bewies, dass die Zellen nicht mehr auf die CIS ansprechen konnten. Zusammenfassend konnte gezeigt werden, dass die Behandlung mit den T_h1 Zytokinen die Selektion von Chromosomenaberrationen innerhalb einer heterogenen Zellpopulation beeinflussen kann. Darüber hinaus wurde gezeigt, dass das Fehlen von Cdkn2a die Induktion von CIS verhindert.

Die Induktion der CIS ist als mögliche Behandlungsoption für unzugängliche oder metastasierte Krebsarten besonders interessant, weil sie zu einem p16^{INK4a}-abhängigen Wachstumsstopp führt. Da TNF aufgrund seiner zytotoxischen Wirkung nicht systemisch verabreicht werden kann, ist die Identifizierung des Signalweges entscheidend, um eine TNF-unabhängige Aktivierung des TNF-Signalweges zu induzieren. Deshalb wurde untersucht, wie die p16^{INK4a} Expression nach IFNγ- und TNF-Stimulation eingeleitet wird. Ein möglicher Kandidat für die Signaltransduktion ist der AP-1 Transkriptionsfak-

tor JunB. Wie in den Experimenten gezeigt wurde, wird die JunB Expression in der CIS induziert. Diese JunB Expression ist TNF abhängig. Weitere Untersuchungen zeigten, dass die TNF-abhängige Induktion von JunB durch NF-κB vermittelt wird. Es wurden verschiedene Techniken zur Herunterregulierung bzw. zum knockout von JunB eingesetzt. Dies würde, so die Hypothese, zu einer reduzierten $p16^{INK4a}$ Expression führen, welche die Induktion von CIS verhindert. Trotz einer reduzierten JunB Expression konnte in keinem der Ansätze die Einleitung der CIS verhindern werden. Es bleibt unklar, ob die verbleibende Menge an JunB ausreicht, um eine $p16^{INK4a}$ Expression zu induzieren, oder ob andere Transkriptionsfaktoren an der $p16^{INK4a}$ Induktion in der CIS beteiligt sind.

Contents

1 Introduction **1**
1.1 Cancer and its characteristics . . . 1
1.1.1 Chromosomal instability enables cancer development . . . 3
1.2 Cancer therapies . . . 5
1.2.1 Classical cancer therapy . . . 5
1.2.2 Targeted therapy . . . 6
1.2.3 Immunotherapy . . . 7
1.3 Senescence . . . 9
1.4 The AP-1 transcription factor . . . 14
1.4.1 The AP-1 transcription factor family member JunB . . . 15
1.5 Aim of this thesis . . . 19

2 Material and Methods **21**
2.1 Material . . . 21
2.1.1 Equipment . . . 21
2.1.2 Consumables . . . 22
2.1.3 Chemicals and reagents . . . 23
2.1.4 Buffers and solutions . . . 25
2.1.5 Kits . . . 27
2.1.6 Laboratory mice . . . 27
2.1.7 Cell lines . . . 28
2.1.8 Mycoplasma testing . . . 28
2.1.9 Plasmids and siRNA sequences . . . 29
2.1.10 Oligonucleotides . . . 29
2.1.11 Antibodies . . . 30
2.1.12 Compounds . . . 30
2.1.13 Software and websites . . . 31
2.2 Methods . . . 31
2.2.1 Cell culture . . . 31
2.2.2 Tumor preparation and β-cancer cell isolation . . . 32
2.2.3 DNA isolation . . . 33
2.2.4 PCR . . . 34
2.2.5 Agarose gel electrophoresis . . . 35
2.2.6 RNA isolation . . . 35
2.2.7 cDNA synthesis . . . 36

2.2.8 qPCR . . . 36
2.2.9 Protein extraction . . . 37
2.2.10 Nuclear and cytoplasmic extraction . . . 38
2.2.11 Protein concentration determination . . . 38
2.2.12 SDS-PAGE and Western Blot . . . 38
2.2.13 Growth arrest assay . . . 39
2.2.14 Senescence-associated β-galactosidase assay . . . 40
2.2.15 LDH assay . . . 40
2.2.16 Crystal violet assay . . . 41
2.2.17 Transfection . . . 41
2.2.18 Comparative genomic hybridization . . . 42
2.2.19 Statistical analyses . . . 44

3 Results **45**
3.1 T_h1 cytokines influence the chromosomal stability of RIP1-Tag2 β-cancer cells . . . 45
3.2 JunB expression is induced by T_h1 cytokines . . . 55
3.3 Inhibition of NF-κB leads to reduced JunB protein expression . . . 60
3.4 Pharmacological downregulation of JunB does not effect the induction of CIS . . . 75
3.5 Downregulation of JunB mediated by siRNA does not influence CIS induction . . . 75
3.6 CRISPR/Cas9-mediated knockdown of JunB has no effect on CIS induction . . . 77

4 Discussion **83**
4.1 Chromosomal aberrations in RT2 and RT2xStat1$^{-/-}$ cancer cell lines after *in vitro* cytokine treatment and *in vivo* ICB therapy . . . 83
4.1.1 No influence on chromosomal aberrations after cytokine treatment in stable RT2 and RIP1-Tag2 x signal transducer and activator of transcription 1$^{-/-}$ cancer cell lines . . . 83
4.1.2 T_h1 cytokine treatment can modify chromosomal aberration in unstable RT2 cancer cell lines . . . 84
4.1.3 *In vivo* selection pressure favors the establishment of a Cdkn2a-negative subpopulation . . . 85
4.2 The role of JunB in CIS . . . 88
4.2.1 JunB expression in CIS is TNF-dependent . . . 88
4.2.2 Strong evidence of NF-κB-mediated induction of JunB expression after T_h1 cytokine treatment . . . 89
4.2.3 Reduction of JunB expression has no influence on the induction of CIS in A204 cancer cells . . . 90

4.2.4 Relationship of JunB and $p16^{INK4a}$ expression in the induction of CIS remains unresolved 91
4.2.5 The complexity of the AP-1 transcription factor impedes the accurate analysis of JunB in CIS 91
4.2.6 Deciphering the TNF signaling pathway in CIS will help to identify potential targets 92
4.3 Conclusion 93

Acronyms **99**

Bibliography **105**

Chapter 1

Introduction

1.1 Cancer and its characteristics

In cancer cells, cellular processes and regulatory mechanisms change in comparison to healthy cells. However, these differences must accumulate before cells can transform into malignant cells. The multi-stage process of cell transformation is defined by so-called ”hallmarks of cancer” (Figure 1.1; Hanahan and Weinberg (2011)). One characteristic of cancer cells is the permanent response to proliferation signals. This responsiveness is achieved at different signaling levels. For example, cells can increase the expression of receptor proteins on their cell surface. Furthermore, mutations of downstream effectors can lead to a constitutively activated form (e.g., B-Raf proto-oncogene (BRAF)V600E, compare Section 1.2.2). Besides, negative feedback loops acting as a cell-internal regulatory mechanism are frequently impaired (Amit *et al.* (2007)). An excessive overexpression of effector proteins such as rapidly accelerated fibrosarcoma (RAF), rat sarcoma (RAS) and cellular myelocytomatosis (MYC) can lead either to apoptosis or to senescence (see Section 1.3; Murphy *et al.* (2008), Pelengaris *et al.* (2002), Lawlor *et al.* (2006), Sarkisian *et al.* (2007)). Although senescent cells do no longer proliferate, they produce and secrete proliferation and inflammation signals known as senescence-associated secretory phenotype (SASP) (compare Section 1.3 and Figure 1.7). Thus, SASP can also promote tumor expansion.

The sustained proliferation of cancer cells is closely associated with their resistance to apoptosis. Apoptosis leads to a non-inflammatory cell death, which can be triggered by extrinsic or intrinsic signals. A key factor of apoptosis induction is the tumor suppressor protein p53 (p53) (Pietsch *et al.* (2008)). This protein acts as a deoxyribonucleic acid (DNA) damage sensor, thereby preventing mutated cells from proliferating as shown in Figure 1.2 (Bartkova *et al.* (2005)). Loss of p53 is found in many tumors highlighting its important role as a tumor suppressor (Donehower and Lozano (2009)). Moreover, the overexpression of anti-apoptotic proteins like B-cell lymphoma 2 (Bcl-2) and B-cell lymphoma-extra large (Bcl-x_L) (Eischen *et al.* (2001)) or the decreased expression of pro-apoptotic proteins such as Bcl-2-like protein 11 (Bim) or Bcl-2-associated X protein (BAX) (Bauer *et al.* (2007), Mccurrach *et al.* (1997)) results in an overall inhibition of apoptosis.

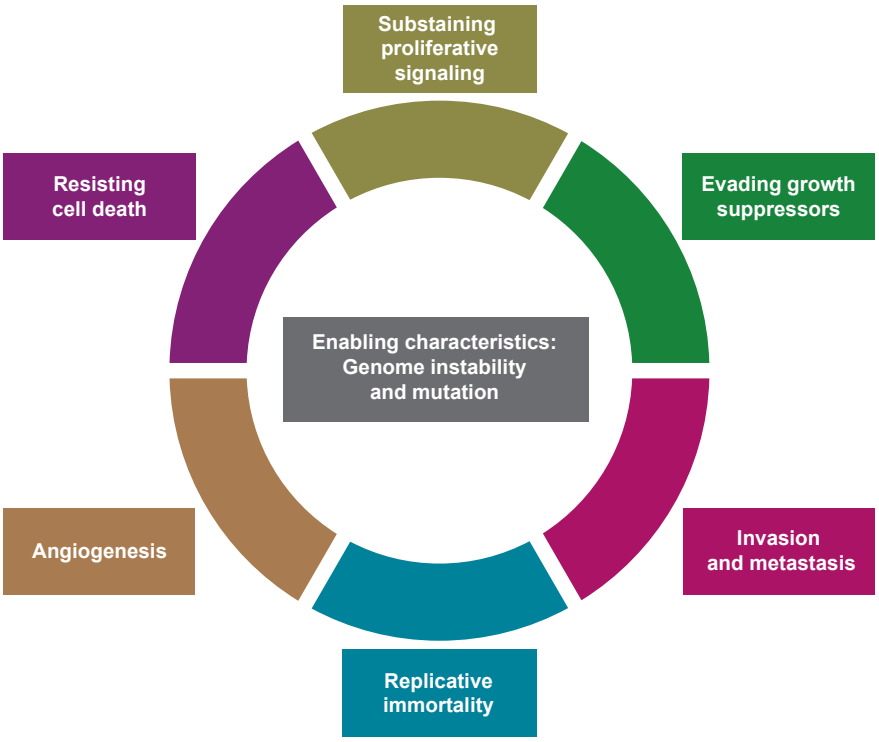

Figure 1.1: Hallmarks of cancer. In order to transform into a cancer cell, the cells must be resistant to cell death and become immortal. Furthermore, they need sustained proliferation. When progressing, cancer cells activate angiogenesis, become invasive and finally metastasize. Genomic instabilities and mutations form the basis of neoplasm development. Modified from Hanahan and Weinberg (2011).

Another feature that has to be acquired by cancer cells is replicative immortality. In healthy cells, the number of potential cell divisions is limited by the length of the telomeres. This limit is called hayflick limit (Hayflick and Moorhead (1961), Shay and Wright (2000)). Telomeres are repetitive nucleotide sequences positioned at the end of each chromosome to stabilize the DNA. In each replication step, the DNA is amplified while telomeres are not, resulting in telomere shortening. After reaching a critical length, the cells do not multiply in order to prevent DNA damage (compare Section 1.1.1; Takai *et al.* (2003), Ledford (2007)). Instead, cells become senescent or apoptotic. In order to overcome the replicative limitation, malignant cells activate telomerase (Greider and Blackburn (1996)). This enzyme, inactivated in normal stromal cells, elongates the telomere ends, enabling unlimited cell division. Thus, reexpression of the telomerase is a characteristic of cancer cells.

As the tumor grows and expands, the increasing need for nutrients and oxygen can no longer be provided by the surrounding blood vessels. Also, oxidative stress accumulates in cancer cells, which can not be effectively eliminated (Sosa *et al.* (2013)). This

insufficient supply eventually leads to upregulation and secretion of vascular endothelial growth factor (VEGF) (Juarez *et al.* (2008), Carmeliet (2005)). Angiogenesis, i.e., the production and growth of new blood vessels, is induced by this protein. Thus, angiogenesis, as another hallmark of cancer, facilitates the growth and progression of tumors.

The potential of cancer cells to invade and metastasize is another important hallmark of cancer. This process is mediated by a mechanism called epithelial-mesenchymal transition (EMT) (Yilmaz and Christofori (2009)). By the downregulation of adhesion proteins, such as E-cadherin, cancer cells can detach from their surrounding tissue and invade into the lymphatic system or the bloodstream (Berx and van Roy (2009)). From there, cancer cells can further migrate into local lymph nodes or into distant tissue, which results in either local or distant metastasis. A fundamental biological mechanism underlying the development of the above-described hallmarks of cancer is the genomic instability of cancer cells.

1.1.1 Chromosomal instability enables cancer development

The integrity loss of the genome is the main driver of tumor development and progression. Genotoxins such as ultraviolet (UV)-light, ionizing radiation, heterocyclic amines and alkylating compounds trigger genomic instability by generating nucleotide mutations or double strand breaks (DSBs) which result in chromosomal aberrations (Roos and Kaina (2006)). The accumulation of mutations is accompanied by the loss or reduced expression of proteins involved in DNA repair.

At a single nucleotide level, point mutations in protein coding regions can induce a silent mutation that do not change the amino acids (AA) code. Therefore, the protein structure and function is not influenced. Nonsense mutations lead to a premature termination of the AA sequence, whereas missense mutation replaces the AA. Those mutations can alter protein function and may result in a hyperactive enzymatic activity promoting tumorigenesis (e.g., BRAFV600E, compare Section 1.2.2). Alterations occurring at the single nucleotide level can be identified by sanger sequencing (classical approach) or, for example, by next-generation sequencing. The described single nucleotide mutations have a minor influence on the overall genomic structure.

However, genotoxins can also cause DNA lesions that interrupt the progression of the replication fork leading to its collapse. As a result, the DNA strand is interrupted creating a DSBs. Severe disturbances of this kind activate the DNA damage sensors ataxia telangiectasia mutated (ATM) and ataxia telangiectasia and Rad3-related protein (ATR). These kinases sense either DNA single strand breaks (ATR) or double strand breaks (ATM) (Ismail *et al.* (2005), Zou and Elledge (2003)). Afterward, downstream proteins, such as checkpoint kinase 1 (CHK1) and checkpoint kinase 2 (CHK2), are phosphorylated and in turn activate p53.

The tumor suppressor p53 has a pivotal role in the subsequent determination of the cell fate (Figure 1.2). A moderate level of phosphorylated p53 results in the activation of cyclin-dependent kinase inhibitor 1 (p21) (El-Deiry *et al.* (1993)). This protein inacti-

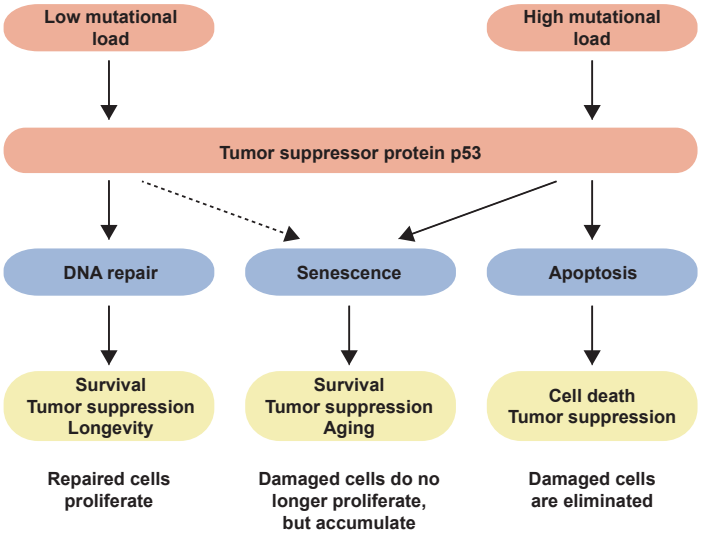

Figure 1.2: The expression level of p53 determines cell fate. Low DNA damage or mutation-induced stress leads to low or moderate p53 expression. In consequence, cells activate the DNA repair mechanism to survive and proliferate, or to survive and become senescent. High mutational load or DNA damage causes high p53 expression resulting in apoptosis induction and cell death. Modified from Wu and Prives (2018).

Abbreviations: p53 (tumor suppressor protein p53).

vates the cyclin E/A - cyclin-dependent kinase 2 (CDK2) complex resulting in a G_1 arrest and senescence (Dulić *et al.* (1994)). High levels of DNA DSBs increases the expression level of p53 until it exceeds a critical threshold. At this point, proapoptotic proteins, such as BAX and p53 upregulated modulator of apoptosis (PUMA), are activated and the expression of the tumor necrosis factor receptor superfamily member 6 (Fas receptor) is induced (Toshiyuki and Reed (1995), Nakano and Vousden (2001), Roos *et al.* (2004)).

These activations initiate the apoptosis cascade, thereby preventing the proliferation of severely damaged cells. Cells can avoid senescence or apoptosis induction by activating the DNA repair mechanisms. The most frequently used repair systems are the classical non-homologous end joining (c-NHEJ) and the homologous recombination (HR). Cofactors are abundant in the c-NHEJ, which is the dominant repair mechanism during the G_0/G_1 and G_2 phases (Chiruvella *et al.* (2013), Karanam *et al.* (2012)). In the c-NHEJ blunt DSBs are ligated independently of sequence homology. This process is error-prone, which can result in the integration of false nucleotides. Nevertheless, c-NHEJ is a fast mechanism to protect DNA integrity and preventing chromosomal instability (Difilippantonio *et al.* (2000)). If the DSBs leaves 3'-single stranded DNA overhangs, the HR process is activated. Mostly active in the mid-S and mid-G_2 phase, the HR is largely error-free as it can use the sister chromatin as a template (Karanam *et al.* (2012)). Impair-

ment of the DSBs repair mechanisms can result in chromosomal translocations as well as amplifications and deletions (Difilippantonio *et al.* (2000), Bassing and Alt (2004), Al-Kuraya *et al.* (2004), Paris *et al.* (2004)).

While most DSBs occur randomly throughout the genome, some regions are more vulnerable to DSBs. During replication, these fragile sites are more prone to severe damage (Sutherland (1977), Yunis *et al.* (1987)). The breakage of particular fragile sites on chromosome 9 and 12, for example, can lead to the Philadelphia chromosome translocation (t[9; 22]) (Kurzrock *et al.* (2003)). In consequence, the fusion gene BCR-ABL is expressed, which drives the malignant transformation of lymphocytes. Chromosomal amplifications and deletions can be analyzed by array comparative genomic hybridization (CGH) (compare Section 2.2.18) whereas translocations are detected by fluorescent DNA *in situ* hybridization (FISH) (Ceccaldi *et al.* (2016), Bassing and Alt (2004), Paulson *et al.* (1998), Pipiras *et al.* (1998)).

Like DSBs, the shortening of the telomeric ends contributes to the destabilization of genomic integrity. As the telomeres reach a critical length, the DSBs sensors ATM or ATR are activated. Since telomeres cannot be repaired in a normal cell, p53 is subsequently activated to induce senescence (Figure 1.3). Cancer cells can overcome this permanent growth arrest by inactivating p53 and/or retinoblastoma protein (Rb) (Shay *et al.* (1991), Hara *et al.* (1991)). Further replication causes the sister chromatins to fuse and finally break during mitosis. This strongly destabilizes the genome which can result in translocation, amplification or deletion of genomic regions (Artandi *et al.* (2000)). Although most cells become apoptotic, some cells manage to survive and become malignant.

1.2 Cancer therapies

1.2.1 Classical cancer therapy

One of the traditional cancer therapies is the surgical removal of the tumor. However, this procedure is only possible with a solid tumor. Moreover, the tumor must be surgically accessible. Further limitations occur if the tumor has infiltrated excessively into the surrounding tissue or if it has already metastasized. Therefore, neoadjuvant therapy options exist in which the tumor is reduced by radiation or chemotherapy before resection. In contrast, adjuvant therapy is applied when potential remaining tumor cells are to be destroyed by irradiation or chemotherapy after the surgery.

In radiation therapy, DNA damage is caused by gamma rays, electrons or X-rays, which in turn induces apoptosis (Wannemacher *et al.* (2006)). Besides, most chemotherapeutic drugs lead to the disruption of DNA repair or replication in fast-proliferating cells (Bruhn *et al.* (2003)). The effect of cytotoxic drugs, however, is limited in large tumors with poor blood circulation due to the low uptake of the drug. Furthermore, resistances often develop, which is why a combination of different drugs is usually administered.

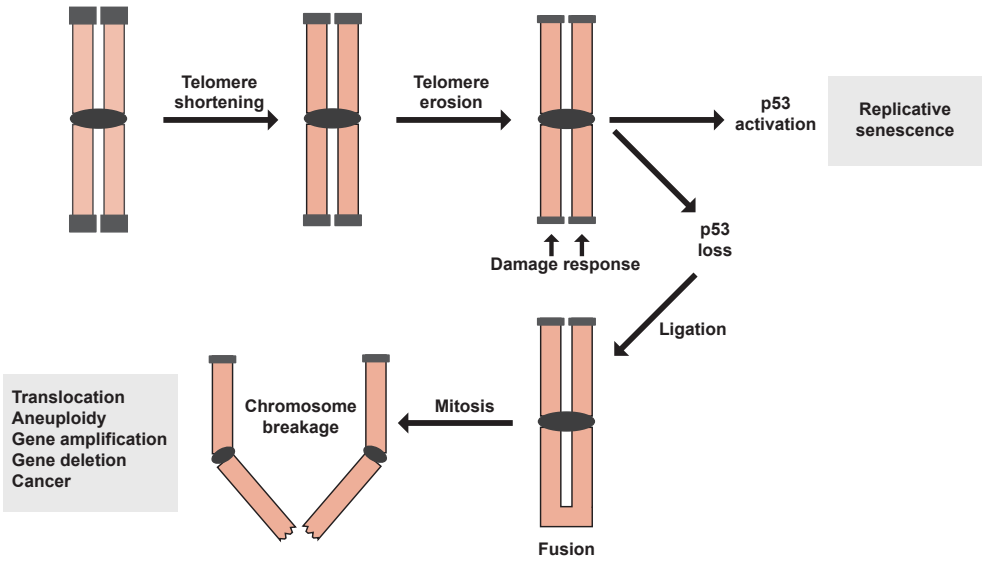

Figure 1.3: Telomere shortening threatens chromosomal stability. With each cell division, the telomeres become progressively shorter. When a critical length is reached, the DNA damage response (DDR) is activated. Subsequent activation of p53 triggers senescence induction. If p53 is deactivated or lost, sister chromatins can fuse and break during mitosis. As a result, chromosomal aberrations, such as translocations, aneuploidy, gene amplification, or deletion, occur, and support cancer development. Modified from Artandi and DePinho (2010).

Abbreviations: p53 (tumor suppressor protein p53).

The disadvantage of radiation therapy and especially cytotoxic therapy is that healthy tissue is also damaged, which leads to severe side effects. Newer cancer therapy methods, therefore, strive for more targeted treatment of tumor cells, which also includes the involvement of the immune system.

1.2.2 Targeted therapy

Nowadays, the progress in cancer therapy enables more specific treatment of the tumor. This is accomplished by so-called small molecules, antibodies, and the manipulation of the immune system. Small molecules focus on disrupting enzymatic activity in tumor cells, while monoclonal antibodies inhibit cell-cell interactions by blocking cell surface receptors. In order to manipulate the immune system, endogenous T cells are transformed to express a chimeric antigen receptors (CAR) in order to kill tumor cells.

Small molecules are successfully used in the clinic to treat a large variety of tumors (Hoelder *et al.* (2012)). They target proto-oncogenes that are mutated or overexpressed. These proteins are highly activated, leading to increased proliferation activity. A pathway that can be targeted with small molecules is the mitogen-activated protein kinase

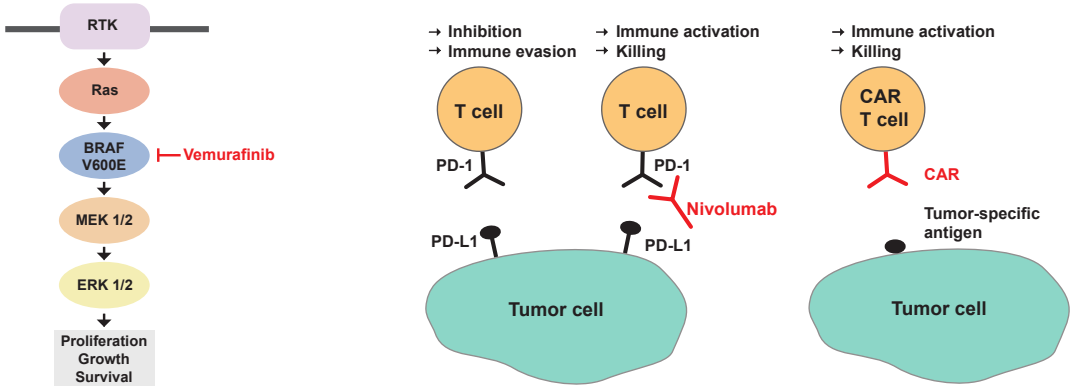

(a) Small molecule therapy (b) Immunotherapy

Figure 1.4: Targeted cancer therapy. (a) Small molecules are used in cancer therapy to impair abnormal enzymatic activity. (b) Principles of immunotherapy. Left: The expression of programmed cell death protein 1 ligand (PD-L1) on cancer cells interacts with programmed cell death protein 1 (PD-1) on T cells to prevent their activation. To overcome this inhibition, the PD-1 antibody nivolumab is used for immune checkpoint blockade therapy. Right: CAR T cells recognize tumor specific antigens and subsequently kill the tumor cell. Modified from Swaika *et al.* (2014), Lim and Soo (2016) and Brown and Mackall (2019).

Abbreviations: BRAF (B-Raf proto-oncogene), CAR (chimeric antigen receptors), MEK (mitogen-activated protein kinase kinase), PD-1 (programmed cell death protein 1), PD-L1 (programmed cell death protein 1 ligand), RAS (rat sarcoma), RTK (receptor tyrosine kinases).

(MAPK) pathway with mutations mainly found in mitogen-activated protein kinase kinase (MEK) or BRAF proteins (Davies *et al.* (2002), Curtin *et al.* (2005)). Around 90% are BRAF mutations that have a missense mutation at the gene location 1799 (T to A), replacing the AA valine (V) to glutamic acid (E). This mutated BRAF(V600E) is constantly activated and found in tumors like melanoma (Ascierto *et al.* (2012)) and non-small-cell lung carcinoma (NSCLC) (Janku *et al.* (2011), Kobayashi *et al.* (2011)). The small molecules vemurafenib (Flaherty *et al.* (2010)) and dabrafenib (Wilmott *et al.* (2012)) are specifically targeting this mutation and disrupting the MAPK pathway.

1.2.3 Immunotherapy

Besides using small molecules to alter tumor metabolism, antibodies are used to interfere with the cell-cell interaction. One example of this immunotherapeutic approach is the inhibition of PD-1. PD-1 is a membrane protein expressed on activated T cells, B cells and macrophages (Yamazaki *et al.* (2002)). Two ligands can bind to PD-1. For example PD-L1, which is constitutively expressed on antigen-presenting cells (APC), T cells (Vibhakar *et al.* (1997)), B cells (Eppihimer *et al.* (2002)), monocytes, epithelial and en-

dothelial cells (Freeman *et al.* (2000), Sharpe and Freeman (2002)). The expression of the other PD-1 ligand, PD-L2, is exclusively found on APC and bone marrow-derived mast cells (Latchman *et al.* (2001), Zhong *et al.* (2007)). Binding of PD-L1 on PD-1 results in T cell inactivation (Carter *et al.* (2002), Latchman *et al.* (2004), Kroner *et al.* (2005), Keir *et al.* (2007)). This mechanism reduces tissue damage caused by a prolonged immune response (Nishimura *et al.* (1999), Okazaki *et al.* (2003)). The described negative regulation of the immune response can be exploited by cancer cells to escape the immune response. Tumors such as melanoma (Kleffel *et al.* (2015)), renal carcinomas (Weinstock and McDermott (2015)), ovarian (Strickland *et al.* (2016)), as well as lung cancer (Sacher and Gandhi (2016)), express PD-L1. Binding to PD-L1 inactivates T cells and inhibits the killing of tumor cells. Nivolumab, a FDA approved antibody binding to PD-1, hence blocking T-cell inhibition, was shown to achieve partial or complete response in patients with NSCLC, renal cell cancer, and melanoma (Figure 1.4; Topalian *et al.* (2012)). In other therapies that exploit the presence of tumor-specific T cells, antibodies against, for example, cytotoxic T-lymphocyte-associated protein 4 (CTLA-4) or lymphocyte-activation gene 3 (LAG-3) are used. The blocking of CTLA-4, which binds with a higher affinity to CD80/CD86, prevents the inhibition of proliferation of the activated T cell (Krummel and Allison (2011)). LAG-3 on the other hand binds to major histocompatibility complex class II (MHC class II) with a higher affinity than the CD4 receptor (Baixeras *et al.* (1992)). By inhibiting LAG-3, a proper activation of T cells can be achieved. These successful therapies demonstrate the potential of immune checkpoint therapies (Wieder *et al.* (2018)).

Nevertheless, these therapies are limited by the availability of T-cell receptors (TCRs), which can recognize tumor-specific antigens. To overcome this limitation, T cells are isolated from the patient and genetically modified to express a synthetic TCR that recognizes tumor-specific antigens. This CAR dramatically increases the specificity of TCR, resulting in efficient tumor killing. First clinical trials showed the efficiency of anti-CD19 CAR T cells in pediatric and adult patients with B-cell non-Hodgkin lymphoma (Kochenderfer *et al.* (2010), Savoldo *et al.* (2011), Brentjens *et al.* (2011)) and chronic lymphatic leukemia (CLL) (Kalos *et al.* (2011), Porter *et al.* (2011)). Other promising targets for CAR T-cell therapy are the CD20 and CD30 receptor (Zhang *et al.* (2016), Wang *et al.* (2017)). Major side effects in this therapy are the cytokine release syndrome (Morgan *et al.* (2010), Hay *et al.* (2017)) and neurotoxicity (Brudno and Kochenderfer (2016), Abken (2017)).

Each of the discussed treatments leads to the killing of the tumor cells. Cancer cells can escape this intense survival pressure by, for example, upregulating other signal pathways through additional mutations. Furthermore, PD-L1 therapy requires the presence of a T-cell clone that can identify the specific and exposed mutation of a tumor cell. In addition, a direct cell-cell contact must exist, similar to CAR T-cell therapy. Since solid tumors can be inaccessible, such therapeutic approaches are not effective. This obstacle can be overcome by using soluble factors such as cytokines. Moreover, the strong survival pressure mediated by killing might be avoided by inducing senescence in the tumor

cell. As a result, the formation and spread of further mutations would be inhibited.

1.3 Senescence

Senescence describes an irreversible state of a metabolically active cell that is unable to divide. The induction of this state can, for example, prevent the proliferation of damaged cells, while maintaining them in the tissue. Thus, senescence serves as a barrier to malignant transformation. This mechanism was discovered in 1961 in cultivated fibroblast (Hayflick and Moorhead (1961)). Senescent cells are cell-cycle arrested in the G_0/G_1 or

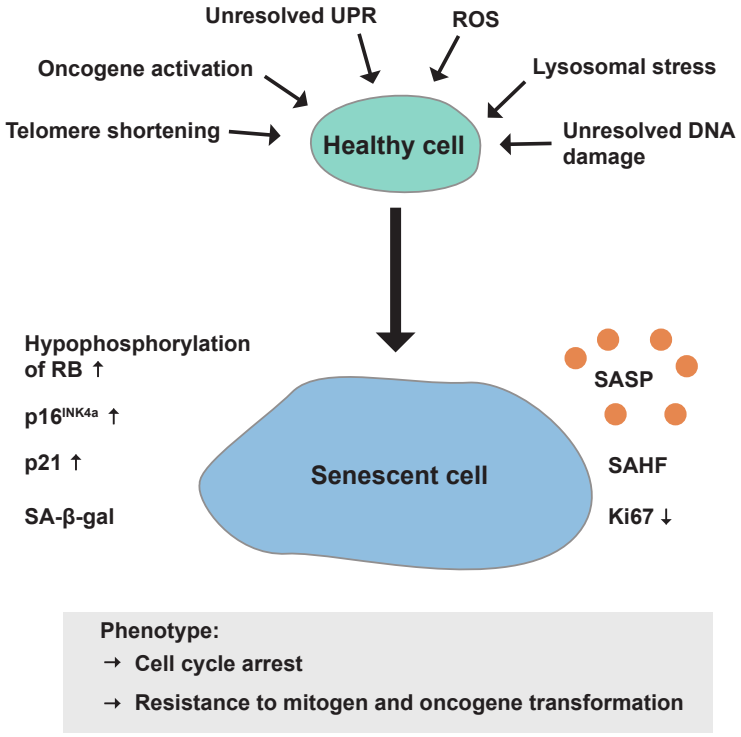

Figure 1.5: Senescence induction. Cell stressors such as telomere shortening, oncogene activation, or ROS can trigger senescence induction. Senescent cells are cell cycle arrested but metabolically active cells. Senescent cells can be characterized by their increased expression of $p16^{INK4a}$ and p21, and the increased hypophosphorylation of Rb. Additionally, they express SA-β-gal, SASP, and SAHF. In contrast, the marker of proliferation Ki67 (Ki67) is downregulated. Modified from Sharpless and Sherr (2015).

Abbreviations: Rb (retinoblastoma protein), $p16^{INK4a}$ (cyclin-dependent kinase inhibitor 2A), p21 (cyclin-dependent kinase inhibitor 1), ROS (reactive oxygene species), SA-β-gal (senescence-associated β-galactosidase), SAHF (senescence-associated heterochromatin foci), SASP (senescence-associated secretory phenotype), UPR (unfolded protein response).

G_2/M stage (Deng *et al.* (1995), Tresini *et al.* (1998)). A hallmark for senescent cells is the hypophosphorylation of Rb (Figure 1.5). Rb is a tumor suppressor protein that is bound to DNA via E2F transcription factor (E2F) in a non-dividing cell (Figure 1.6; (Graña *et al.* (1998)). In this state, the protein is hypophosphorylated and thus prevents E2F-induced DNA replication. When a cell enters the cell cycle, Rb is phosphorylated by the kinases cyclin-dependent kinase 4/6 (CDK4/6) and further hyperphosphorylated by CDK2 (Suzuki-Takahashi *et al.* (1995)). The hyperphosphorylation of Rb leads to the inactivation and, in consequence, to the dissociation of Rb from the DNA. By releasing E2F, the cell can enter the cell cycle in order to proliferate. The hypophosphorylation of

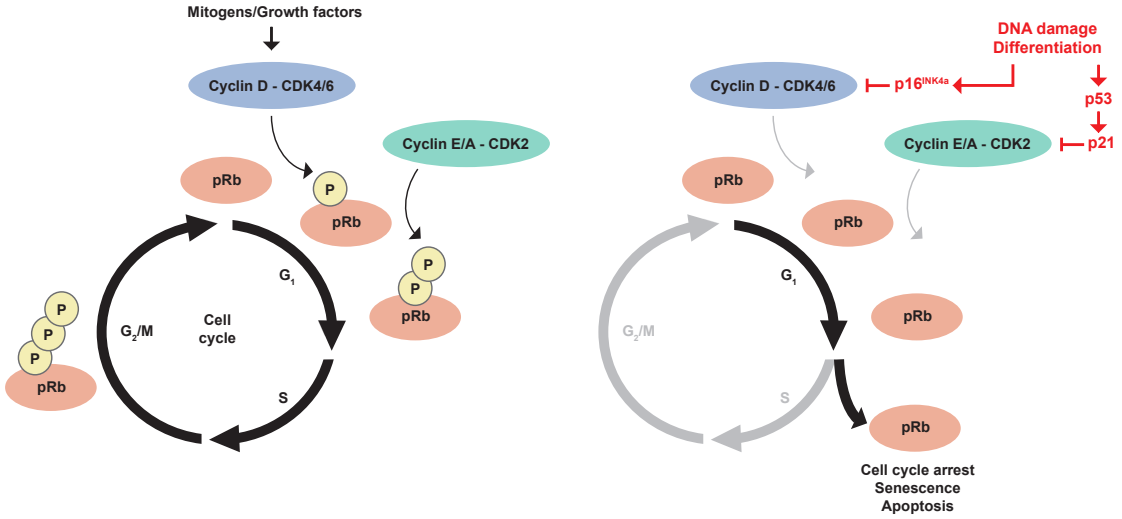

Figure 1.6: Cell cycle arrest is mediated by p53 and $p16^{INK4a}$. In order to enter the cell cycle, Rb is phosphorylated by the cyclin D - CDK4/6 complex and then hyperphosphorylated by the cyclin E/A - CDK2 complex. This process is inhibited by the stress-induced expression of p53 and $p16^{INK4a}$, resulting in cell cycle arrest, senescence, or apoptosis. Modified from Sachdeva and O'Brien (2012)).

Abbreviations: Rb (retinoblastoma protein), CDK2 (cyclin-dependent kinase 2), CDK4/6 (cyclin-dependent kinase 4/6), $p16^{INK4a}$ (cyclin-dependent kinase inhibitor 2A), p21 (cyclin-dependent kinase inhibitor 1), p53 (tumor suppressor protein p53).

Rb is associated with the increased expression of p53, p21 and cyclin-dependent kinase inhibitor 2A ($p16^{INK4a}$), which is another hallmark of senescence (Serrano *et al.* (1997), Alcorta *et al.* (1996)). The tumor suppressor p53 acts as a sensor for stress and especially for DNA damage (Figure 1.2). If these damages cannot be sufficiently eliminated, the cell either undergoes apoptosis or becomes senescent. When the cell chooses to become senescent, the activation of p53 leads to the direct activation of the downstream factor p21. This inhibitor blocks the cyclin E/A - CDK2 complex, preventing the cell from entering the cell cycle. Expression of the other tumor suppressor $p16^{INK4a}$ is mediated by a variety of signaling pathways. For example, activation of the oncogene RAS

leads to expression of HMG-box transcription factor 1 (HBP1) which in turn induces $p16^{INK4a}$ (Ohtani *et al.* (2001)). Furthermore, the expression of $p16^{INK4a}$ can be induced by the transcription factors protein C-ets-1 (ETS-1) and JunB proto-oncogene (JunB) (Ohtani *et al.* (2001), Passegué and Wagner (2000)). As a cell cycle inhibitor, $p16^{INK4a}$ prevents cyclin D - CDK4/6 complex formation. In consequence, the cell do no longer proliferate. Therefore, the expression of $p16^{INK4a}$ is positively associated with aging and senescence, whereas $p16^{INK4a}$ loss is often connected with the development of malignant cells (Krishnamurthy *et al.* (2004)). Contrary to the expression of the described tumor suppressors, the proliferation marker Ki67 is strongly reduced or not expressed at all (Lawless *et al.* (2010)). The induction of senescence leads to metabolic changes and, thus, to a different cytokine expression profile. This SASP is composed of different cytokines and chemokines. Inflammatory and immunomodulatory cytokines such as interleukin 6 (IL-6) and interleukin 8 (IL-8) promote tumorigenesis and inflammation (Coppé *et al.* (2008)). The composition of the SASP may vary so that, in other cases, anti-inflammatory properties dominate in the SASP. In consequence, the SASP may also prevent fibrosis and suppress tumor growth (Figure 1.7; Krizhanovsky *et al.* (2008), Acosta *et al.* (2013)). Besides these metabolic changes, epigenetic modifications are found in senescent cells as well (Narita *et al.* (2003)). In addition to the increased expression of the trimethylated histone H3 lysine 9 (H3K9me3), which is frequently used as a marker for senescence, numerous heterochromatin foci are found. This characteristic is called senescence-associated heterochromatin foci (SAHF). Another hallmark of senescence is the expression and activation of senescence-associated β-galactosidase (SA-β-gal). The enzymatic activity of SA-β-gal can be measured in senescent cells at a suboptimal pH value of 6.0 pH (Dimri *et al.* (1995)). Usually, the activity of β-galactosidase is measured at 4.5 pH. In SA-β-gal-positive cells, the perinuclear compartment is stained in blue. So far it is unclear why the pH shift occurs in senescent cells (Lee *et al.* (2006)). Finally, the morphology of senescent cells differs from normal cells. For example, a flattened and enlarged cell body could be found in oncogene-induced senescence (Serrano *et al.* (1997), Denoyelle *et al.* (2006)). This altered morphology is also observed in aging BRAFV600E-mutated melanoma cells and in oxidative stress-induced senescent human fibroblasts (Michaloglou *et al.* (2005), Chen and Ames (1994)). Furthermore, this phenotype was found in osteosarcoma cells, where senescence was induced by the reexpression of Rb (Hinds *et al.* (1992)).

In order to define a senescent cell as such, at least two of the described characteristics must be fulfilled. Moreover, senescence can be induced by a variety of mechanisms.

Initially, senescence was discovered in aging cells as a result of the continuous shortening of telomeres (Hayflick and Moorhead (1961), de Lange (2005), Zglinicki *et al.* (2005)). This form of senescence is named replicative senescence. It is characterized by continuous shortening of telomeres. This, in turn, activates DNA damage response (DDR), resulting in a p53 activation and, eventually, senescence induction. Thus, replicative senescence represents a mechanism of tumor suppression as it prevents the proliferation of damaged cells (Feldser and Greider (2007)). Surprisingly, the expression of

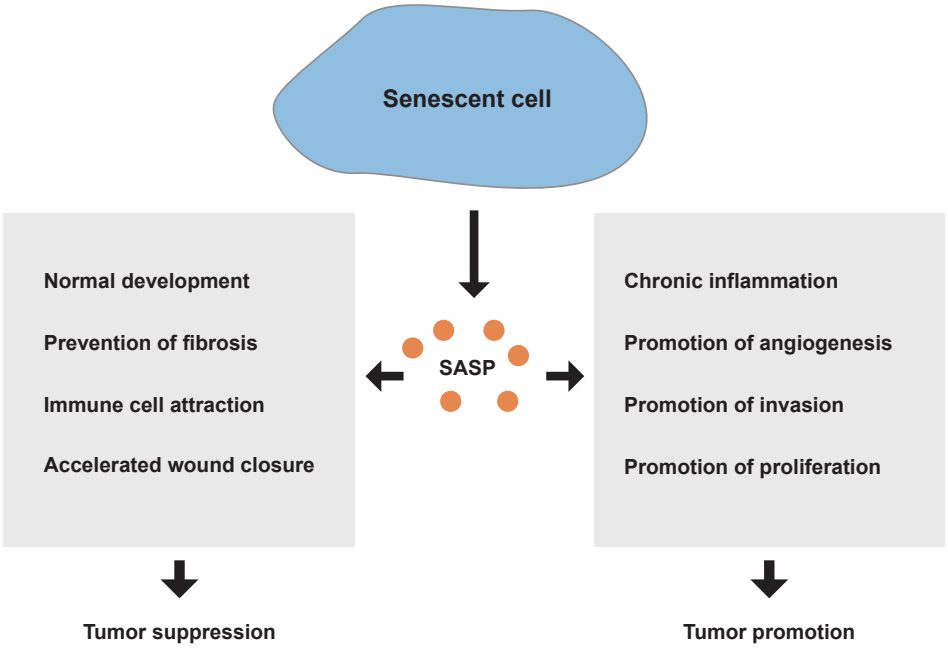

Figure 1.7: Divergent effects of the SASP. Secreted molecules from senescent cells can prevent fibrosis, accelerate wound healing, and lead to the attraction of immune cells, which all together prevent tumor progression. Nevertheless, SASP may also cause chronic inflammation and induce angiogenesis, cell invasion, and proliferation, thus leading to tumor promotion. Modified from Lecot *et al.* (2016).

Abbreviations: SASP (senescence-associated secretory phenotype).

oncogenes can also result in senescence induction. The first oncogene that was shown to induce senescence is H-RAS (Serrano *et al.* (1997)). H-RAS-mediated senescence induction is enabled by the activation of signaling pathways controlling survival, proliferation, cytoskeleton changes or the generation of oxidative stress (Malumbres and Pellicer (1998)). The accumulation of oxidative stress triggers the activation of DDR and the MAPK/p38 pathway. Hence, the downstream effector proteins p53 and p21 and/or $p16^{INK4a}$ are activated, which eventually lead to a permanent cell cycle arrest (Sewing *et al.* (1997), Lin *et al.* (1998), Zhu *et al.* (1998)). Another protein that induces oncogene-induced senescence is also located in the MAP-kinase signaling pathway. The expression of BRAF(V600E) is found in numerous tumors, particularly in melanoma. However, the oncogene is also expressed in 80% of all nevi (Pollock *et al.* (2003)). Despite the expression of BRAF(V600E), these cells are not malignant and, in contrast to melanoma cells, have an intact $p16^{INK4a}$ activity (Wellbrock *et al.* (2004), Dhomen *et al.* (2009)). This prevents the entry into the cell cycle and thus malignant transformation.

If the intracellular control mechanisms have failed, and a malignant cell has developed, senescence can be induced nevertheless and prevent the proliferation of malignant cells. For example, senescence can be caused by radiation therapy and treatment with cytotoxic drugs. The mechanism of action is the same: substances such as doxorubicin and hydroxyurea, but also camptothecin, intervene in DNA replication (Wang *et al.* (1998), Park *et al.* (2000)), Han *et al.* (2002), te Poele *et al.* (2002)). As a result, the amplification of DNA and its repair in these rapidly proliferating cells is significantly impeded. Chromosomal instability occurs, and the cell either becomes apoptotic or initiates senescence. In addition, the kinase inhibitor palbociclib, a drug already used in breast cancer therapy, also leads to therapy-related senescence (Finn *et al.* (2009), Vijayaraghavan *et al.* (2017)). It resembles the $p16^{INK4a}$ induction by inhibiting the cyclin D - CDK4/6 complex, thereby inducing a G_0/G_1 arrest.

Besides replicative, oncogene- and therapy-induced senescence, other induction mechanisms were discovered recently. The $CD4^+$ T-helper cell 1 (T_h1) cytokines interferon gamma (IFNγ) and tumor necrosis factor (TNF) can induce senescence in cancer cells which is therefore termed cytokine-induced senescence (CIS) (Braumüller *et al.* (2013)). For this study, a tumor mouse model developing an endocrine pancreatic tumor within 12 weeks of age was used (compare Section 2.1.6). The combined treatment of cancer-prone mice with IFNγ- and TNF-producing T_h1 cells caused an increase of SA-β-gal activity, an increase of the senescence marker pHP1γ in the nucleus and high $p16^{INK4a}$ levels. In addition, Rb was hypophosphorylated, indicating DNA binding and thereby preventing the cells from entering the S phase. Furthermore, isolated RIP1-Tag2 (RT2) cells became growth-arrested when treated with both cytokines *in vitro*. Treatment with one cytokine alone failed to induce growth arrest. Moreover, the expression levels of SA-β-gal or pHP1γ were not as high compared to the double-treated cells. In an *in vivo* study, an adoptive T-cell transfer resulted in an infiltration of injected Tag-T_h1 cells in the surrounding tumor tissue. In consequence, the tumor volume of Tag-T_h1-treated mice was sharply reduced, accompanied by a prolonged survival. Cells from RIP1-Tag2 x sig-

nal transducer and activator of transcription $1^{-/-}$ (RT2xStat1$^{-/-}$) and RIP1-Tag2 x tumor necrosis factor receptor $1^{-/-}$ (RT2xTNFR1$^{-/-}$) mice showed little to no SA-β-gal expression. *In vivo* studies using RT2xTNFR1$^{-/-}$ mice demonstrated that the adoptive T-cell therapy did not reduce tumor volume and failed to induce p16^{INK4a} expression in RT2 tumors. The expression of p16^{INK4a} seems to be essential for senescence induction in this tumor model since a knockdown of p16^{INK4a} via small hairpin RNA (shRNA) impaired RT2 cancer cells to become senescent after treatment with IFNγ and TNF.

1.4 The AP-1 transcription factor

Activator protein 1 (AP-1) is a dimeric transcription factor composed of proteins from the ATF (ATF1-7), JUN (c-Jun, JunB, and JunD), FOS (FOS, FOSB, FOSL1, and FOSL2) and MAF (v-maf, c-Maf, and MafA) families (Hai and Curran (1991), Kataoka *et al.* (1994), Kerppola and Curran (1994a), Kerppola and Curran (1994b)). These proteins can either form homo- or heterodimers. Dimer formation is enabled by the binding of two activator protein 1 (AP-1) proteins via their leucine-zipper motif which leads to a coiled coil structure (Figure 1.8, Curran and Franza (1988), Rauscher *et al.* (1988)). Subsequent DNA binding is facilitated by a basic motif present on both proteins. To mediate DNA binding, AP-1 must recognize and bind specifically to the cAMP response element (CRE) consensus sequences (5'-TGACGTCA-3') or to the 12-*O*-tetradecanoylphorbol 13-acetate (TPA)-responsive element (5'-TGA G/C TCA-3') (Hirai and Yaniv (1989), Lee *et al.* (1987), Angel *et al.* (1987)). The transcription factor AP-1 has a broad and diverse role in the regulation of signaling pathways. These include pathways involved in proliferation, apoptosis, angiogenesis and DNA methylation (Zenz *et al.* (2003), Kasibhatla *et al.* (1998), Marconcini *et al.* (1999), Bakin and Curran (1999)). Control of these diverse and in part opposing signaling pathways is achieved by a different composition and thereby different DNA-binding affinity of AP-1 (Halazonetis *et al.* (1988), Ryseck and Bravo (1991)). However, the formation of the dimers depends on the relative amount of expressed AP-1 members (Kovary and Bravo (1991), Kovary and Bravo (1992)). The expression of AP-1 proteins, in turn, is regulated extracellular mitogens and cytokines (Gurzov *et al.* (2008), Gurzov *et al.* (2012)). Furthermore, AP-1 proteins can regulate other AP-1 proteins as well. For instance, studies demonstrated that the Jun proto-oncogene (c-Jun) homodimer has a higher DNA binding affinity than JunB homodimer. However, JunB prefers to form heterodimers e.g., with c-Jun. Thereby, JunB can prevent c-Jun homodimer formation and can thus inhibit the transcription of c-Jun homodimer targets (Deng and Karin (1993), Kovary and Bravo (1991), Kovary and Bravo (1992)).

The most prominent member of the AP-1 is c-Jun. Its function is often associated as tumor-promoting and initiating (Young *et al.* (1999), Eferl *et al.* (2003)). On the other hand, the other members of the JUN family, JunB and JunD proto-oncogene (JunD), are primarily regarded as tumor suppressors (Passegué *et al.* (2001), Pfarr *et al.* (1994)).

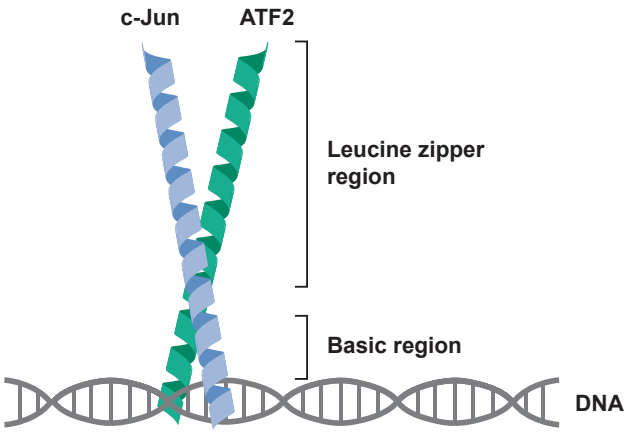

Figure 1.8: Structure of the AP-1 transcription factor. Depending on their abundance, AP-1 proteins form either homo- or heterodimers. As basic leucine zipper (bZIP) proteins, they interact with each other via the leucine zipper region. The interaction with the DNA is mediated by their basic region. Here, a c-Jun/ATF2 heterodimer is shown which binds to the DNA. Modified from Eferl and Wagner (2003).

Abbreviations: ATF2 (activating transcription factor 2), c-Jun (Jun proto-oncogene), DNA (deoxyribonucleic acid).

1.4.1 The AP-1 transcription factor family member JunB

The transcription factor JunB is a member of the JUN protein family and part of the transcription factor AP-1. In humans, JUNB is found on chromosome 19, while in mice it is found on chromosome 8 (National Center for Biotechnology Information (2019a), National Center for Biotechnology Information (2019b)). However, the gene and protein sequence in humans and mice is conserved and share 86% similarity (Kawakami *et al.* (1992)). Both gene loci are about 2 kb long and contain only one exon. The subsequent transcription and translation of JUNB leads to a 347 AA (human) and 344 AA (mouse) long protein with a molecular weight of 42 kDa. Compared to other AP-1 members, JunB is more likely to act as a heterodimer. This is caused by small AA change compared to e.g., c-Jun, which eventually decreases its homodimerization affinity (Deng and Karin (1993)).

Although JunB is classically regarded as a tumor suppressor, it has a much more diverse role in regulating cellular processes. His crucial role in angiogenesis was found early on. In pregnant mice, JunB knockout led to embryonic lethality at the age of E9.5 as a result of a defect in the extraembryonic tissue, especially in the placenta (Schorpp-Kistner *et al.* (1999)). Due to its high demand for vascularization and rapid growth, the placenta depends on the formation of new blood vessels. In this model, angiogenesis was induced by increased hypoxia. This resulted in an activation of nuclear factor kappa-light-chain-enhancer of activated B-cells (NF-κB), which led to the expression of

JunB (Schmidt *et al.* (2007)). JunB then bound to the promoter of VEGF and induced its transcription. After that, VEGF was secreted to induce the generation of blood vessels. Thus, JunB is a direct transcription factor of VEGF independent from hypoxia-inducible factors (HIF). Further studies confirmed this relationship. For instance, the stimulation of MCF-7 breast cancer cells led to an activation of JunB and subsequent expression of VEGF (Yin *et al.* (2009)). Furthermore, in hypoglycemic mouse embryonic fibroblasts (MEF), the expression of VEGF was also regulated by JunB (Textor *et al.* (2006)). However, in this model, the expression of JunB was induced by extracellular signal-regulated kinase (ERK) rather than by NF-κB.

Invasiveness and metastasis are also regulated by JunB. In a metastatic head and neck squamous cell carcinoma (HNSCC) model, the knockout of JunB reduced the frequency of metastases and extends survival *in vivo* (Hyakusoku *et al.* (2016)). In addition, IL-6/STAT3 expression of JunB led to an increased expression of EMT factors such as MMP-2, MMP-4, MMP-9, Snail and Twist (Gong *et al.* (2018)).

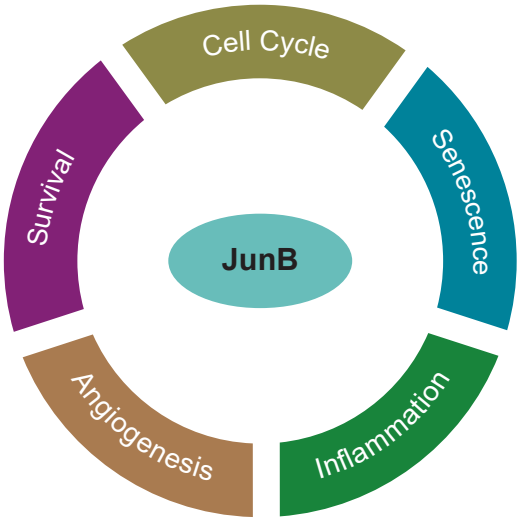

Figure 1.9: JunB is involved in various cellular events. The AP-1 protein member JunB mediates survival and promotes cell cycle progression. In contrast, it is also involved in senescence induction. Additionally, JunB triggers angiogenesis and promotes inflammation. Modified from Fan *et al.* (2017).

Abbreviations: JunB (JunB proto-oncogene).

The involvement of JunB in inflammation is even more prominent. In psoriatic lesions JunB expression has been found to be interrupted (Zenz *et al.* (2005)). A psoriatic phenotype was recreated in a mouse model with JunB/c-Jun double knockout in the epidermis. In detail, the loss of JunB led to an altered cytokine and chemokine secretion, which recruited macrophages and neutrophils into the epidermis. The invasion of innate immune cells resulted in the psoriatic phenotype. On the other hand, a single JunB

knockout in the epidermis led to the establishment of a systemic lupus erythematosus (SLE)-similar disease (Pflegerl *et al.* (2009)). Here, it was shown that JunB bound to the IL-6 promoter and inhibited its expression. This study showed that the binding of an AP-1 factor not only initiates transcription but also suppresses gene expression. Another study emphasizes the protective function of JunB in inflammation. In type I diabetes, infiltrating immune cells secrete various cytokines, for example TNF and IFNγ (Gurzov *et al.* (2012)). These cytokines activated NF-κB which led to the upregulation of JunB in pancreatic β-cells and subsequently initiated the expression of ATF3. The expression of ATF3 was essential to prevent apoptosis induction in the β-cells. Similar results were found in purified rat primary β-cells and an insulin-producing cell line (INS-1E) (Gurzov *et al.* (2008)). Here, JunB expression was activated by NF-κB after stimulation of IL-1β and IFNγ. In this model, the loss of JunB resulted in an increase in endoplasmic reticulum (ER) stress and inducible nitric oxide synthase (iNOS), which eventually triggered apoptosis induction. Based on the examples given, it becomes evident that JunB has an essential role in the survival of the cells as well. This role was also demonstrated in breast cancer cell lines (Hicks *et al.* (2014)). There, treatment with the CDK9 inhibitor Flavopiridol stimulated the upregulation of JunB, which protected the cells from apoptosis induction. Furthermore, the overexpression of JunB in human lymphoma cells protected against H_2O_2-induced apoptosis (Son *et al.* (2010)).

A loss of JunB expression in malignant cells can drive and accelerate the progression of the disease, as shown in a prostate cancer model (Thomsen *et al.* (2015)). Immunohistological analyses in low-grade prostate cancer lesions showed an intact JunB expression which further decreased in progressive disease. This negative correlation was also identified in prostate metastasis, in which JunB expression is mostly absent. In a model for human myeloid leukemia JunB was shown to be a transcription factor with tumor-suppressive properties in myelopoiesis (Passegué *et al.* (2001)). Here, a knockout of JunB, specifically in the myeloid cells, induced tumor formation. This tumor was transplantable and progressed to a blast crisis. In summary, this highlights the role of JunB as a tumor suppressor.

The impact of JunB is not only found in angiogenesis, inflammation, survival, and tumor formation. It has also been identified as a regulator of cell cycle and senescence. In murine fibroblast, the loss of JunB did not have an impact on their survival but slowed down their proliferation rate (Andrecht *et al.* (2002)). Analyses revealed a reduced expression dynamic of cyclin A in JunB knockout cells. As a result, these cells accumulated in the S phase. Further investigations confirmed cyclin A as a direct transcriptional target of JunB. Additionally, JunB was shown to inhibit the expression of cyclin D and MYC in response to mammalian target of rapamycin (mTOR) inhibitor treatment in MEF cells with activated AKT signaling (Vartanian *et al.* (2011)).

In addition to the cyclins mentioned above, JunB regulates the expression of the tumor suppressor $p16^{INK4a}$. A study by Passegué and Wagner (2000) has shown that the overexpression of JunB in a murine fibroblast cell line reduced their proliferation rate. The cells remained longer in the G_1 phase. Furthermore, primary MEF cells with JunB

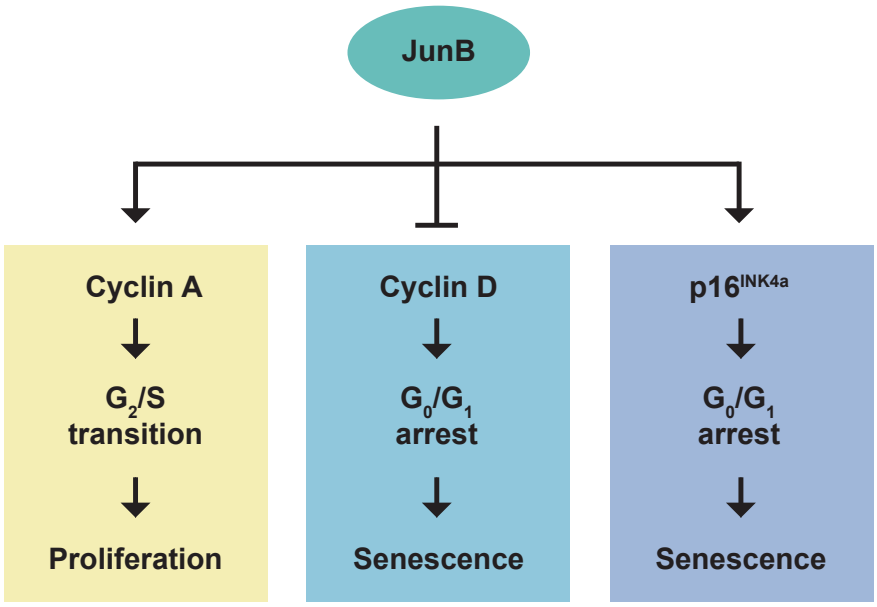

Figure 1.10: JunB has a dual role in cell cycle regulation. Progression of the cell cycle is promoted by the JunB-dependent induction of cyclin A (left). In contrast, cells can become senescent through JunB-mediated suppression of cyclin D (middle) as well as by JunB-induced expression of the tumor suppressor $p16^{INK4a}$ (right). Modified from Piechaczyk and Farràs (2008).

Abbreviations: JunB (JunB proto-oncogene), $p16^{INK4a}$ (cyclin-dependent kinase inhibitor 2A).

overexpression became more rapidly senescent. In both cases, the increased expression of $p16^{INK4a}$ was identified as the underlying mechanism. A reporter gene assay confirmed that $p16^{INK4a}$ is a direct transcriptional target of JunB. The collected information shows that the timing of JunB expression, the cell type, the stimuli, and also the presence of other AP-1 members affects its function as a proto-oncogenic or tumor suppressor protein.

1.5 Aim of this thesis

In the first part of this thesis, the genomic stability of RT2 cancer cell lines was investigated before and after treatment with T_h1 cytokines TNF and IFNγ. The underlying question was whether the genomic stability of RT2 cancer cell lines is affected by CIS induction. In this context, genomic material from two different time points (before and after 96 h of treatment with and without cytokines) was collected and analyzed by CGH. In addition, the genomic stability of a subcutaneously transplanted RT2 cancer cell line was examined after failing immune checkpoint therapy. The aim was to find out whether the genomic stability of cancer cells is affected by an inflammatory *in vivo* environment.

In the second part of the project, the signal transduction in CIS was aimed to be deciphered (Figure 1.11). Currently, it is not possible to induce CIS by the application of IFNγ and TNF in humans. Although IFNα is approved for the treatment of malignant melanoma, the systemic application of TNF is too toxic. By decoding the signaling pathways, proteins should be identified that could, for example, be exploited as therapeutic targets. In the analysis of the signal transduction pathway of CIS, the AP-1 transcription factor JunB appears to be a possible mediator between the initiation of senescence by IFNγ and TNF and the downstream activation of $p16^{INK4a}$.

In order to investigate the involvement of JunB in CIS, JunB mRNA and protein expression during the induction of CIS was investigated in murine RT2 cancer cells as well as in the human rhabdomyosarcoma cell line A204. Moreover, the IKK-1 and IKK-2 inhibitor IKK-16 was used to decipher whether TNF-dependent activation of JunB was mediated by NF-κB. In addition, small interfering RNA (siRNA)-mediated knockdown and CRISPR/Cas9-induced knockout of JunB was performed to analyze the behavior of the cells in CIS. According to the signaling pathway scheme in Figure 1.11, a JunB knockout should lead to an impaired expression of $p16^{INK4a}$ which in turn impaires senescence induction.

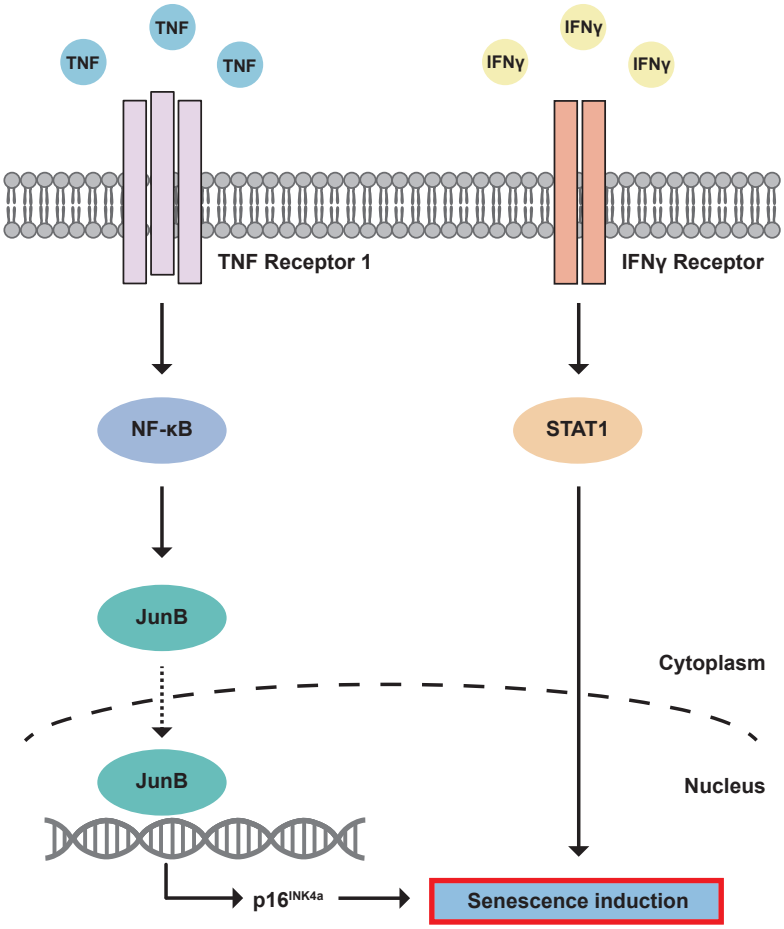

Figure 1.11: Visualization of the proposed signaling pathway model. To induce CIS in cancer cells, both T_h1 cytokines (IFNγ and TNF) must be present. While IFNγ signaling is mediated by STAT1, the signal transduction via the TNF pathway is yet unclear. In the presented model, the expression of the AP-1 transcription factor JunB is induced by the TNF-dependent activation of NF-κB. JunB in turn binds to the AP-1 binding sites of the $p16^{INK4a}$ promoter and thus initiates its transcription. Combined with the activation of the IFNγ signaling pathway, CIS is induced in cancer cells.

Abbreviations: IFNγ (interferon gamma), JunB (JunB proto-oncogene), NF-κB (nuclear factor kappa-light-chain-enhancer of activated B-cells), $p16^{INK4a}$ (cyclin-dependent kinase inhibitor 2A), STAT1 (signal transducer and activator of transcription 1), TNF (tumor necrosis factor).

Chapter 2

Material and Methods

2.1 Material

2.1.1 Equipment

Table 2.1: Equipment.

Equipment	Vendor
Axiovert 200	Zeiss
BigSquid magnetic stirrer	Yellowline
Biofuge pico	Heraeus
BioPhotometer	Eppendorf
Cryo 1 °C freezing container	Nalgene
DNA Microarray Scanner G2505C	Agilent
Electroblotting unit Gelco 102B for 4 gels	biostep GmbH
Electrophoresis system	Bio RAD
Fume hood mc6	Waldner
Gel documentation E.A.S.Y 442 K	Herolab
Hera cell 240	Thermo Scientific
Hera freeze	Kendro Laboratory Product
Hera safe culture hood	Thermo Scientific
HBO 100 Power-Supply	Zeiss
Hybridization Oven	Agilent
Leitz DMIL microscope	Leica
Licor scan	LI-COR Biosciences
Liebherr comfort refrigerator	Liebherr
LightCycler 480 II	Roche
Mastercycler gradient	Eppendorf
Microbiological incubator	Heraeus
Mini PROTEAN System Glass Plates	Bio RAD
Mini-PROTEAN Tetra System	Bio RAD
Multifuge 3 S-R	Heraeus

Continuation of Table 2.1

Equipment	Vendor
Multiskan EX	Thermo Scientific
Nanophotometer	Implen
Odyssey Sa Infrared Imaging System	LI-COR
Otigrid	Visitron Systems GmbH
PeqlabSTAR Thermocycler 96x Universal Gradient	Peqlab
Power Pac 300	Bio RAD
Retsch MM300 TissueLyser	Retsch
Sky Line Shaker DRS-12	Elmi
Table centrifuge	Neolab
Thermomixer comfort	Eppendorf
Waterbath	GFL

2.1.2 Consumables

Table 2.2: Consumables.

Consumable	Vendor
Amersham Hybond P 0.45 PVDF Blotting Membrane	GE Healthcare Life Science
Cell Culture flask 175 cm^2	Sarstedt
Cell Culture flask 25 cm^2	Sarstedt
Cell Culture flask 75 cm^2	Sarstedt
Cell culture plate 10 cm	Falcon
Cell culture plate 6-well	Falcon
Cell culture plate 96-well	Sarstedt
Cell culture slides	Falcon
Cell scraper	Falcon
CGH Microarray (2x105k), Amadid 014699 mouse	Agilent
Chambered Cell Culture Slides, 8-well	Falcon
Combitip advanced 0.5 mL	Eppendorf
Combitip advanced 2.5 mL	Eppendorf
Combitip advanced 5 mL	Eppendorf
Cryo.s vials	Greiner Bio-One
Gasket Slide Kit	Agilent
Immobilon-FL Transfer Membranes	Merck
Inject 10 ml, Luer, eccentric	Braun
Microlance Hypodermic Needle 24G x 1”	BD

Continuation of Table 2.2

Consumable	Vendor
Microlance Hypodermic Needle 30G x 1/2”	BD
Millex-GP Syringe Filter Unit, 0.22 µm	Merck Millipore
Neubauer improve counting chamber	Hecht-Assistent
PCR Tubes	Biozym
Pipetboy	Integra
Pipette 0.5 - 10 µL	Eppendorf
Pipette 10 - 100 µL	Eppendorf
Pipette 100 - 1000 µL	Eppendorf
Pipette filter tips 0.5 - 20 µL, Biospehere plus	Sarstedt
Pipette filter tips 100 - 1250 µL, Biospehere plus	Sarstedt
Pipette filter tips 2 - 100 µL, Biospehere plus	Sarstedt
Pipette multichannel 50 - 300 µL	Eppendorf
Pipette multistepper	Eppendorf
Pipette tips 0.5 - 20 µL	Starlab
Pipette tips 100 - 1000 µL	Starlab
Pipette tips 2 - 100 µL	Starlab
Reaction tube 0.5 mL	Eppendorf
Reaction tube 1.5 mL	Eppendorf
Reaction tube 15 mL	Falcon
Reaction tube 2.0 mL	Eppendorf
Reaction tube 50 mL	Falcon
Serological pipette 10 mL	Corning Life Sciences
Serological pipette 25 mL	Corning Life Sciences
Serological pipette 5 mL	Corning Life Sciences
Slide Holder	Agilent
UV transparent disposable cuvettes	Sarstedt
Whatman	GE Healthcare Life Science

2.1.3 Chemicals and reagents

Table 2.3: Chemicals and Reagents.

Chemical	Vendor
2-log-DNA-Ladder	NEB
10x Fast Digest Buffer	Thermo Scientific
Acetonitrile	Merck
Agar	Sigma-Aldrich
Agarose	Roth

Continuation of Table 2.3

Chemical	Vendor
Albumin Fraktion V	Roth
Ammonium persulfate	Sigma-Aldrich
Ampuwa	Fresenius Kabi
Bromophenol Blue	Sigma-Aldrich
Collagenase NB8	Serva
Complete Tablets, Mini, EDTA-free, EASYpack	Roche
Cot-1 DNA ($1\,\mu g\,mL^{-1}$)	Agilent
Crystal violet	Roth
Dako Protein Block	Dako
DharmaFECT Transfections Reagent	Dharmacon
DirectPCR Lyse Reagent	7BioScience
DMEM	Merck Millipore
DMSO	Roth
dNTP-Mix $10\,mmol\,L^{-1}$ each	Genaxxon
Effectene Transfection Reagent	Qiagen
Ethanol	VWR
EDTA	Roth
FastDigest buffer, 10x	Thermo Scientific
Fetal bovine serum	Sigma-Aldrich
G418 (geneticin)	Invivogen
GelRed GelStain	Biotium
Glycerol	Sigma-Aldrich
Glycin	Roth
Hanks Solution	Merck Millipore
HEPES, 50x	Merck Millipore
Isopropyl alcohol	VWR
KAPA SYBR FAST LC480	Sigma-Aldrich
MEM Non-essential amino acid solution	Merck Millipore
Methanol	VWR
Non-fat dry milk	Roth
Nonident P40 Substitute	Fluka BioChemie
Odyssey Blocking Buffer (PBS)	LI-COR
Oligo aCGH/ChIP-on-Chip Wash Buffer 1	Agilent
Oligo aCGH/ChIP-on-Chip Wash Buffer 2	Agilent
Orange G	Roth
PageRuler Plus Prestained Protein Ladder	Thermo Scientific
PBS	Sigma-Aldrich
Penicillin/Streptavidin	Merck Millipore
PhosSTOP EASYpack	Roche
Plasmid Transfections medium	Santa Cruz

Continuation of Table 2.3

Chemical	Vendor
Proteinase K Powder	GENAXXON
Puromycin dihydrochloride	Santa Cruz
Rotiphorese Gel 30 (37,5:1) (Polyacrylamide)	Roth
RPMI	Merck Millipore
Sodium dodecyl sulfate (SDS)	Roth
SOC Medium	New England Biolabs
Sodium chloride	Sigma-Aldrich
Sodium deoxycholate	Sigma-Aldrich
Sodium Pyruvat, 100 mM	Merck Millipore
Stabilization and Drying Solution	Agilent
Taq DNA-Polymerase	Genaxxon
TEMED	Roth
Tris ultrapure	AppliChem
Trypan Blue Solution, 0.4%	Thermo Scientific
Trypsin-EDTA	Invitrogen
Tryptone	Sigma-Aldrich
Tween 20	Roth
UltraCruz Plasmid Transfections Reagent	Santa Cruz
Yeast Extract	Sigma-Aldrich

2.1.4 Buffers and solutions

Table 2.4: Buffers and Solutions. Buffers and solutions are diluted in dd-H_2O (double-distilled water) if not indicated otherwise.

Buffer	Ingredient
Crystal violet staining	12 mM crystal violet 20% (v/v) MeOH
Collagenase solution	3.5 mL Mouse Prep A 6 mg Collagenase 10 mM $CaCl_2$
DNA loading buffer	2 mL Orange G (10 mg dissolved in 1x TAE-Buffer 1:2 with glycerol) 1 µL Gel Red
Laemmli buffer	4% (w/v) SDS 10% (v/v) 2-mercaptoethanol 20% (v/v) glycerol 0.004% (w/v) bromophenol blue

Continuation of Table 2.4

Buffer	Ingredient
	0.125 M Tris-HCl adjust to 6.8 pH
Mouse Prep A	500 mL Hanks solution 3 mM glucose
Mouse Prep B	250 mL Mouse Prep A 0.871 g BSA
RIPA buffer	50 mM Tris-HCl 8.0 pH 150 mM NaCl 1% (v/v) NP-40 0.5% (w/v) sodium deoxycholate 0.1% (w/v) SDS
10x Running Buffer	248 mM Tris 1.9 M Glycin 1% (w/v) SDS For 1x Running Buffer: Dilute 1:10 in dd-H_2O
Semi-Dry Buffer	48 mM Tris 29 mM Glycin 0.038% (w/v) SDS 20% (v/v) MeOH adjust to 8.5 pH
50x TAE Buffer	0.4 M Tris-HCl 1.142% (v/v) acetic acid 10 mM EDTA (8.0 pH) filtrate For 1x TAE: Dilute 1:50 in dd-H_2O
10x TBS Buffer	0.2 M Tris 1.37 M NaCl adjust to 7.6 pH For 1x TBST: Dilute 1:10 in dd-H_2O, add 0.5% (v/v) Tween20
Tris, lower	0.5 M Tris 0.4% (w/v) SDS adjust to 6.8 pH
Tris, upper	1.5 M Tris

Continuation of Table 2.4

Buffer	Ingredient
	0.4% (w/v) SDS adjust to 8.8 pH

2.1.5 Kits

Table 2.5: Kits.

Kit	Vendor
AllPrep DNA/RNA Mini Kit	Qiagen
β-Galactosidase Staining Kit	Biomol
DNeasy Blood and Tissue Kit	Qiagen
GeneJet Endo-Free Plasmid Maxiprep Kit	Thermo Scientific
iScript cDNA Synthesis Kit	BioRad
NE-PER Nuclear and Cytoplasmic Extraction Reagent	Thermo Scientific
NucleoSpin RNA Plus	Macherey Nagel
Oligo aCGH/ChIP-on-Chip Hybridization Kit	Agilent
Pierce BCA Protein Assay Kit	Thermo Scientific
Pierce LDH Cytotoxicity Assay Kit	Thermo Scientific
Suretag Complete DNA Labeling Kit	Agilent

2.1.6 Laboratory mice

Mice used in this thesis were kept under specific-pathogen-free conditions according to the ”Tierschutz-Versuchstierverordnung - TierSchVersV”. Animal experiments were approved in the animal experiment application HT5/15 by the Regierungspräsidium Tübingen. The following mouse lines were used:

C3HeB/FeJ: C3H wild type mouse purchased from the Jackson Laboratory. The breeding of these mice is homozygotic.

C3HeB/FeJ-Tg(RIP1-TAg)2/DH (RIP1-Tag2 (RT2)): The mouse strain was established 1985 by the microinjection of the fusion gene RIP1-TAG into fertilized mouse embryos (Hanahan (1985)). The fusion gene is compromised of the SV40 large T-cell antigen (TAG2) oncogene, which is expressed under a rat insulin promoter (RIP). In consequence, TAG2 is expressed in β-cells of the pancreas. As early as embryonic stage E9, TAG2 expression can be detected (Alpert *et al.* (1988)). At the age of 4-6 weeks, although all β-cancer cells express oncogenic TAG2, 50-75% of islets cells become hyperplastic (Teitelman *et al.* (1988)). At the age of 8-10 weeks, angiogenic switch leads to the growth of new blood capillary in 10% of the islets (Folkman *et al.* (1989)). After 11-12 weeks, 1-2% of all islets have developed into solid encapsulated tumors. The growth of β-cancer cells leads to an increase of the serum insulin level (2 to 10 fold),

although it is not correlating with the number of insulin-producing cells (>100 fold increase) (Hanahan (1985)). Nevertheless, RT2 mice become hypoglycemic and die within 12-14 weeks of age. Tumors arising from RT2 β-cancer cells show an inhibition of pRb and p53 by TAG2 oncoprotein. Although every β cell harbors this mutation, it is insufficient to transform β-cells into pancreatic tumors. Other factors like the different regulation of apoptosis, is needed to convert β-cells into β-cancer cells (Naik *et al.* (1996)). The breeding of these mice is heterozygotic. In this thesis, this mouse is referred to as RIP1-Tag2 (RT2).

C3HeB/FeJ-Tg(Stat1.ko-(RIP1-TAg)2)/DH: This double-transgenic mouse was provided by Taconic and originated from a 129S6/SvEv-Stat1tm1Rds mice34 backcrossed to C3HeB/FeJ mice (Braumüller *et al.* (2013)). These mice develop β-cancer cells tumors just as the C3HeB/FeJ-Tg(RIP1-TAg)2/DH strain but has an additional knockout of the signal transducer and activator of transcription 1 (STAT1) receptor. Mice of this genotype do not display a phenotype different from the C3HeB/FeJ-Tg(RIP1-TAg)2/DH strain except for their incapability to transduce signals from the signal transducer and activator of transcription 1 (STAT1) receptor. The breeding of these mice is heterozygotic. In this document, this mouse is referred to as RIP1-Tag2 x signal transducer and activator of transcription $1^{-/-}$.

2.1.7 Cell lines

For most of the experiments performed in this thesis the human tumor cell line A204 (purchased from Cell line service) is used. The A204 cancer cell line is a rhabdomyosarcoma cell line from a one-year-old female child and was first established in 1973 (Giard *et al.* (1973)). A204 tumor cells are adherent and grow as a monolayer. This cell line is cultivated in RPMI medium (see Table 2.12 and Section 2.2.1). Primary β-cancer cells tumors were isolated according to Section 2.2.2 and cultivated in DMEM medium (see Table 2.12 and Section 2.2.1). The murine colon cancer (CT26) cell line was kindly provided by Ralph Mocikat (Munich) and is cultivated in DMEM medium (see Table 2.12 and Section 2.2.1). The murine cell line lewis lung carcinoma (LLC) is also cultivated in DMEM medium (see Table 2.12 and Section 2.2.1). Unfortunately, the origin of the LLC cell line was no longer retraceable.

2.1.8 Mycoplasma testing

Cells used in this thesis were all mycoplasma free as determined by regularly testing for mycoplasma contamination.

2.1.9 Plasmids and siRNA sequences

Table 2.6: Sequences of siRNA.

Name	Order Nr.	Vendor	Sequence 5'-3'
ON-TARGETplus Non-targeting Pool	D-001810-10-05	Dharmacon	UGGUUUACAUGUCGACUAA UGGUUUACAUGUUGUGUGA UGGUUUACAUGUUUUCUGA UGGUUUACAUGUUUUCCUA
Accell Human JUNB (3726) siRNA - SMARTpool	E-003269-00-0005	Dharmacon	UUAUUGAAUCUAUUUAAGU CCUUCCACCUCGACGUUUA GCCUCUCUCUACACGACUA GAGUUUAUUUUAAGACGUG

Table 2.7: Sequences of CRISPR/Cas9 plasmids.

Name	Order Nr.	Vendor	Sequence 5'-3'
JunB CRISPR/Cas9 KO Plasmid (h2)	sc-400493-Ko-2	Santa Cruz	Sequences available on request
Control CRISPR/Cas9 Plasmid	sc-418922	Santa Cruz	Sequences available on request

2.1.10 Oligonucleotides

Table 2.8: Oligonucleotides. Human and murine primers for PCR or qPCR are listed below. All primers were purchased from Eurofins Genomics.

Name	Method	Species	Sequence 5'-3'
ACTIN sense	qPCR	human	AGCCTCGCCTTTGCCGA
ACTIN antisense	qPCR	human	CTGGTGCCTGGGGCG
GAPDH sense	PCR	human	GACAACAGCCTCAAGATCATC
GAPDH antisense	PCR	human	CACCCTGTTGCTGTAGCCA
GAPDH sense	qPCR	human	CAGCCTCAAGATCATCAGCAATG
GAPDH antisense	qPCR	human	ATACCAAAGTTGTCATGGATGACCTT
HPRT sense	qPCR	human	TGATAGATCCATTCCTATGACTGTAGA

Continuation of Table 2.8

Name	Method	Species	Sequence 5'-3'
HPRT antisense	qPCR	human	AAGACATTCTTTCCAGTTAAAGTTGAG
JUNB sense	PCR, qPCR	human	ATACACAGCTACGGGATACGG
JUNB antisense	PCR, qPCR	human	GCTCGGTTTCAGGAGTTTGT
RT2 sense	PCR	murine	GGACAAACCACAACTAGAATGCAGTG
RT2 antisense	PCR	murine	CAGAGCAGAATTGTGGAGTGGG
TBP sense	qPCR	human	CACGAACCACGGCACTGATT
TBP antisense	qPCR	human	TTTTCTTGCTGCCAGTCTGGAC

2.1.11 Antibodies

Table 2.9: Antibodies for Western Blot analysis.

Compound	Species	Dilution	Order Nr.	Vendor
α-Tubulin	mouse	1:2000	NB100-690	Novus Biologicals
β-Actin (C4)	mouse	1:5000	MAB1501R	Millipore
β-Actin (13E5)	rabbit	1:1000	4970S	Cell Signaling
IκBα (L35A5)	mouse	1:1000	4814S	Cell Signaling
pIκBα (Ser32)(14D4)	mouse	1:1000	2859S	Cell Signaling
IRDye 680RD	goat	1:15000	926-68071	LI-COR
IRDye 680RD	goat	1:15000	926-68070	LI-COR
IRDye 800CW	goat	1:15000	926-32210	LI-COR
IRDye 800CW	goat	1:15000	926-32211	LI-COR
JunB (C-11)	mouse	1:1000	sc-74	Santa Cruz
JunB (C37F9)	rabbit	1:1000	3753	Cell Signaling
Lamin A and C	mouse	1:1000	MAB 3538	Millipore

2.1.12 Compounds

Table 2.10: Compounds

Compound	Order Nr.	Vendor
IKK-16 (IKK Inhibitor VII)	S2882	Selleckchem
Recombinant human IFNγ [100 µg]	285-IF-100	R&D Systems
Recombinant human TNF [20 µg]	210-TA-020	R&D Systems
Recombinant mouse IFNγ [100 µg]	485-MI/CF	R&D Systems
Recombinant mouse TNF [50 µg]	410-MT-050	R&D Systems

2.1.13 Software and websites

Table 2.11: Software and Websites.

Software/Websites	Vendor
Adobe Photoshop CS2	Adobe
Adobe Illustrator CS6	Adobe
Agilent Scan Control	Agilent
Agilent Extraxtion 10.5.1.1	Agilent
Agilent Genomic Workbench Lite Edition 6.5.0.18	Agilent
Agilent Analytics 4.0.85	Agilent
Ascent Software Version 2.6	Thermo Labsystem Oy
Axiovision 40x64 V 4.9.1.0	Zeiss
FlowJo V10	FlowJo LLC
GNU Image Manipulation Program 2.10.8	The GIMP Team
GrapPad Prism 8	GraphPad
ImageJ 1.47v	Wayne Rasband, NIH, USA
Imagestudio lite 3.1.4	LI-COR Biosciences
Lightcycler 480 SW 1.5.1	Roche
Mendeley	Elsevier
Microsoft Office 10	Microsoft
Odyssey Sa Infrared imagine system	LI-COR Biosciences
Odysses Sa Application software 1.1.7	LI-COR Biosciences
qBase+	Biogazelle
SnapGene Viewer	GSL Biotech LLC
VisiView	Visitron Systems GmbH
http://www.premierbiosoft.com/netprimer/	Primer design
https://www.eurofinsgenomics.eu/de/	Primer order
https://www.overleaf.com	LaTex

2.2 Methods

2.2.1 Cell culture

In order to cultivate human or murine cancer cells, the cell culture medium is mixed according to Table 2.12. Dulbecco's modified eagle's medium (DMEM) is used for human cells, while Roswell park memorial institute medium (RPMI) is used for murine cells. Cells are placed in a 37 °C cell culture incubator with 100% humidity and 5% CO_2 for human, and 7.5% CO_2 for murine cancer cells.

To passage cells, cell culture medium is aspirated and discarded. Next, cells are

washed once with phosphate-buffered saline (PBS) and incubated with 37 °C prewarmed trypsin for 5 to 10 min at 37 °C. As soon as cells are detached, prewarmed cell culture medium is added to the cells to stop the enzymatic activity of trypsin. After centrifuging cells at 545 x g for 5 min at room temperature (RT), cells are resuspended in fresh medium.

To determine the cell count, a defined volume of cells is mixed with trypan blue (1:2 diluted in PBS) and transferred in a Neubauer counting chamber. After counting cells in all four quadrants, cell number can be determined with the Equation (2.1).

In order to cryoconserve cells, cell pellets are resuspended in FCS mixed with 10% DMSO, placed in a cryo freezing container and stored in a freezer at −80 °C. After 24 h, cells are entirely frozen and can be stored at −80 °C for up to one year. For long term storage, cells are transferred in a liquid N_2 tanks.

In order to thaw frozen cells, the cryotube is incubated in a water bath at 37 °C until the pellet is almost completely thawed. Cells are transferred in a 15 mL tube, then 10 mL of the prewarmed cell culture medium is slowly added to the cells. The suspension is centrifuged at 545 x g for 5 min at RT. After discarding the supernatant, cells are resuspended and seeded in a cell culture flask. Cells are placed in a cell culture incubator for 24 h, after which the medium is replaced.

$$\text{Cell count per ml} = \frac{\text{counted cell number}}{\text{no. of quadrants}} \times 10^4 (\text{Neubauer factor}) \times \text{ dilution factor} \tag{2.1}$$

Table 2.12: Cell Culture medium recipes

Reagents for DMEM and RPMI cell culture medium
500 mL DMEM or 500 mL RPMI
10% (v/v) fetal bovine serum (FCS)
1% (v/v) HEPES
1% (v/v) MEM Non-essential amino acid solution
1% (v/v) sodium pyruvate
0.2% (v/v) β-mercaptoethanol (only for murine cell culture)

2.2.2 Tumor preparation and β-cancer cell isolation

Experiments with murine tumor cells were performed with isolated β-cancer cell from 12 week old RT2 mice (see Section 2.1.6).

After sacrificing the mouse with CO_2 inhalation and following cervical dislocation, the mouse is immersed in 80% EtOH. Next, the mouse is dissected, and the ductus hepaticus is tightened with a thread. Subsequently, the duodenum is clamped before and

after the duodenal papilla, which is carefully cut open in the following step. In total, 3 mL of collagenase solution are injected (Table 2.4). The pancreas is dissected, placed in a 50 mL tube and put into a waterbath for 10 min at 37 °C. Next, the collagenase is inactivated by adding 10 mL of mouse prep B buffer (Table 2.4). After centrifuging at 19 x *g* for 3 min the supernatant is discarded. The pellet is washed once again with 10 mL of mouse prep B buffer, briefly vortexed and centrifuged. Afterward, the supernatant is discarded, and the tumors are resuspended in 10 mL of mouse prep B buffer and put inside a 6 cm Petri dish. The tumors are collected under a binocular, transferred into a 1.5 mL tube, and covered with mouse prep B buffer.

Tumors which are going to be analyzed by array comparative genomic hybridization (CGH) (Section 2.2.18) are separately snap-frozed in liquid N_2 without any remaining liquid.

For β-cancer cell line preparation, the tube containing the collected tumors is centrifuged, and the supernatant is removed. Under a sterile workbench, 500 µL of 37 °C prewarmed trypsin are added. With a small scissor, tumors are cut open for 5 min. Afterward, tumors are incubated in a water bath for 5 min at 37 °C. Next, trypsin is inactivated by adding 500 µL of DMEM and the tube is centrifuged for 5 min at 500 x *g*. The supernatant is removed, and the pellet is resuspended in DMEM in an appropriate volume for counting cells. Adherent β-cancer cells are cultivated in plastic culture dishes with DMEM and penicillin/streptavidin (P/S) and placed inside an incubator with 37 °C and 5% CO_2.

2.2.3 DNA isolation

Different methods are used to extract deoxyribonucleic acid (DNA) from samples depending on the following assay.

In order to isolate DNA for the CGH analysis in Section 2.2.18, the AllPrep DNA/RNA Mini Kit from Qiagen is used according to the manufacturer's instructions. First, frozen tumor tissue needs to be disrupted and homogenized. For this, 350 µL of RLT Plus Buffer are added to 20 µg tissue and homogenized in a tissue lyzer. Samples need to be cooled on ice at all times. Both homogenized tissue and culture cells are placed in a QIAshredder and centrifuged for 2 min at 13000 x *g*. Next, the lysate is transferred into an AllPrep DNA spin column and centrifuged for 30 sec at 8000 x *g*. The flow-through contains ribonucleic acid (RNA) whereas DNA is bound to the spin column. The DNA is washed with 500 µL AW1 Buffer and centrifuged for 15 sec at 8000 x *g*. In the next step, 500 µL of 80% EtOH are used to wash. After centrifuging for 2 min at 13000 x *g*, the DNA can be eluted by adding 50 µL of nuclease-free H_2O and centrifugation for 1 min at 8000 x *g*. The eluted DNA is measured in a photometer, and subsequently stored at -20 °C. An A_{260}/A_{280} extinction ratio of 1.7 - 2.0 and an A_{260}/A_{230} extinction ratio >1.7 indicate high quality DNA.

For the isolation of control DNA from the spleen of a male C3HeB/FeJ mouse, the DNeasy Blood & Tissue Kit from Qiagen is used. Up to 25 mg of spleen tissue is cut

into a 1.5 mL tube and 180 µL of ATL Buffer and 20 µL of proteinase K are added. The tube is incubated at 56 °C at 300 revolutions per minute (rpm) in a thermomixer until the sample is completely lyzed. After shortly vortexing, 200 µL of AL Buffer are added, and the lysate is vortexed. Next, 200 µL of 100% EtOH are mixed with the sample and vortexted once more. The lysat is transferred onto a DNeasy Mini spin column and centrifuged for 1 min at 5100 x *g*. The DNA is bound to the membrane which is washed with 500 µL of AW1 Buffer and centrifuged for 1 min at 5100 x *g*. Next, the membrane is washed with 500 µL of 80% EtOH and centrifuged for 3 min at 13000 x *g*. The DNA is eluted by adding 200 µL nuclease-free H_2O, incubated for 1 min, and centrifuged for 1 min at 5100 x *g*.

For mouse genotyping, ear punches are used. First, 100 µL of DirectPCR Lysis Reagent from Viagen, mixed 1:20 with proteinase K, are added to the sample and incubated over night (o/n) at 55 °C. After that, proteinase K is inactivated by incubating samples at 85 °C for 45 min. Samples are cooled down on ice and ready to use for polymerase chain reaction (PCR) (compare Section 2.2.4).

2.2.4 PCR

PCR is a method used to amplify single-stranded DNA with target specific primers. Besides DNA as a template and specific primers, taq-polymerase, which can withstand high temperature and amplifies DNA, is needed (compare Table 2.13). Initially, DNA is denaturated at 95 °C in order to produce single-stranded DNA (see Table 2.14). In the first step of the amplification phase, primers anneal on the single-stranded DNA. Subsequently, the Taq polymerase can bind to the primers and amplify DNA at 72 °C. The amplified DNA is denaturated afterward. The amplification step is repeated 30 times. Then, incomplete ends are filled in the extension phase, which runs for 3 min at 72 °C. Finally, DNA is stored at 4 °C.

Table 2.13: PCR master mix recipe. The annotations refer to one sample.

Chemicals
14.4 µL nuclease-free H_2O
2 µL 10x PCR Buffer with $MgCl_2$
1 µL sense primer
1 µL anti-sense primer
0.4 µL NTP (25 nM each)
0.2 µL Taq DNA polymerase
1 µL DNA sample

Table 2.14: PCR standard program is displayed below. The annealing temperature depends on the primers used.

step		temperature [°C]	time	cycle
1	denaturation	95	3 min	1
2	amplification	95	30 sec	30
3		56 - 60	30 sec	
4		72	30 sec	
5	extension	72	3 min	1
6	store	4	∞	

2.2.5 Agarose gel electrophoresis

Agarose gel electrophoresis is used to separate DNA, RNA, or proteins along an electric gradient based on their electric charges. The agarose gel is composed of 1.5% weight per volume (w/v) agarose in 300 mL 1x TAE-Buffer (see Table 2.4) and heated in a microwave until the agarose is liquefied. After cooling down shortly, the gel is poured into a tray holding a comb in order to load samples into the gel. Samples are mixed with DNA-loading buffer (Table 2.4) containing orange G to observe the running front and GelRed to visualize the probe under UV-light. After loading samples into the gel, samples run along an electric field at 120 V towards the anode due to their negatively charged residues. Finally, the probes are visualized under UV-light.

2.2.6 RNA isolation

To isolate RNA, the NucleoSpin RNA Plus Kit from Macherey-Nagel is used according to the manufacturer's instructions. First, cells are trypsinized and washed once with PBS. After removing the supernatant, samples are snap-frozen in liquid (N_2). To start the RNA extraction cell pellets are lyzed in 350 µL LBP. The lysat is transferred onto the NucleoSpin gDNA Removal Column and centrifuged at 13000 x *g* for 30 sec. The flow-through is mixed with 100 µL of BS and transferred onto the NucleoSpin RNA Plus Column. After centrifuging at 13000 x *g* for 15 sec, the flow-through is discarded. The column is washed with 200 µL of Buffer WB1 and centrifuged at 13000 x *g* for 15 sec. Subsequently, the column is washed twice with Buffer WB2, first with 600 µL and centrifuged at 13000 x *g* for 15 sec, next with 250 µL and centrifuged at 13000 x *g* for 2 min to dry the membrane completely. Lastly, the RNA is eluted with 40 µL of RNase-free H_2O. RNA concentration and purity is measured in a photometer. An A_{260}/A_{280} extinction ratio of 1.8 - 2.2 and an A_{260}/A_{230} extinction ratio >1.7 indicate high quality RNA.

2.2.7 cDNA synthesis

In order to measure the expression of specific genes, transcripted messenger RNA (mRNA) from Section 2.2.6 must be translated into complementary DNA (cDNA). In the beginning, 1 µg of RNA are mixed according to Table 2.15 with reverse transcriptase and iScript reaction mix. Next, reverse transcription is performed in a thermocycler with the program shown in Table 2.16. To control the successful transcription 1 µL of cDNA is used in a GAPDH test PCR (see Section 2.2.4).

Table 2.15: cDNA synthesis master mix. For each reaction 1 µg RNA is used.

Reagents per sample
4 µL 5x iScript Reaction Mix
1 µL iScript Reverse Transcriptase
1 µg RNA
add 20 µL nuclease-free H_2O

Table 2.16: RNA synthesis thermocycler program.

	step	temperature [°C]	time [min]
1	priming	25	5
2	reverse transcription	46	20
3	reverse transcription inactivation	95	1
4	store	4	∞

2.2.8 qPCR

Quantitative polymerase chain reaction (qPCR) is a method to measure the amount of mRNA by performing a fluorescence based PCR with synthesized cDNA from Section 2.2.7. In order to measure the amount of specific cDNA, a dye emitting fluorescent light when intercalating into DNA (SYBR green) is used. After each amplification step, the fluorescence intensity, which directly correlates with the amount of amplified cDNA, is measured. The cycle at which the amplified cDNA crosses the threshold line is named threshold cycle (C_t) and used for relative measurement of the amount of cDNA. The C_t value of a gene of interest (GOI) is correlated with the C_t value of at least two housekeeping genes.

In the preamplification step, a cDNA pool composed of cDNA from all samples is diluted 1:5. From this pool, 1 µL is mixed in a 96-well plate with 9 µL of a master

mix containing KAPA SYBR FAST qPCR mix with specific primers for the GOI and housekeeping genes (Table 2.8 and Table 2.17). After the preamplification, the amplified cDNA is used to dilute a standard curve ranging from 10^{-4} to 10^{-10} in order to determine the primer efficiency. Next, each sample is tested in duplicate with the specific primers. The qPCR is performed with the settings displayed in Table 2.18. Resulting data are analyzed either with the LightCycler 480 SW 1.5.1 software or with qBase^{+}.

Table 2.17: Recipe for qPCR master mix.

Reagents per sample
5 µL KAPA SYBR FAST
1 µL sense primer
1 µL anti-sense primer
2 µL nuclease-free H_2O
1 µL cDNA

Table 2.18: qPCR lightcycler program.

	step	temperature [°C]	time	cycle
1	denaturation	95	5 min	1
2	amplification	95	10 sec	45
3		60	10 sec	
4		72	10 sec	
5	melting curve	95	10 sec	1
6		65	1 min	1
7		95	0.06 °C/ sec at 65 °C	1
8	cooling	40	10 sec	1

2.2.9 Protein extraction

In order to analyze the protein expression under specific treatment conditions, cell culture supernatant is removed, and cells are washed once with ice-cold PBS. Cells are detached from the culture plate with a cell scraper and harvested on ice in 100 - 300 mL cold denaturating radio immuno precipitation assay buffer (RIPA) containing sodium dodecyl sulfate (SDS) and NP-40 to break cellular membrans (Table 2.4). To inhibit protease activity RIPA buffer is supplemented with 10% (w/v) phospho stop (PS) and 10% (w/v) protease inhibitor (PI). Lysates are stored at −80 °C.

2.2.10 Nuclear and cytoplasmic extraction

To analyze the location or translocation of a protein, respectively, the cytoplasm and nuclear fraction need to be separated. For this, the NE-PER nuclear and cytoplasmic extraction Kit from Thermo Scientific is used. According to the manufacturer's protocol, cells are trypsinized, washed once with PBS, and centrifuged. The supernatant is removed, and the cell pellet is resuspended in ice-cold CERI solution. After vortexing and incubating for 10 min, ice-cold CerII is added, vortexed, and incubated for 1 min on ice. Next, the suspension is centrifuged, and the supernatant consisting of the cytoplasmic extract is transferred into a pre-chilled tube and stored on ice. The pellet containing the nuclei is resuspended in ice-cold NER buffer. The suspension is vortexed every 10 min for a total of 40 min. After centrifuging, the nuclear extract is in the supernatant and transferred into a pre-chilled tube. Samples are stored on ice for a subsequent determination of the protein concentration or at $-80\,^{\circ}\mathrm{C}$ until used.

2.2.11 Protein concentration determination

In order to measure the protein concentration, the Pierce BCA Protein Assay Kit from Thermo Scientific is used. Here, proteins with more than three AA reduce Cu^{2+} to Cu^{1+} in an alkaline medium. One molecule of Cu^{1+} forms a chelate with two bicinchoninic acid (BCA), resulting in a color switch from light-blue to intense violet. A protein standard dilution from 1500 ng/µL to 50 ng/µL is prepared using RIPA and bovine serum albumin (BSA). According to the manufacture's protocol, 10 µL of protein standard dilution, RIPA buffer as blank and samples are pipetted as duplicates into a 96-well plate. Then, 200 µL BCA solution (50x BCA Reagent A + 1x BCA Reagent B) are added to each sample and incubated at 37 °C for 30 min. The extinction switch is measured in a photometer at 540 nm.

2.2.12 SDS-PAGE and Western Blot

The sodium dodecyl sulfate – polyacrylamide gel electrophoresis (SDS-PAGE) is a method to separate proteins based on their mass. SDS binds to the protein and negatively charges it in proportion to its length. Along an electric field, small proteins travel faster through a polyacrylamide gel towards the anode than larger ones.

The polyacrylamide gel is composed of a separating gel (Table 2.19) and a stacking gel (Table 2.19). First, the separating gel is poured between two glass chambers and covered with isopropanol. After its polymerization isopropanol is removed and the stacking gel is added over the separating gel. A separating comb is placed on top of the stacking gel to create pockets in which the protein samples can be loaded. The glass chamber containing the polyacrylamide gel is fixed in a cassette, which in turn, is placed inside a tank chamber. The chamber is filled with 1x running buffer (Table 2.4). A total of 20 µg protein per samples is mixed in a 1:2 ratio with Laemmli-Buffer (Table 2.4). After

heating the samples to 95 °C for 5 min, probes are cooled on ice, centrifuged, and are ready to be loaded into the pockets of the stacking gel. Along an electric field, negatively charged proteins travel through the stacking and the following separating gel towards the anode.

In the subsequent blotting step, proteins are transferred from the polyacrylamide gel to a polyvinylidene fluoride (PVDF) membrane. First, the PVDF membrane is activated by immersing it in methanol and stored in semi-dry buffer (Table 2.4). The polyacrylamide gel is placed on the activated PVDF membrane, inserted between two whatman-paper and two sponges, which are soaked up in semi-dry buffer and transferred into a tank blot chamber covered with semi-dry buffer. After 120 min at 100 V and 300 mA, proteins are transferred onto the PVDF membrane.

In order to prevent unspecific antibody binding, the membrane is blocked with odyssey blocking buffer or 5% w/v non-fat dry milk in 1x TBST (Table 2.4) for 1 h. The membrane is then incubated o/n with a primary antibody detecting the antigen in question diluted according to the manufacture's protocol in 1x TBST and odyssey blocking buffer in a 1:2 ratio or, if blocked with milk, in 5% w/v non-fat dry milk in 1x TBST.

On the following day, the membrane is washed three times for 15 min in 1x TBST. Next, the membrane is incubated protected from light with the secondary antibody in 1x TBST and odyssey blocking buffer mixed 1:2. After 1 h, the membrane is washed three times with 1x TBST and finally with 1x TBS for 10 min. The membrane can now be scanned with the Odyssey Sa Infrared Imaging System. In order to quantitatively determine protein expression, the signal intensity of the bands was measured with the Imagestudio lite 3.1.4 program. Subsequently, the target/reference ratio was determined. This value is shown in the densiometric evaluation.

Table 2.19: SDS-PAGE recipe for separating and stacking gels.

Chemicals	5% stacking gel [ml]	10% separating gel [ml]	7.5 % separating gel [ml]
dd-H_2O	3.4	3.9	3.8
Polyacrylamide 30%	0.85	3.3	2
Tris, upper (6.8 pH)	0.625	-	-
Tris, lower (8.8 pH)	-	2.5	2
10% (w/v) SDS	0.05	0.1	0.08
10% (w/v) APS	0.05	0.1	0.08
TEMED	0.005	0.004	0.008

2.2.13 Growth arrest assay

Senescent cells are, by definition, non-dividing, growth-arrested cells. This growth inhibition can be analyzed in a growth arrest assay. Here, a defined cell number is seeded

in a 10 cm cell culture dish one day before the treatment. This data point is called passage -1. To induce CIS in murine cancer cells, cells are treated with a combination of 100 ng mL^{-1} of recombinant mouse IFNγ and 10 ng mL^{-1} of recombinant mouse TNF. For human A204 cancer cells, 100 ng mL^{-1} of recombinant human IFNγ and 400 pg mL^{-1} of recombinant human TNF are used. Cells are treated for a total of 96 h. In order to determine the cell number, cells are trypsinized, and viable cells (trypan-blue negative) are counted in a Neubauer counting chamber (compare Section 2.2.1). This data point is defined as passage 0. For the next passage (passage 1), the same cell number as in passage -1 is seeded in a new 10 cm cell culture dish and incubated without any cytokines for additional 96 h. Cells are trypsinized and counted as described before. To calculate the proliferation index, the formula in Equation (2.2) is used.

$$\text{Proliferation index} = \frac{\text{Counted cell number}}{\text{Seeded cell number}} \times \text{Proliferation value from previous passage} \tag{2.2}$$

2.2.14 Senescence-associated β-galactosidase assay

Unlike other cells, senescent cells have a characteristic SA-β-gal activity at 6.0 pH. To measure this activity, the SA-β-gal Staining Kit by US Biological is used according to the manufacturer's instructions. Cells are seeded in a 96-well plate and treated for 96 h to induce CIS. To start, cells are washed twice with PBS and subsequently fixed for 15 min in 100 µL of a 1:10 dilution of the Fixation Solution. Next, cells are washed twice with PBS. To each well, 100 µL of Staining Solution are added and incubated o/n in an incubator at 37 °C without CO_2. On the following day, cells are washed twice with PBS. To stain the nuclei, 100 µL of a 300 nM DAPI solution are added to the cells and incubated for 5 min at RT. Finally, cells are washed once with PBS. For microscopic analysis, 50 µL of PBS are added to each well, and cells were counted under a microscope.

2.2.15 LDH assay

The lactate dehydrogenase (LDH) assay is a method to measure cytotoxicity. Here, damaged cells release LDH, which is used to enzymatically reduce tetrazolium salt (INT) to formazan, which can be colorimetrically measured at 490 nm. For this experiment, the Pierce LDH Cytotoxicity Assay Kit from Thermo Scientific is used according to the manufacturer's instructions. First, cells seeded one day before the experiment in a 96-well plate are treated with the compound in duplicates for 24 h at 37 °C with 5% CO_2. In one duplicate, without any compound, 10 µL of ultrapure H_2O are added and used later as the spontaneous LDH activity. In another compound-free duplicate, 10 µL 10x lysis buffer are added and incubated at 37 °C with 5% CO_2 for 45 min. This sample is referred to as maximum LDH activity. After transferring 50 µL of each well in a new 96-well plate,

50 µL of reaction mix are added. Samples are incubated for 30 min at RT protected from light. Finally, 50 µL stop solution is added to each well. The LDH assay is measured in a photometer at 490 nm and 680 nm. To calculate the LDH activity, the recorded values from the 680 nm absorbance are subtracted from the 490 nm values. The cytotoxicity of the compound-treated cells is calculated as displayed in Equation (2.3).

$$\% \text{ Cytotoxicity} = \frac{\text{Compound-treated LDH activity - Spontaneous LDH activity}}{\text{Maximum LDH activity - Spontaneous LDH activity}} \times 100 \tag{2.3}$$

2.2.16 Crystal violet assay

The crystal violet assay is an assay to quantify the cell number by staining cell nuclei with crystal violet. The intensity of bound crystal violet correlates to the cell number. First, cells are seeded in a 96-well plate together with medium only wells (used as blank), sit for 24 h in a cell culture incubator, and treated with a compound for additional 24 h. Next, the medium is discarded and 50 µL of 0.5% crystal violet solution (Table 2.4) are added to the cells and incubated for 20 min at RT. The 96-well plate is carefully washed under tap water and air-dried. To dissolve the bound crystal violet, 200 µL of methanol are added to each well and incubated for 20 min at RT. The plates are measured in a photometer at 570 nm.

2.2.17 Transfection

In order to knockdown protein expression in human cancer cells, the DharmaFECT Transfection protocol from Dharmacon is used. First, cells are seeded one day before transfection in a 6-well plate with confluency of 15-75% in a cell culture medium without antibiotics. On the day of transfection, 10 µL of siRNA are mixed with 190 µL of serum-free medium. In another tube, 10 µL of DharmaFECT reagent are diluted with 190 µL of serum-free medium. After 5 min, the siRNA mixture is added to the DharmaFECT solution and incubated for 20 min at RT. Next, the medium is removed from the cells and replaced with 1.6 mL of fresh cell culture medium. The transfection mixture is added to the cells and mixed by carefully swirling the 6-well plate. The incubation time of the siRNA varies between 24 to 72 h, depending on the performed assay. Here, cells were incubated for 24 h.

To induce a gene knockout by clustered regularly interspaced short palindromic repeats/crispr associated protein 9 (CRISPR/Cas9), the CRISPR KO Transfection Protocol by Santa Cruz is used. This technique is designed to cut a specific target sequence from the genome. The DNA is subsequently ligated. Here, cells are seeded in a 6-well plate in antibiotic-free medium one day prior to the transfection. The confluency of the cells should be between 40-80% on the day of transfection. In the beginning, 1 µg of plasmid

DNA is mixed with 140 µL of Plasmid Transfection Medium. Next, 10 µL of UltraCruz Transfection Reagent are diluted with 140 µL of Plasmid Transfection Medium. After incubation for 5 min, the Plasmid DNA solution is added drop by drop to the Transfection mixture and incubated for 20 min at RT. At the same time, cell culture medium is removed from the cells and replaced with 3 mL of fresh cell culture medium. The Plasmid DNA transfection solution is added drop by drop to the cells and incubated for 24 to 48 h. Successfully transfected cells express green fluorescent protein (GFP) and can, therefore, be sorted in a fluorescence activated cell sorter (FACS).

2.2.18 Comparative genomic hybridization

The array comparative genomic hybridization (CGH) is a method used to identify DNA copy number variations such as deletions or amplifications. Target DNA is labeled with cyanine 5 (Cy5) while reference DNA is labeled with cyanine 3 (Cy3). Both samples are mixed and compete to hybridize with oligonucleotides coated on a microarray surface. If the target DNA contains amplification, it will bind more to the array and the spot will fluoresce red (670 nm). If the target DNA has a deletion, the spot will fluoresce green (570 nm) since more reference DNA binds to this spot.

In the first step, the concentration of DNA from Section 2.2.3 is measured with a nanodrop. Furthermore, DNA should not be degraded and is therefore analyzed with an agarose gel electrophoresis according to Section 2.2.5. For the following steps, the SureTag Complete DNA Labeling Kit from Agilent is used. First, 1 µL of target and reference (from the spleen of male wild typ C3HeB/FeJ mice, Section 2.2.3) DNA is adjusted to 20.2 µL with nuclease-free H_2O. Next, DNA is digested by adding digestion master mix (Table 2.20). The samples are incubated in a thermocycler for 2 h at 37 °C followed by 20 min at 65 °C and stored at 4 °C until use.

Table 2.20: CGH digestion master mix.

Reagents per sample
2 µL nuclease-free H_2O
2.6 µL 10x Restriction Enzyme Buffer
0.2 µL BSA
0.5 µL Alu I
0.5 µL Rsa I

To enable fluorescence labeling of the DNA, 5 µL of random primer are added to each sample and incubated for 3 min at 98 °C and cooled down to 4 °C until the next step. Subsequently, 19 µL of labeling master mix (see Table 2.21) are added to the probes.

After incubating samples for 2 h at 37 °C followed by 10 min at 65 °C, samples are cooled down to 4 °C. Next, labeled DNA is cleaned-up with purification columns. First,

Table 2.21: CGH labeling master mix.

Reagents per sample
10 µL 5x Reaction Buffer
5 µL 10x dNTP
3 µL Cy3-dUTP or Cy5-dUTP
1 µL Exo (-) Klenow

nuclease-free H_2O is added for a total volume of 430 µL and transferred onto the purification columns. After centrifuging the samples for 10 min at 14000 x *g*, the flow-through is discarded and 430 µL nuclease-free H_2O are added to the column. After another centrifugation for 10 min at 14000 x *g*, the column is inverted and placed on a new 2 mL collection tube. The samples are centrifuged for 1 min at 1000 x *g*. Next, the volume of the cleaned-up DNA is measured (around 20 µL to 32 µL) and diluted with nuclease-free H_2O to a volume of 79 µL. After that, the dye and DNA concentration is measured with a nanodrop. The dye concentration (pmol µg^{-1}) is used to determine the yield and specific activity of labeled samples. The equations are displayed in Equation (2.4) and Equation (2.5) and compared to the expected values in Table 2.22.

$$\text{Specific Activity} = \frac{\text{pmol}\,\mu\text{L}^{-1}\ \text{dye}}{\mu\text{g}\,\mu\text{L}^{-1}\ \text{gDNA}} \tag{2.4}$$

$$\text{Yield (µg)} = \frac{\text{DNA concentration (ng}\,\mu\text{L}^{-1})\ \ \text{Sample Volume (µL)}}{1000\ \text{ng}\,\mu\text{g}^{-1}} \tag{2.5}$$

Table 2.22: CGH labeling control.

Input gDNA [µg]	Yield [µg]	Specific Activity of Cy3 labeled sample [pmol µg^{-1}]	Specific Activity of Cy5 labeled sample [pmol µg^{-1}]
1	9 to 12	25 to 40	20 to 35

Comparable yields of Cy3 and Cy5 labeled DNA are mixed. Next, 181 µL hybridization master mix (Table 2.23) are added and mixed by carefully pipetting up and down five times.

After incubating samples for 3 min at 98 °C followed by 30 min at 37 °C, probes are directly pipetted on a gasket slide and transferred in an Agilent SureHyb chamber. After that, the SureHyb chamber cover is put on top of the microarray and tighten with

Table 2.23: CGH hybridization master mix.

Reagents per sample
25 µL Cot-1 DNA (1.0 µg mL^{-1})
26 µL 10x aCGH Blocking Agent
130 µL 2x HI-RPM Hybridization Buffer

the clamp. The chamber is placed inside the rotating hybridization oven for 48 h at 67 °C. In order to wash the microarray, the slides are disassembled in Agilent Oligo aCGH/ChIP-on-Chip Wash Buffer 1. Next, the microarray is transferred in fresh Agilent Oligo aCGH/ChIP-on-Chip Wash Buffer 1 and washed for 5 min at RT. Subsequently, the microarray is washed in 37 °C prewarmed Agilent Oligo aCGH/ChIP-on-Chip Wash Buffer 2 for 5 min. Afterward, the microarray is placed in acetonitrile for 1 min at RT after which it is transferred in Agilent Stabilization and Drying solution for 1 sec at RT. The array is placed inside a slide holder and measured in the DNA Microarray Scanner G2505C. The data is subsequently analyzed with the Agilent Genomic Workbench Lite Edition 6.5.0.18.

2.2.19 Statistical analyses

For statistical analyses, the data was evaluated using GraphPad Prism 8. For the SA-β-gal assay (Figure 3.10b), the paired t-test was used. The paired t-test was also used for the densiometric analysis of Figure 3.17, Figure 3.19a, Figure 3.19b, Figure 3.29b where the signal ratio of the cytokine-treated inhibitor sample was compared with the cytokine-treated DMSO control.
Evaluation of mRNA expression in Figure 3.29c was done using one-way ANOVA.
Statistical analysis of the LDH and the crystal violet assays of Figure 3.15a to Figure 3.15e were performed with the two-way ANOVA test (Dunnett's multiple comparison test).
For inhibitor treatment with simultaneous cytokine titration in Figure 3.20 to Figure 3.21d, the LDH, and crystal violet assays were analyzed with the two-way ANOVA test (Turkey's multiple comparison test).
Western Blots of Figure 3.23a to Figure 3.25c, in which the JunB protein expression was measured after cytokine treatment at different inhibitor concentrations, were analyzed with a one-way ANOVA test. *P $\leq$ 0.05, **P $\leq$ 0.01, ***P $\leq$ 0.001, ****P $\leq$ 0.0001, NS, not significant.

Chapter 3

Results

3.1 T_h1 cytokines influence the chromosomal stability of RIP1-Tag2 β-cancer cells

In the first part of the results, the influence of the T_h1 cytokines (IFNγ and TNF) on the chromosomal stability of murine RT2 cancer cell lines was examined. It is well known that epigenetic changes can be found in the genome through the induction of replicative senescence (De Cecco *et al.* (2013)). This leads, for example, to gene silencing, which ultimately suppresses the expression of proteins and thus strengthens the senescence phenotype. However, it is unclear whether there are additional mutations in the genome, for example, in the form of amplification or deletion of chromosomes or chromosomal segments. At this point, the question arose whether induction of senescence with IFNγ and TNF can influence the stability of existing chromosomal aberrations.

For this purpose, different primary RT2 and RIP1-Tag2 x signal transducer and activator of transcription $1^{-/-}$ cancer cell lines isolated from 12 weeks old female RT2 and RIP1-Tag2 x signal transducer and activator of transcription $1^{-/-}$ mice were used. At the beginning of the experiment, cells were trypsinized and counted (compare Figure 3.1). A fraction of the cells was removed at this time, centrifuged and frozen as cell pellets. This sample corresponds to the sample ”untreated”. The other cells were seeded for treatment either with medium alone (medium control) or with medium mixed with the T_h1 cytokines IFNγ and TNF (referred to as IFNγ + TNF). After a total treatment time of 96 h, cells were harvested, and the cell pellets were frozen. Thereafter, DNA was isolated and analyzed by CGH.

In Figure 3.2, the CGH of RT2 cancer cell line 1 is shown. The genome shown for the different treatment groups reveals a variety of chromosomal aberrations. For example, the untreated sample has a loss of chromosomes 1, 3, 6, 9, and 16. On the other hand, chromosomes 4, 13, and 15 are amplified. The strong amplification of the X chromosome is caused by using male control DNA in the CGH assay. In addition to a complete loss or an amplification of the entire chromosome, amplification of chromosomal segments can also be observed. In this case, on chromosome 2. The analysis of

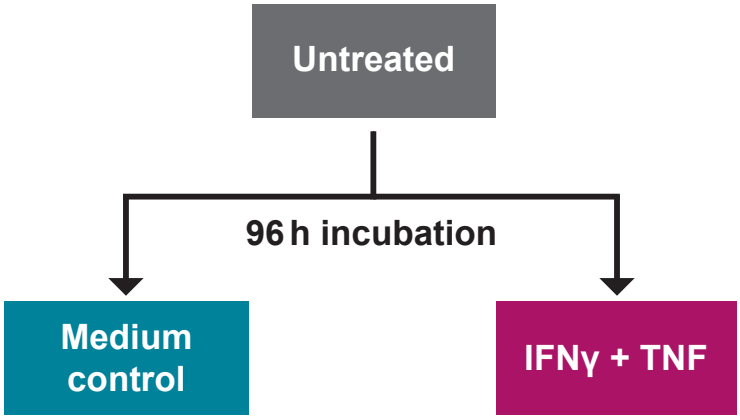

Figure 3.1: CGH treatment scheme. The RT2 cancer cells were trypsinized and counted. At this point, a part of the cells was removed and frozen as pellets (Untreated). The remaining cells were seeded and either treated with medium (Medium control) or with the cytokine mix (IFNγ + TNF) for 96 h. Afterward, the cells were harvested and stored as frozen pellets until DNA was isolated and CGH analyses were performed.

the other treatment groups (medium control and IFNγ + TNF) shows that they have a similar chromosomal aberration pattern. The overlay reveals that these are identical in untreated, medium-treated or cytokine-treated cells.

The CGH result of the RT2 cancer cell line 2, originating from another RT2 mouse, is shown in Figure 3.3. Although originating from an identical genetic background, the aberrations differ from those shown in Figure 3.2. In contrast to this CGH, the untreated group in Figure 3.3 shows no amplification of an entire chromosome. Only the amplification of a section of chromosome 2, which is also found in Figure 3.2, can be observed here. As shown in Figure 3.3, chromosome 3 and 9 are also deleted as well. However, partial deletions, as found in the RT2 cancer cell line 1 in Figure 3.2, are not present in this example. The results of the overlay do not reveal any pronounced differences. This is another example where none of the treatments influenced the chromosomal aberrations.

Next, it was investigated whether a RT2xStat1$^{-/-}$ cancer cell line also had chromosomal aberrations and whether the different treatments influenced these. In this cancer cell line, no CIS can be induced due to the absence of the STAT1 receptor. Similar to the results in Figure 3.2 and Figure 3.3, the RT2xStat1$^{-/-}$ cancer cell line shows partial amplification of chromosome 2 in the untreated sample (Figure 3.4). A further partial amplification, as well as partial deletion, can be seen on chromosome 6. Chromosome 4 is completely amplified in this cancer cell line, as shown in Figure 3.4. However, a deletion of a whole chromosome is not present here. The overlay clearly shows that none of the treatments

influence the formation and stability of chromosomal aberrations.

The following CGH analyses are derived from an *in vivo* experiment in which the genome was examined after failure of immune checkpoint blockade (ICB) therapy. In this experiment, $1x10^6$ cells of the RT2 cancer cell line 3 were injected subcutaneously into the flank of $CD8^+$-depleted C3HeB/FeJ mice (experiment performed by Ellen Brenner, Brenner *et al.* (2020)). In total, four mice were used. A growth arrest assay, which was performed prior to the injection, demonstrated that the RT2 cancer cell line 3 responded to CIS (experiment performed by Ellen Brenner). After tumor attachment ($>$3 mm), an ICB therapy was administered to the mice. The mice were treated once a week with either anti-programmed cell death protein 1 ligand (PD-L1) and anti-lymphocyte-activation gene 3 (LAG-3) or anti-programmed cell death protein 1 (PD-1) and anti-cytotoxic T-lymphocyte-associated protein 4 (CTLA-4). Contrary to expectations, successful ICB therapy could not be induced in any of the mice. As the tumors reached a size of $>$10 mm, the mice were sacrificed, and the tumors were taken into culture (hereinafter referred to as mSc cancer cell line #3, #4, #5, and #6). Subsequently, an *in vitro* growth arrest was started with these cells. The results showed that the tumor cells no longer responded to the CIS (experiment performed by Ellen Brenner, data not shown). To identify the cause of these altered responses to the CIS and whether this might have genetic causes, a CGH was performed.

In Figure 3.5, the CGH of the four different tumors are shown (see also Brenner *et al.* (2020)). All four tumors display multiple amplifications of whole chromosomes or chromosome segments, for example, chromosome 10 or chromosome 8. Deletions of whole chromosomes are, however, rarely found. As the overlay shows, the occurrence of chromosomal aberrations is independent of the ICB treatment. The majority of aberrations are similar in all tumors (chromosomes 2, 4, 5, 7, 9, 10, 14, 16, 18, and 19). The mSc cancer cell line #4 has specific partial amplifications on chromosomes 1 and 8. Chromosomes 3 and 15, on the other hand, show partial amplification for the mSc cancer cell line #5. If the chromosomal aberrations are not in alignment, these aberrations (in this experiment exclusively amplifications) are more pronounced in two or three tumors (chromosome 11, 12, 13, 15, and X chromosome).

Since the expression of $p16^{INK4a}$ is essential for the induction of CIS, the question emerged whether Cdkn2a, the gene for $p16^{INK4a}$, is lost in these cell lines. When zooming in on chromosome 4, a specific loss of Cdkn2a is found in all four mSc cancer cell lines (Figure 3.6). This, in turn, led to the question of whether this specific loss of Cdkn2a was already present in the parent RT2 cancer cell line 3. Hence, a vial of the RT2 cancer cell line 3 was thawed and cultured. The same passage that was used for the first growth arrest assay was used for a new growth arrest assay and a CGH analysis after treatment, according to Figure 3.1. Figure 3.7 displays the result of the CGH analysis (see also Brenner *et al.* (2020)). As demonstrated in the first growth arrest assay (prior to injection), cells responded to the CIS (experiment performed by Ellen Brenner, data not show). Comparing the CGH overlay from this experiment (Figure 3.7) with the CGH

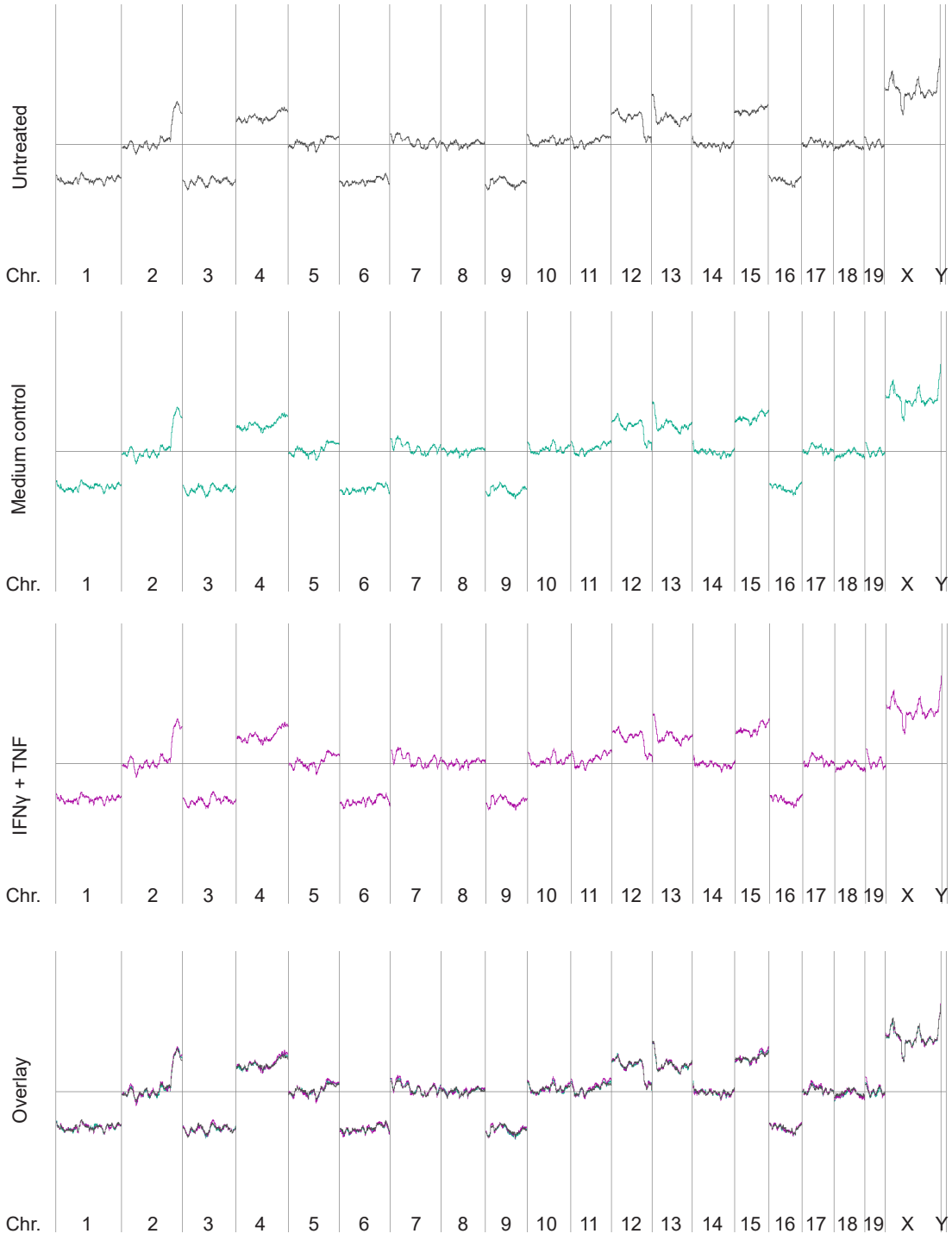

Figure 3.2: CGH of the RT2 cancer cell line 1. Various chromosomal aberrations are seen in three different treatment groups. Nevertheless, none of the different treatments influence the chromosomal aberrations, as seen in the overlay.

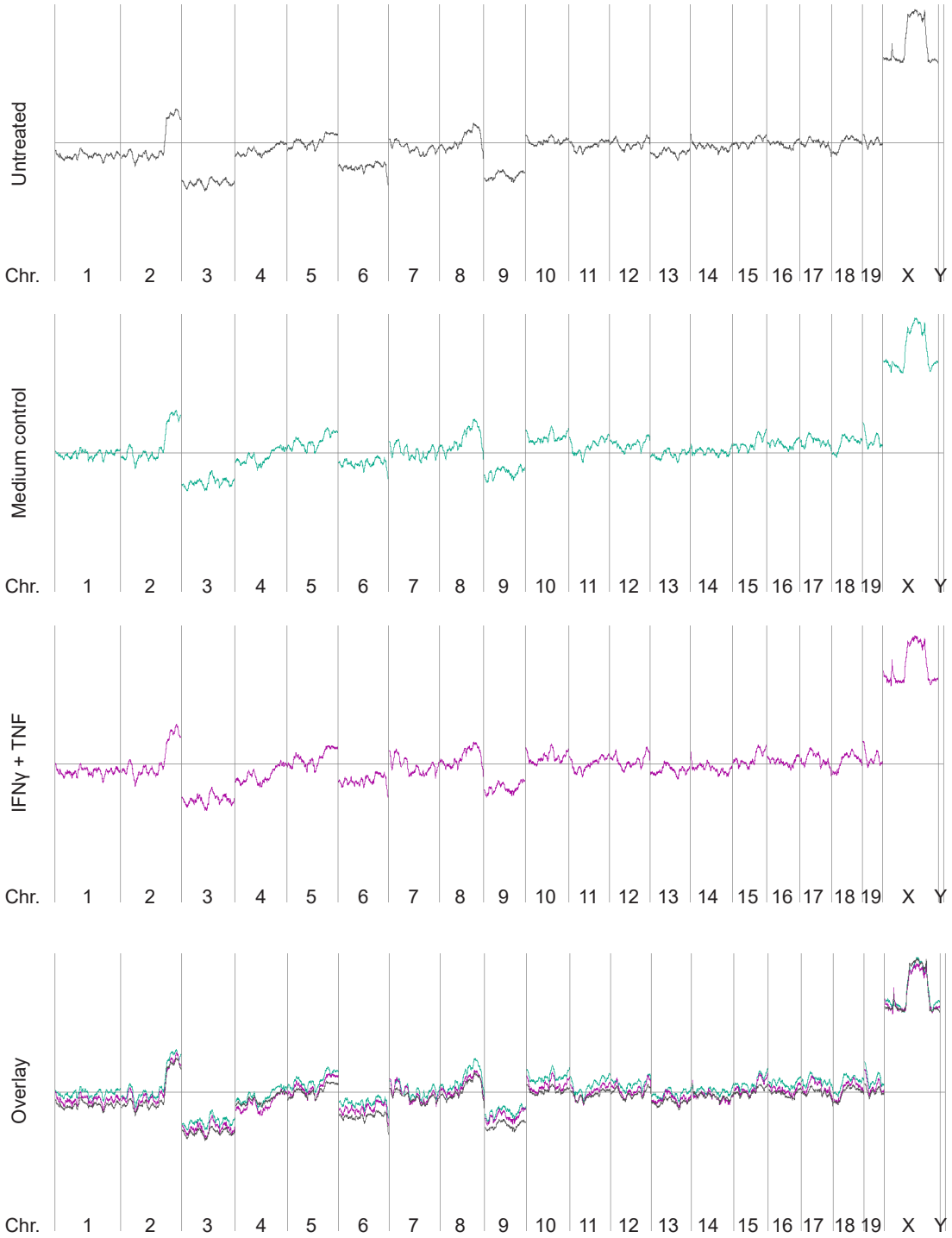

Figure 3.3: CGH of the RT2 cancer cell line 2. In this primary cancer cell line few chromosomal aberrations are found. The overlay shows that none of the treatments influence the appearance of chromosomal aberrations.

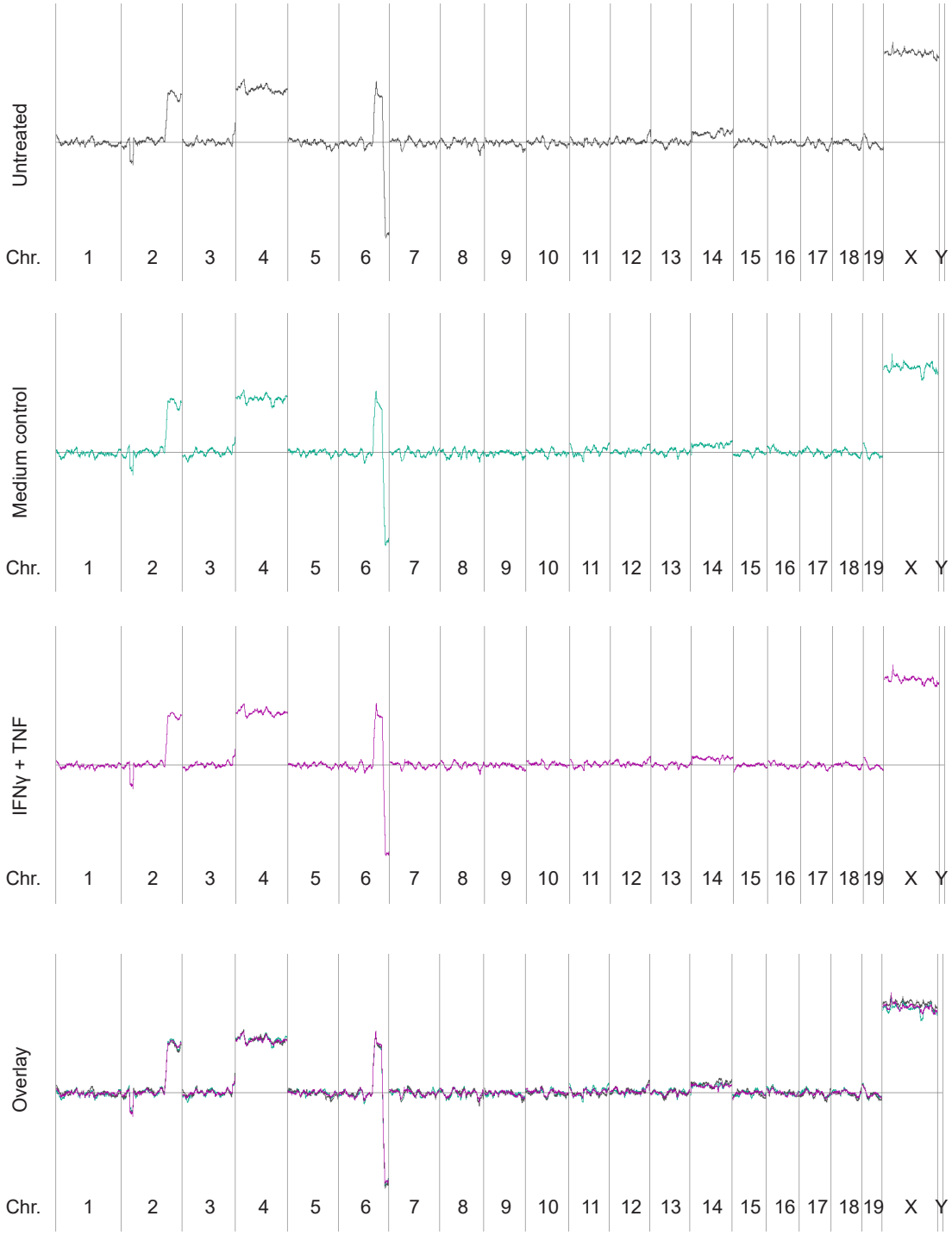

Figure 3.4: CGH of the RIP1-Tag2 x signal transducer and activator of transcription $1^{-/-}$ cancer cell line. The RIP1-Tag2 x signal transducer and activator of transcription $1^{-/-}$ cancer cell line displays only few chromosomal aberrations. As shown in the overlay, the different treatments do not influence chromosomal aberrations.

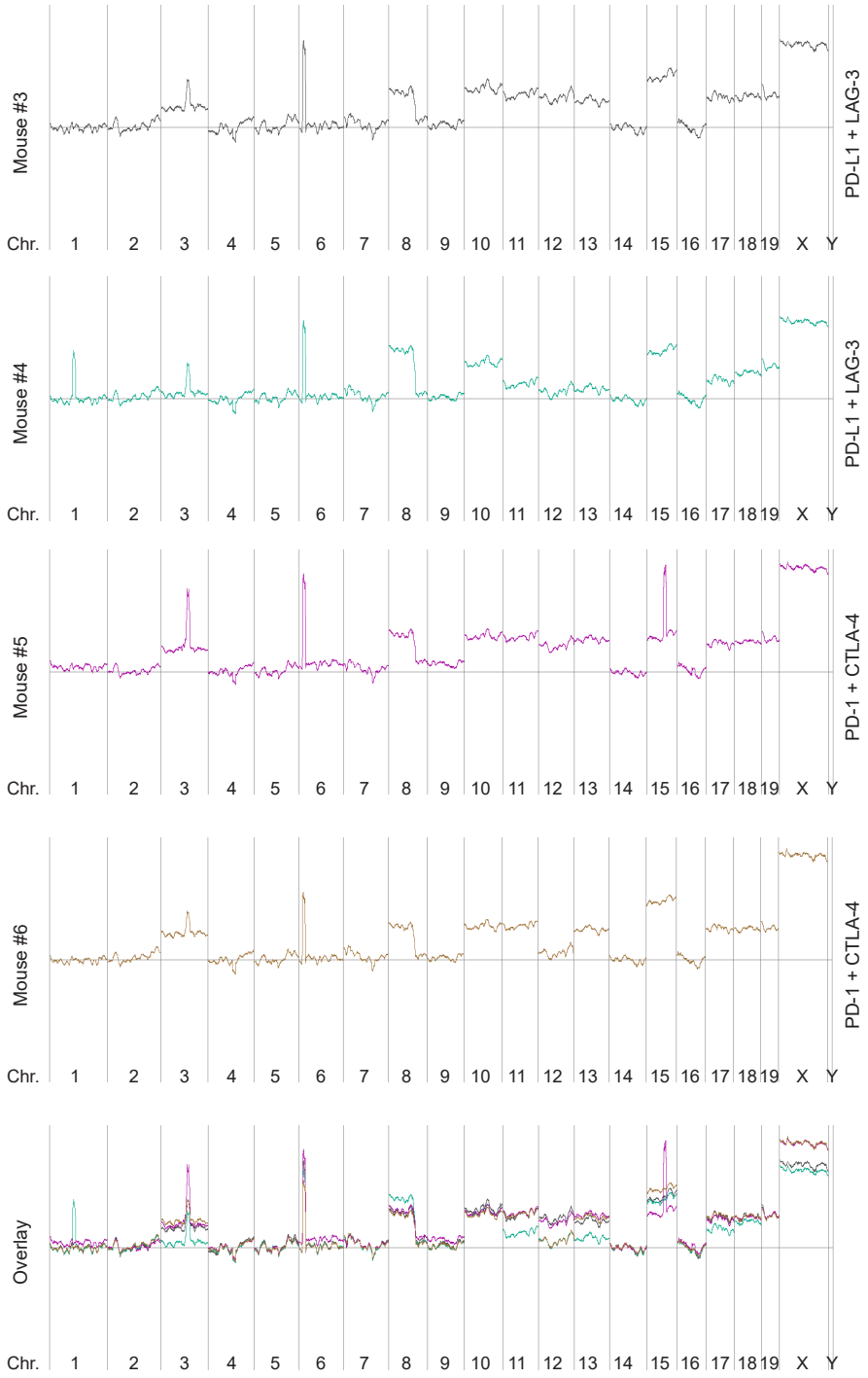

Figure 3.5: CGH of four subcutaneously transplanted RT2 tumors (mSc). The overlay highlights similarities and differences in the chromosomal aberrations (modified from Brenner *et al.* (2020)).

Abbreviations: CTLA-4 (cytotoxic T-lymphocyte-associated protein 4), LAG-3 (lymphocyte-activation gene 3), PD-1 (programmed cell death protein 1), PD-L1 (programmed cell death protein 1 ligand).

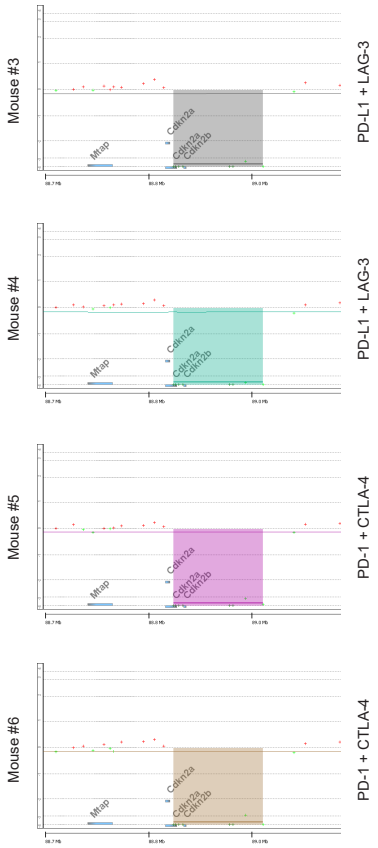

Figure 3.6: Specific loss of the $p16^{INK4a}$ gene locus cyclin-dependent kinase inhibitor 2A (Cdkn2a) in all four mSc tumors.

Abbreviations: CDKN2A (cyclin-dependent kinase inhibitor 2A), CTLA-4 (cytotoxic T-lymphocyte-associated protein 4), LAG-3 (lymphocyte-activation gene 3), PD-1 (programmed cell death protein 1), PD-L1 (programmed cell death protein 1 ligand).

results from the *in vivo* experiment in Figure 3.5, different chromosomal aberrations can be seen. While in the subcutaneous tumors the chromosome 3 shows an amplification (Figure 3.5), a deletion can be found in the *in vitro* samples (Figure 3.7). The partial amplification of chromosome 3 is observed in both. Furthermore, the partial amplification of chromosome 8 (Figure 3.5) is not seen in the *in vitro* samples (Figure 3.7). The same applies to chromosomes 10, 11, 12, 13, 15, 17, 18, 19, and X chromosome. At most, a trend can be seen in the *in vitro* samples. In contrast to the *in vitro* samples (Figure 3.7), no deletion can be found on chromosomes 9, 14, and 16 in the tumors from the *in vivo* experiment (Figure 3.5). The specific partial amplification on chromosome 6 from Figure 3.5 is absent in the *in vitro* samples (Figure 3.7).

The CGH analysis shows no aberrations in the untreated control for chromosome 4 (Figure 3.7) or for Cdkn2a itself (Figure 3.8). However, if the cells are subsequently

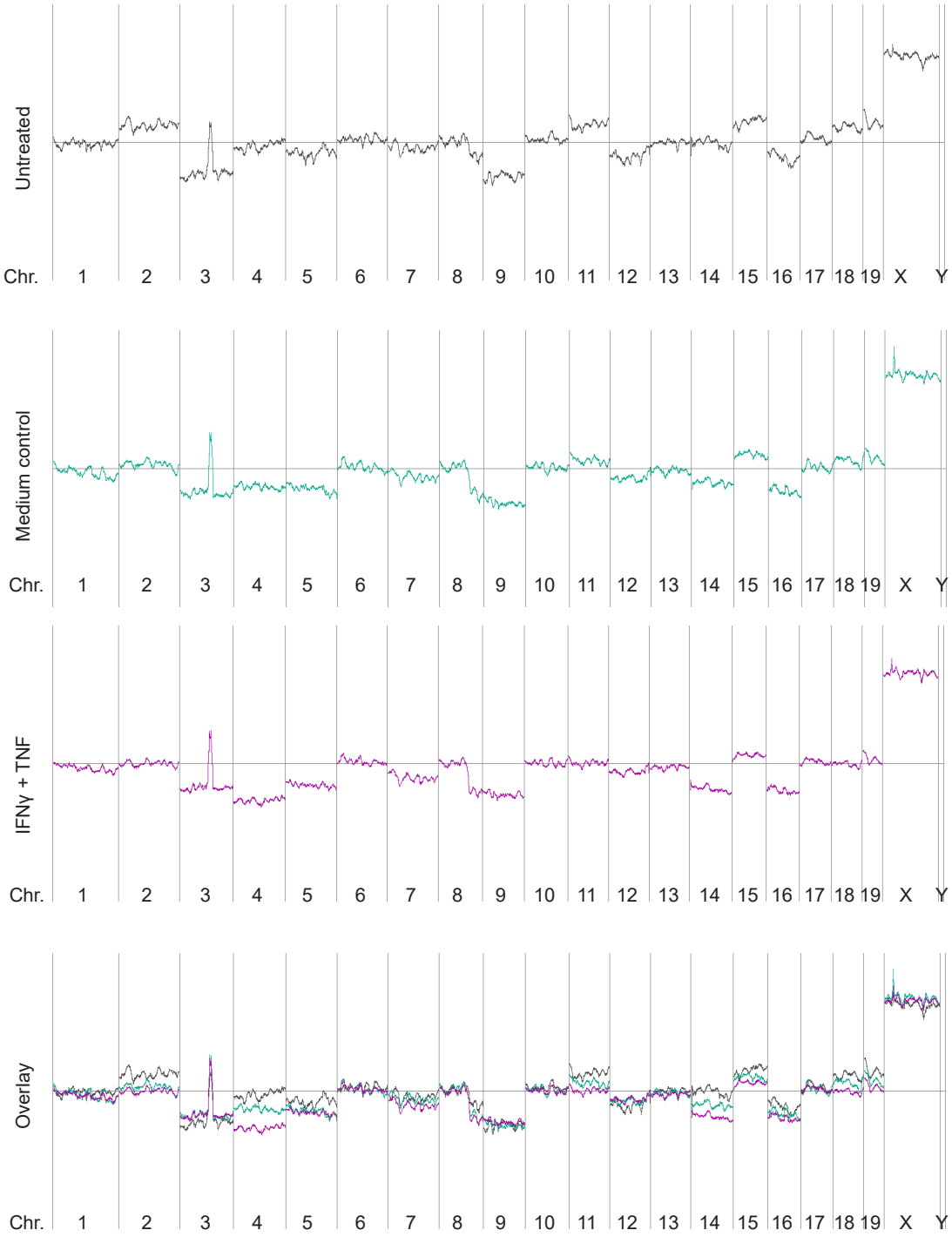

Figure 3.7: The CGH of the RT2 cancer cell line 3 reveals a gradual loss of the chromosomes 4 and 14 (modified from Brenner *et al.* (2020)).

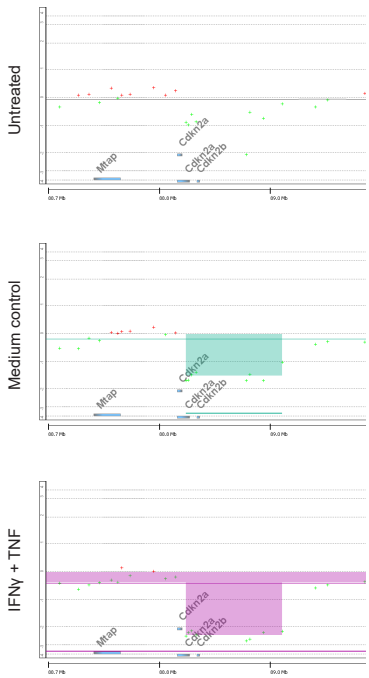

Figure 3.8: Close-up of chromosome 4 shows the progressive loss of the $p16^{INK4a}$ transcription site Cdkn2a.

treated, a downwards shift of chromosome 4 is observed. The increasing loss of this chromosome can already be seen in the medium control (Figure 3.7). The deletion of chromosome 4 is even more pronounced in the cytokine-treated sample. A closer look at chromosome 4 shows a loss of Cdkn2a already present in the medium control (Figure 3.8). The deletion becomes more pronounced in the cytokine-treated sample. A close-up on chromosome 4 shows the progressive loss of the $p16^{INK4a}$ transcription site Cdkn2a. The examples in Figure 3.5 to Figure 3.8 show how crucial the expression of $p16^{INK4a}$ is for the induction of CIS and for ICB therapy (Brenner *et al.* (2020)).

However, it is still unclear how the expression of $p16^{INK4a}$ is induced in CIS. Neither the IFNγ nor the TNF pathway directly lead to its expression. A possible link is the AP-1 transcription factor JunB. It is a published transcription factor for $p16^{INK4a}$ and can in turn be expressed by TNF-mediated NF-κB signaling. The following sections will examine whether there is a relationship between the $p16^{INK4a}$ expression, and thus senescence induction, and the AP-1 transcription factor JunB.

3.2 JunB expression is induced by T_h1 cytokines

In order to investigate a possible relationship between $p16^{INK4a}$ and JunB in CIS, it was first examined whether the expression of the AP-1 transcription factor is induced in CIS. For this purpose, cells were treated either with medium or with the T_h1 cytokines IFNγ and TNF. Cells were harvested after 0 h, 4 h, 8 h, 24 h, 48 h, 72 h and 96 h. Thus, the entire period of 96 h, which is necessary for a stable senescence induction, was covered. The results of protein expression are presented as Western Blots in Figure 3.9. The first three Western Blots show murine cells, in detail a primary RT2 cancer cell line (Figure 3.9a), as well as the LLC (Figure 3.9b), and the CT26 cancer cell lines (Figure 3.9c). Within the first four hours, an induction of JunB expression is found in the cytokine-treated samples. In the medium control, on the other hand, the induction of JunB expression is not or only slightly present. During the progression of senescence induction, the JunB expression peaks after 8 h, and it remains stable for 96 h of treatment. Similar time dynamics and strong expression are found in the human rhabdomyosarcoma cell line A204 (Figure 3.9d).

This cell line is well established, genetically robust, and shows a stable proliferation. Also, CIS can be induced in A204 cancer cells. This is demonstrated in Figure 3.10 showing a growth arrest induction (Figure 3.10a) and the expression of senescence-associated β-galactosidase (SA-β-gal) (Figure 3.10b and Figure 3.10c). For this reason, the following experiments are performed with the A204 cancer cell line.

To induce CIS, a combined treatment with both IFNγ and TNF is crucial. To identify which cytokine stimulates JunB expression, the cytokines are added separately to A204 cancer cells. Figure 3.11 shows that in the first 4 h to 8 h JunB expression is found in TNF-treated samples as well as in IFNγ and TNF-treated samples. In the medium control and the IFNγ single treatment no JunB expression is observed at this time points. With progressive induction of senescence, JunB expression decreases in the TNF single treatment (from 24 h). Only the double treatment shows, as in Figure 3.9, stable expression of the transcription factor until the end of the treatment. Surprisingly, the IFNγ single treatment displays, to a small extent, a JunB expression after 24 h. However, the expression of JunB by TNF is no longer detectable after 48 h.

The increased expression of JunB at the protein level could be shown after addition of TNF alone or after combining IFNγ and TNF. To find out if the mRNA levels of JUNB also increases, a qPCR was performed (Figure 3.12). While JUNB mRNA expression is almost undetectable in the medium control, an increase in JUNB mRNA is already visible after 4 h in the cytokine-treated samples. The increased expression remains elevated and nearly stable over the course of 96 h. An exception is the mRNA value at 24 h. Here, a decreased transcription of JUNB mRNA is observed.

The previous Western Blots, both the combination treatment from Figure 3.9 and the

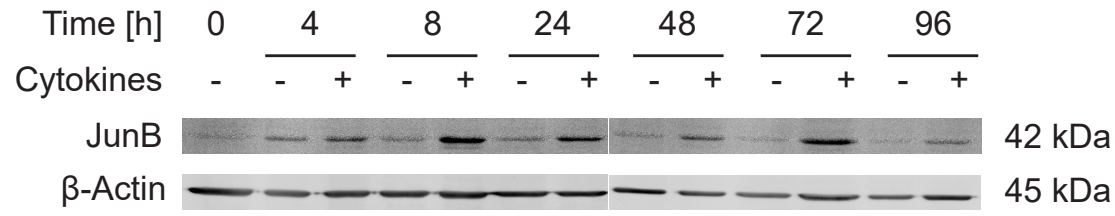

(a) Murine RT2 cancer cell line.

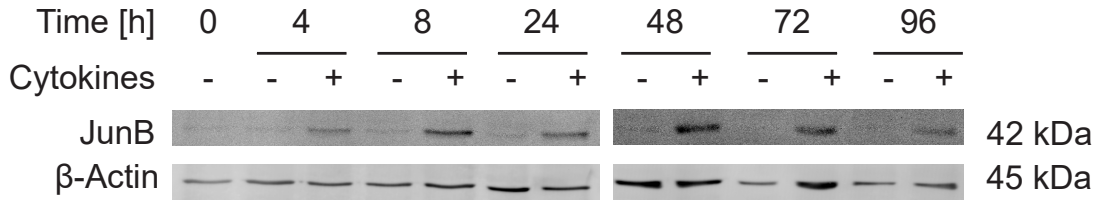

(b) Murine lewis lung carcinoma cell line (LLC).

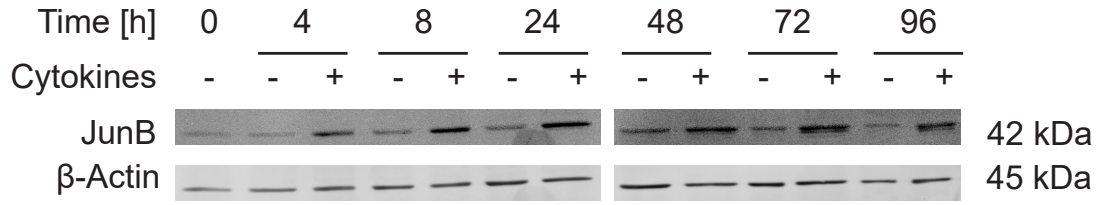

(c) Murine colon cancer cell line (CT26).

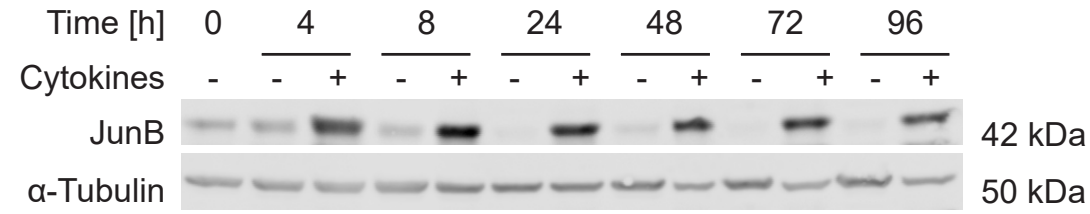

(d) Human rhabdomyosarcoma cell line A204.

Figure 3.9: Upregulation of the JunB protein level in various cancer cells lines after stimulation with the T_h1 cytokines. Four representative Western Blot analyses are displayed showing the upregulation of JunB protein as early as 4 h after treatment with IFNγ and TNF. The expression levels remain elevated during the senescence induction phase. ((a) n=3, (b) and (c) n=1, (d) n=3)

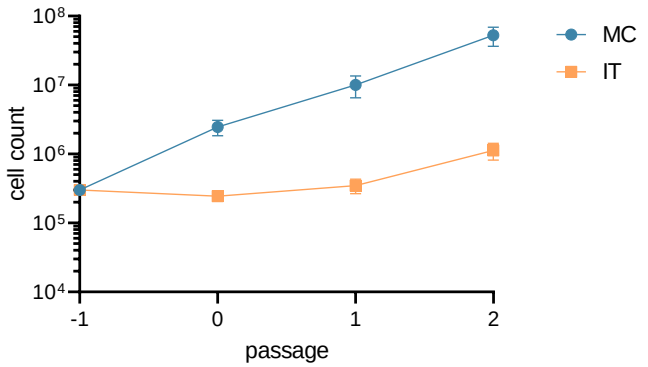

(a) Growth arrest assay.

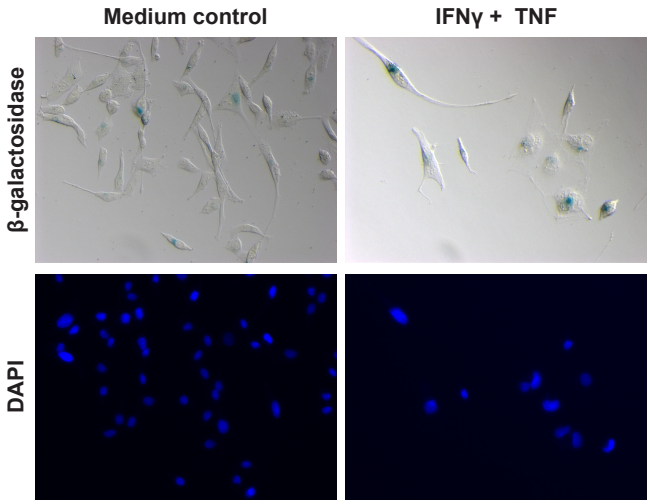

(b) SA-β-gal microscopic images.

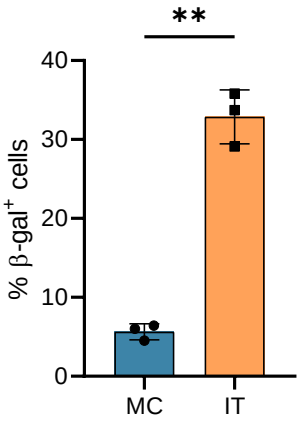

(c) SA-β-gal assay.

Figure 3.10: The T_h1 cytokines IFNγ and TNF induce senescence in A204 cancer cells. To induce CIS, combined treatment with 100 ng mL^{-1} of IFNγ and 400 pg mL^{-1} of TNF over a period of 96 h is necessary. Successful inhibition of proliferation (a) as well as increased expression of SA-β-gal activity ((b) and (c)) are characteristics of cellular senescence. Representative microscopic images displayed in (b). (n=3)

Abbreviations: CIS (cytokine-induced senescence), IT (IFNγ + TNF), MC (medium control), SA-β-gal (senescence-associated β-galactosidase).

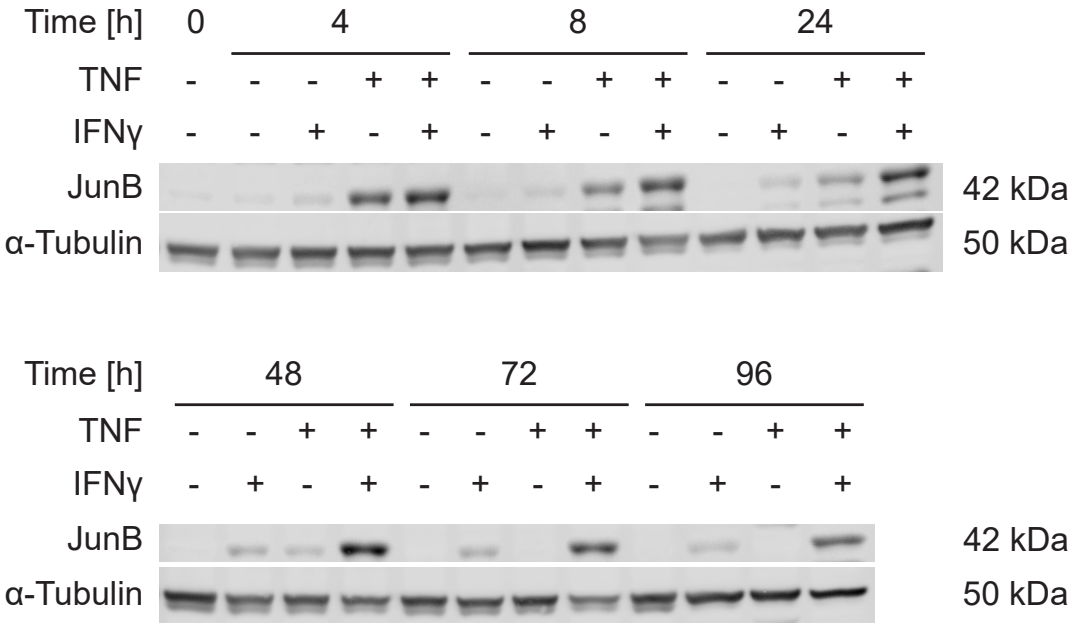

Figure 3.11: Treatment with TNF leads to the initial expression of JunB. After 24 h of incubation, the JunB protein level remains stable only in double-treated cells. However, a slight increase in JunB expression is seen after 24 h in IFNγ-treated cells. Representative Western Blots are shown. (n=3)

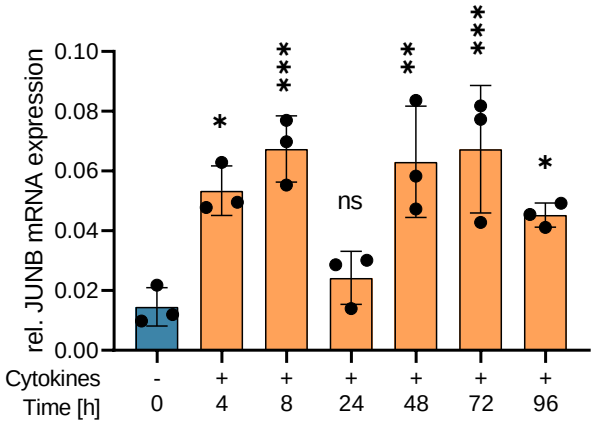

Figure 3.12: Increased JUNB expression on mRNA level after cytokine treatment. The induced transcription of JUNB remains present and elevated (except at 24 h) over the time course of CIS induction for up to 96 h. (n=3)

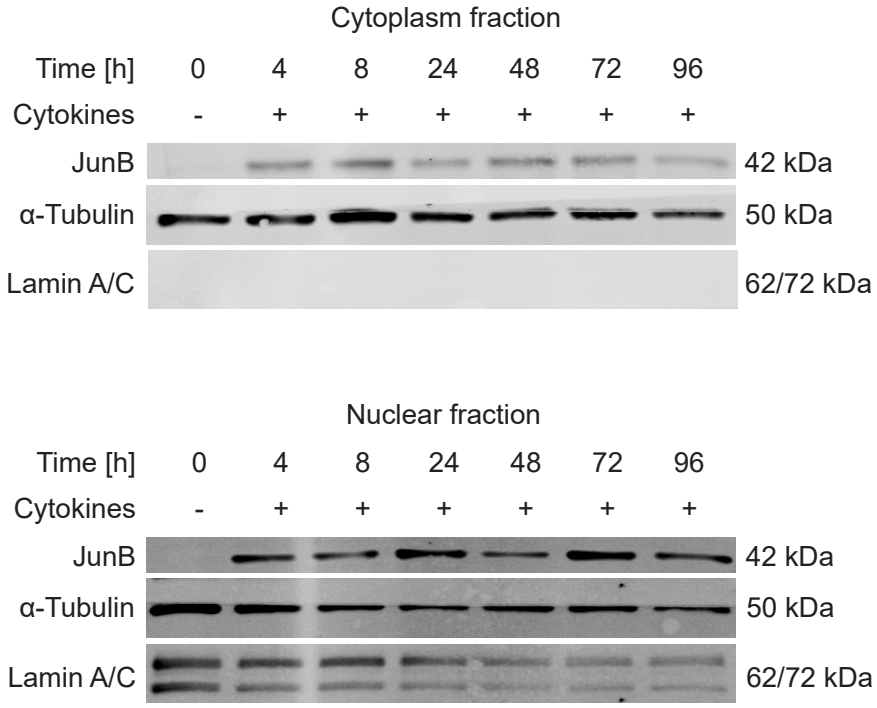

Figure 3.13: Translocation of JunB into the nucleus during CIS induction. After the cells have been treated with IFNγ and TNF, JunB expression is induced. Subsequently, and as early as 4 h of treatment, JunB translocates into the nucleus where it can act as a transcription factor. Representative Western Blots are shown. (n=3)

single treatment from Figure 3.11, were generated with whole-cell lysate. Since JunB is a transcription factor, it must translocate into the nucleus. To address this question, a nuclear/cytoplasmic fractionation was performed. In the upper part of Figure 3.13, the cytoplasm fraction is shown. Here, a low expression of JunB is seen during 4 h to 96 h of cytokine treatment (TNF and IFNγ). In the medium control (0 h), no JunB protein is found. The cytoplasmic fraction is free of nuclear material, which is indicated by the absence of detectable Lamin A/C. The lower part of Figure 3.13 shows the nuclear fraction. No clear separation of the two fractions has been achieved here, as α-Tubulin is still detectable in the nuclear fraction. Nevertheless, the enrichment of the nuclear fraction is only found here, since Lamin A/C is exclusively detectable in the nuclear fraction. Regarding the JunB expression, an evident accumulation of JunB can be observed in comparison to the cytoplasm fraction. This remains constant during the induction of CIS.

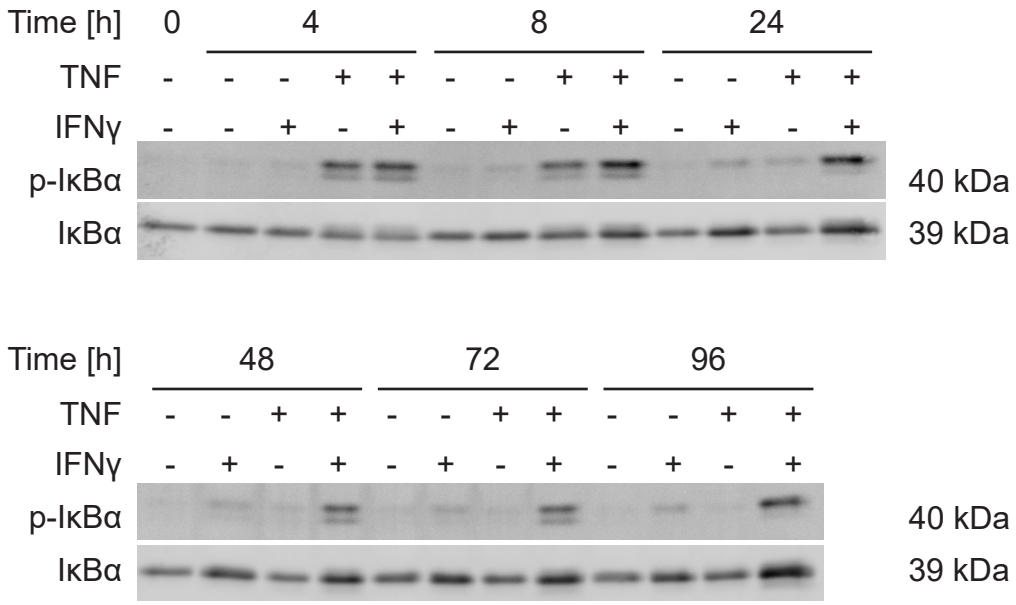

Figure 3.14: TNF leads to activation of the NF-κB signaling in CIS. After 48 h, the activation is no longer visible in the single TNF treatment, in contrast to the double treatment where JunB is expressed throughout 96 h. Representative Western Blots are shown. (n=3)

3.3 Inhibition of NF-κB leads to reduced JunB protein expression

The next step was to further decipher the signaling pathway between TNF and JunB (Figure 1.11). One promising option was the signal transduction of the TNF stimulation via NF-κB. To verify this, Western Blot analyses with the same samples used in Figure 3.11 were performed. The activation of the NF-κB signaling pathway was determined by the expression of IκBα and its activation via pIκBα, respectively. In Figure 3.14, the protein expression of both targets is shown. The expression of the unphosphorylated IκBα remains mostly constant in all samples. In contrast, phosphorylation of IκBα occurs in TNF as well as in IFNγ and TNF-treated samples, but not in the medium control or the IFNγ single treatment.

To investigate a causal relationship between the NF-κB activation and JunB expression, the inhibitor IKK-16 was used. This inhibitor selectively blocks the IκB kinases IKK-1 and IKK-2, thus preventing phosphorylation of downstream IκBα. In consequence, the NF-κB signaling pathway is inhibited.

Initially, the inhibitor's influence on the viability of A204 cancer cells was tested in a LDH and crystal violet assay in order to be able to use an effective but low-toxic

concentration of the inhibitor. In Figure 3.15a, a LDH cytotoxicity assay is shown after 24 h treatment. The A204 cancer cells were treated with the specified concentration of inhibitor, either with or without the addition of the T_h1 cytokines IFNγ and TNF. A concentration of 50 µM proved to be too toxic for the cells, independent of the addition of the cytokine (cytotoxicity value approx. 50%). At concentrations from 5 µM to 10 µM, a moderate cytotoxicity is observed (cytotoxicity value approx. 10%). Between 0.01 µM and 1 µM of IKK-16, no difference to the DMSO control (0 µM) is found (cytotoxicity value approx. 5%).

The results of the crystal violet assays are shown in Figure 3.15b to Figure 3.15e. This assay stains the nuclei, which indirectly provides information on the cell number (high extinction value correlates with a higher cell count). After an incubation time of 24 h, low extinction values are measured at concentrations from 5 µM to 100 µM IKK-16 (extinction value approx. 0.05), especially in cytokine-treated samples (extinction value approx. 0.02, Figure 3.15b). Only at a concentration of equal or less than 1 µM, the extinction values and thus the cell mass increases for both medium and cytokine-treated cells (extinction value approx. 0.2).

The extinction values for medium or cytokine-treated cells are extremely low after 48 h incubation for concentrations equal or higher than 5 µM IKK-16 (extinction value approx. 0.05, Figure 3.15c). For concentrations below 1 µM, the measured extinction values strongly increase in medium-treated cells (extinction value approx. 0.4). In contrast, the cytokine-treated cells display only a slight increase in the extinction values (extinction value approx. 0.1).

After additional 24 h (Figure 3.15d), i.e., a total incubation time of 72 h, the extinction value for the medium-treated cells have further increased (extinction value approx. 0.7) between an IKK-16 concentration from 0 µM to 1 µM. At these inhibitor concentrations, the cytokine-treated cells show no further increase in the extinction values (extinction value approx. 0.1). For concentrations higher than 5 µM, hardly any extinction values can be measured (extinction value approx. 0.05).

At the end of the complete induction time of the CIS (96 h), the extinction values of the medium-treated samples further increase at an inhibitor concentration from 0 µM to 0.1 µM (extinction value approx. 1.3, Figure 3.15e). However, between these IKK-16 concentrations, no difference regarding the extinction values are observed. The application of 1 µM IKK-16 also leads to an increase of the extinction value (extinction value approx. 1.0), albeit not as strong as in comparison to the lower IKK-16 concentrations. At concentrations from 0 µM to 1 µM low extinction values are measured when cells are simultaneously treated with the T_h1 cytokines (extinction value approx. 0.1). For inhibitor concentrations equal to or higher than 5 µM, only a marginal extinction is measured, regardless of whether the cells were treated with medium or the T_h1 cytokines (extinction value approx. 0.05).

Overall, it can be observed that an IKK-16 concentration of 5 µM is considered as too toxic, especially when incubated for 96 h. However, the aim is to apply the inhibitor over the incubation time of CIS to determine whether a possible inhibition of IKK-1 and

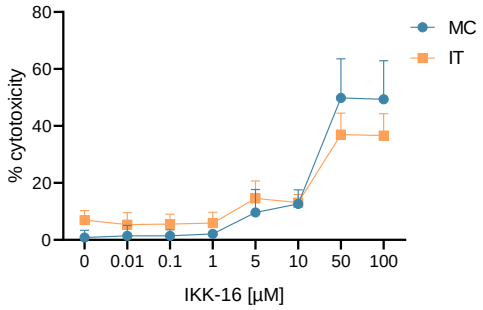

(a) LDH cytotoxicity assay after 24 h.

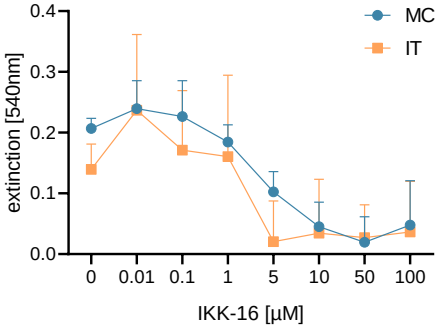

(b) Crystal violet assay after 24 h.

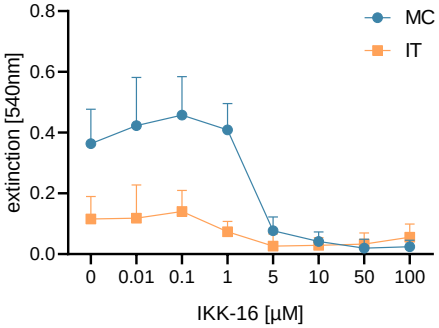

(c) Crystal violet assay after 48 h.

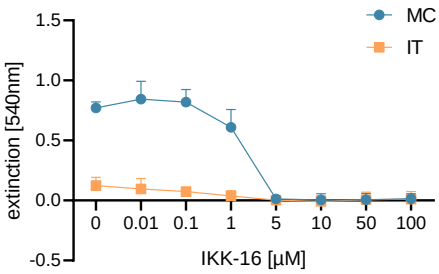

(d) Crystal violet assay after 72 h.

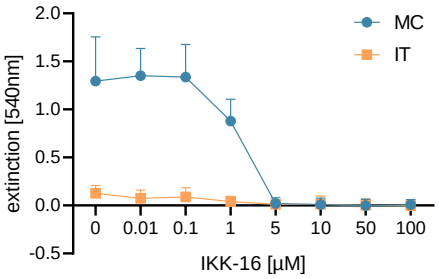

(e) Crystal violet assay after 96 h.

Figure 3.15: Titration of the IKK-1 and IKK-2 inhibitor IKK-16. Concentrations from 0.01 µM up to 100 µM IKK-16 were tested, either alone or in combination with IFNγ and TNF. Here, a LDH cytotoxicity assay after 24 h incubation (a) and crystal violet assays after 24 h, 48 h, 72 h and 96 h incubation are shown ((b) to (e)). (n=4)

IKK-2 leads to a decreased expression of JunB, thus preventing A204 cancer cells from becoming senescent. For this reason, the following experiments were conducted with an IKK-16 concentration of 1 µM to 0.1 µM.

The subsequent approach was used to test whether the inhibitor effectively inhibits the IKK-1 and IKK-2 kinases and whether this results in a decreased expression of JunB. For this purpose, A204 cancer cells were treated with DMSO (negative control) or an IKK-16 concentration of 0.1 µM, with or without the addition of the T_h1 cytokines IFNγ and TNF (Figure 3.16). The cells were harvested at four different time points (0.5 h, 1 h, 2 h, 4 h) after treatment start and subsequently analyzed by Western Blot.

At the beginning of the treatment, no JunB expression is detected in any of the treatment groups (0.5 h, Figure 3.16). After 1 h of incubation, a slight increase of JunB protein expression is detectable in the DMSO cytokine-treated samples. During the course of treatment, the expression of JunB increases continuously in the cytokine-treated DMSO samples and is highest after 4 h. In the samples that were treated with medium alone, no JunB induction is seen, independent of the application of IKK-16. Comparing the DMSO-treated cells with the IKK-16-treated samples, no difference regarding the JunB protein expression is observed. Thus, the treatment with 0.1 µM IKK-16 has no influence on the cytokine-dependent expression of JunB.

Next, the experiment was repeated with 1 µM IKK-16 (Figure 3.18). Similar to Figure 3.16, no JunB expression is found in any of the treatment groups after 0.5 h (Figure 3.18a). However, an increased expression of JunB can be seen after 2 h in the cytokine-treated DMSO sample. Comparing the JunB expression of the DMSO and 1 µM IKK-16 sample after 2 h incubation with the T_h1 cytokines, a significant decreased expression of JunB can be found (Figure 3.18a and Figure 3.19a).

After a total incubation time of 4 h, the expression of JunB becomes more intense in the cytokine-treated DMSO control. However, the expression of JunB increases slightly in the cytokine-treated inhibitor sample, too. Nevertheless, the difference of the JunB expression between the cytokine-treated DMSO control and the cytokine-treated 1 µM IKK-16 sample is significant (Figure 3.19a). In sum, the application of 1 µM IKK-16 reduces the cytokine-dependent expression of JunB.

Subsequently, another Western Blot was performed with the lysates of the 2 h and 4 h samples to analyze the impact of the inhibitor on the phosphorylation of IκBα. As Figure 3.18b and Figure 3.19b show, the use of 1 µM IKK-16 prevents the IKK-1 and IKK-2 -mediated phosphorylation of IκBα within 2 h of incubation. The overall expression of IκBα itself is not affected. Hence, the application of 1 µM IKK-16 leads to a reduced phosphorylation of IκBα.

The results of the above described experiments show that the concentration of 0.1 µM IKK-16 has a tolerable cytotoxicity (Figure 3.15), but is not sufficient to inhibit the expression of JunB (Figure 3.16 and Figure 3.17). In contrast, a satisfactory inhibition of

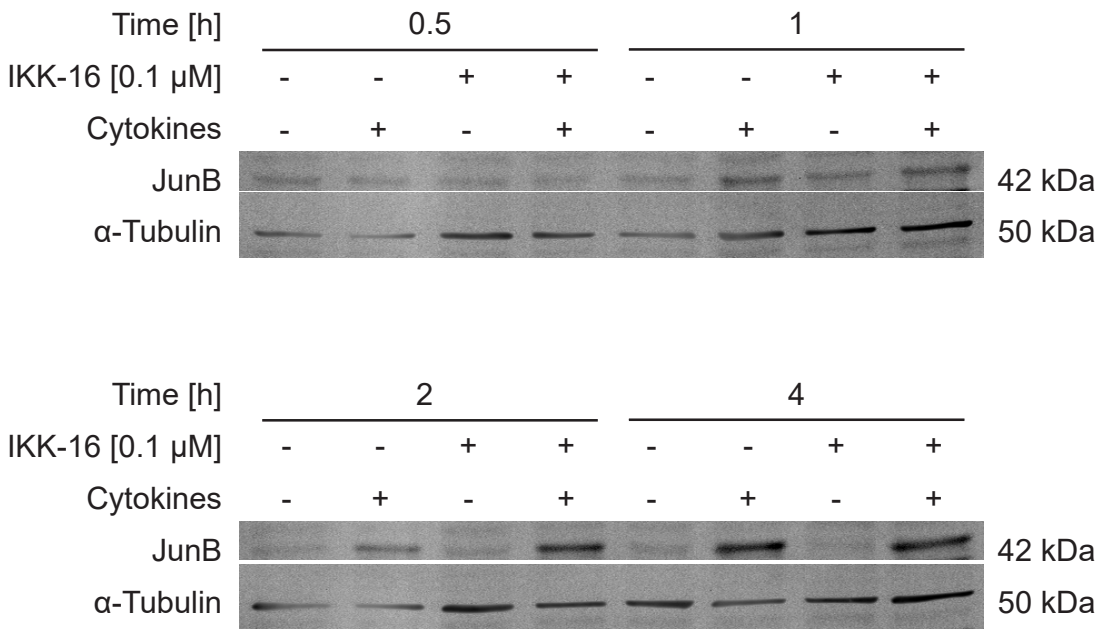

Figure 3.16: Incubation of A204 cancer cells with 0.1 µM IKK-16 inhibitor. JunB expression is not observed until 1 h of treatment with IFNγ and TNF. Moreover, the application of 0.1 µM IKK-16 cannot suppress the cytokine-dependent expression of JunB. Representative Western Blots are shown. (n=3)

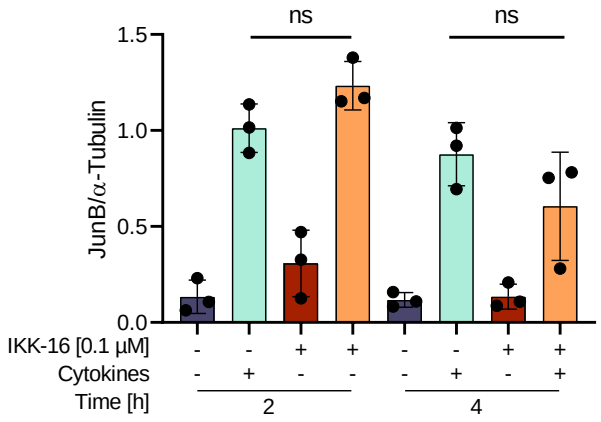

Figure 3.17: Application of 0.1 µM IKK-16 is not sufficient to inhibit the expression of JunB. Despite incubation with 0.1 µM IKK-16 for up to 4 h, the cytokine-dependent JunB expression cannot be reduced (compare Figure 3.16). (n=3)

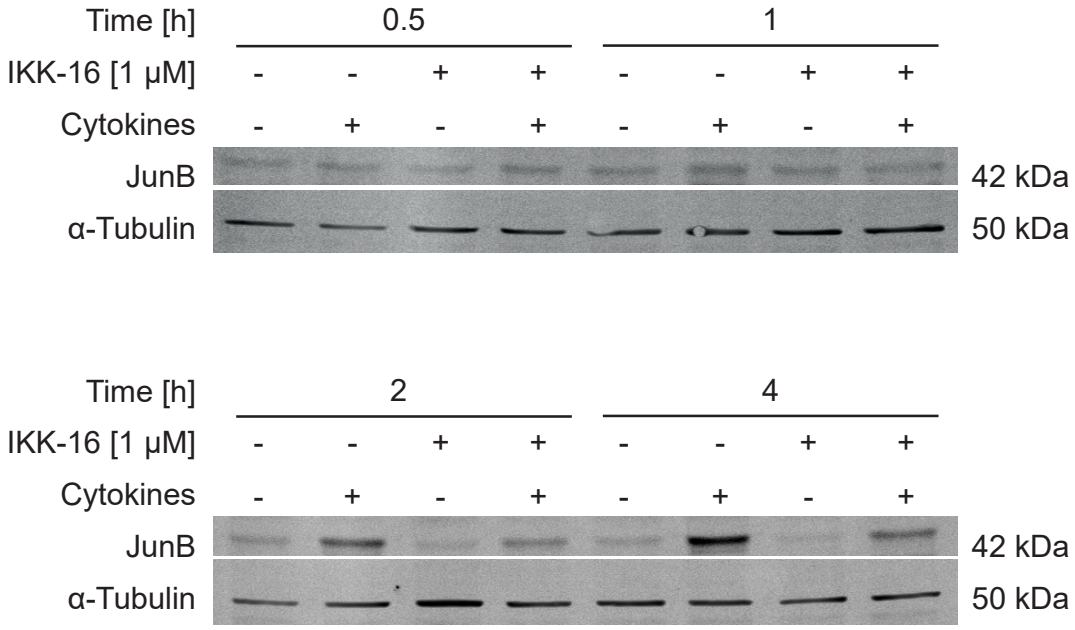

(a) JunB protein expression.

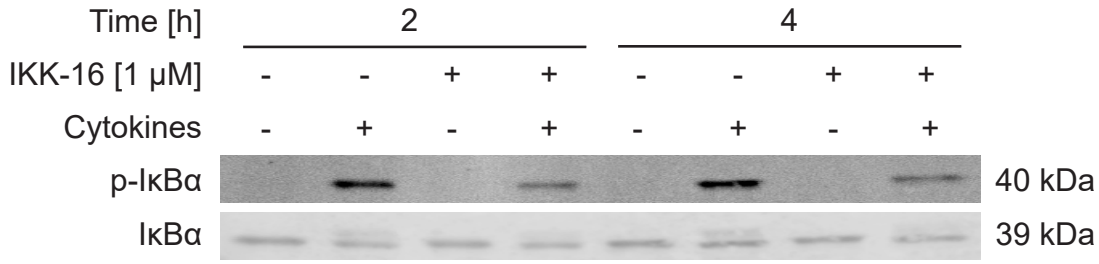

(b) pIκBα and IκBα protein expression.

Figure 3.18: Inhibition of JunB expression after treatment with 1 µM IKK-16. The cytokine-dependent expression of JunB continuously increases over the course of 4 h (a). This effect is suppressed by the addition of 1 µM IKK-16. Furthermore, the inhibitor successfully suppresses the IKK-1 and IKK-2-mediated phosphorylation of IκBα (b). Representative Western Blots are shown. (n=3)

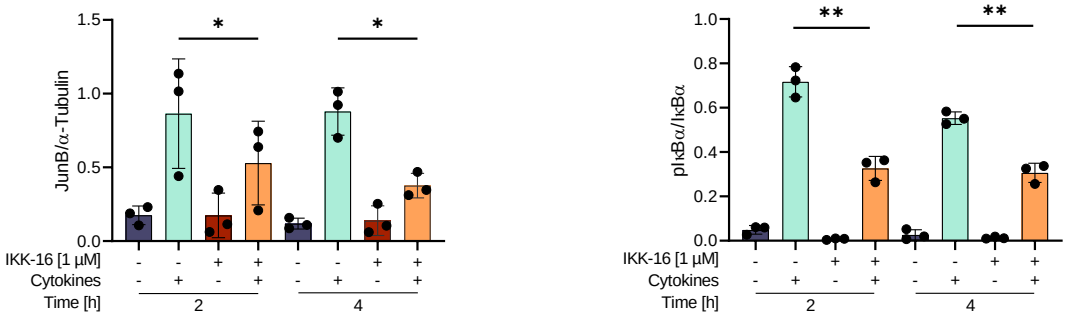

(a) Densiometric quantification of JunB protein expression.

(b) Densiometric quantification of pIκBα protein expression.

Figure 3.19: Inhibition of cytokine-dependent phosphorylation of IκBα leads to a significant reduction of JunB protein expression. The densiometric analyses of Figure 3.18 show that an incubation time of 2 h to 4 h is necessary to detect a significant difference in protein levels of JunB and pIκBα. (n=3)

the cytokine-dependent expression of JunB or phosphorylation of IκBα, respectively, is achieved by using 1 µM IKK-16 (Figure 3.18, Figure 3.19). However, this concentration has shown increased cytotoxicity in the crystal violet assay, especially for longer incubation times (Figure 3.15). Since the aim is to incubate the inhibitor together with the T_h1 cytokines for 96 h with the A204 cancer cells, the inhibitor had to be titrated once more.

For this purpose, an IKK-16 concentration of 0.5 µM was tested for its cytotoxic properties. In addition to the treatment with medium or the combination of the T_h1 cytokines, IFNγ and TNF were added separately in decreasing concentrations to test for cytokine specific sensitivities.

Figure 3.20 shows the results of the LDH assay after 24 h incubation time. Similar to Figure 3.15, a treatment with both IFNγ and TNF leads to a slight increase in cytotoxicity (cytotoxicity value approx. 7%). However, there is no difference between DMSO and inhibitor-treated samples. The IFNγ single treatments (100 ng mL^{-1} to 10 ng mL^{-1}) on the other hand do not display any cytotoxic effects. Its cytotoxicity value is comparable to the medium control-treated cells (cytotoxicity value approx. 2%). In contrast, the treatment with 400 pg mL^{-1} of TNF alone shows increased cytotoxicity, comparable to the double cytokine-treated cells (cytotoxicity value approx. 7%). The cytotoxic effects decline with decreasing TNF concentration from an approximately cytotoxicity value of 7% to 4% (200 pg mL^{-1} to 40 pg mL^{-1} of TNF). Overall, no significant differences are found between the DMSO-treated cells and the 0.5 µM or 1 µM IKK-16-treated cells, regardless of the cytokines used.

In order to investigate the cytotoxic and proliferation-inhibiting effects of inhibitor treatment in combination with cytokine titration, crystal violet assays were performed 24 h, 48 h, 72 h, and 96 h after treatment start.

In Figure 3.21a, the 24 h value of the crystal violet assay is shown. At this time point, a reduced extinction is detectable in the double cytokine-treated cells compared to the medium-treated cells (extinction value approx. 0.15 versus 0.25). On the other hand, as in Figure 3.20, there is no effect found in cells treated with IFNγ alone, independent of the concentration used (extinction value approx. 0.27). The analysis of the extinction values of the TNF single treatments shows a reduced extinction for all TNF concentrations. Here, the DMSO-treated cells displays an extinction value of approx. 0.25, whereas the 0.5 µM and 1 µM IKK-16-treated cells have a lower extinction value (extinction value approx. 0.15). In conclusion, no differences are found between the application of 0.5 µM or 1 µM IKK-16 within in first 24 h of treatment.

After 48 h, the difference of the extinction values between the medium-treated cells (extinction value approx. 0.4) and the double cytokine-treated cells (extinction value approx. 0.15) became more pronounced (Figure 3.21b). Within these groups, however, only a marginal difference between DMSO-treated cells and IKK-16-treated cells is observed. Moreover, the IFNγ single-treated cells display no differences regarding the average extinction value (extinction value approx. 0.35) compared to the medium-treated cells (extinction value approx. 0.4). Nevertheless, significant differences of the extinction are found within the IFNγ-treated group between the DMSO and 0.5 µM IKK-16-treated cells. The treatment with 400 pg mL^{-1} TNF shows a lower extinction value (approx. 0.3) compared to the medium-treated cells (extinction value approx. 0.4). The additional treatment with 0.5 µM or 1 µM IKK-16 results in even lower extinction values (extinction value approx. 0.2). However, the extinction values are still higher compared to the double cytokine-treated cells. Furthermore, it can be observed that with decreasing TNF concentrations the extinction values increase (extinction value of 200 pg mL^{-1} TNF approx. 0.2, extinction value of 40 pg mL^{-1} TNF approx. 0.3). In summary, no differences are found between the treatment with 0.5 µM or 1 µM IKK-16 after 48 h.

An incubation time of 72 h results in an average extinction value approx. 0.7 for the medium-treated control (Figure 3.21c). Here, no difference can be found between the DMSO control and the IKK-16-treated cells. Looking at the double cytokine treatment, no difference between the DMSO and the inhibitor-treated samples are observed. Here, however, the lowest extinction value is found again (extinction value approx. 0.1). With regard to the single IFNγ-treated cells, no difference can be observed between the different IFNγ concentrations, as well as between DMSO and inhibitor treatment. The average extinction value is approx. 0.5. The single treatment with 400 pg mL^{-1} TNF shows an extinction value of approx. 0.5 for the DMSO treatment. In contrast, the inhibitor applications display an average extinction value of approx. 0.3. However, the difference is not significant. As already shown in Figure 3.21b, the extinction values increase with decreasing TNF concentration. In summary, no increased sensitivity of the inhibitor-treated

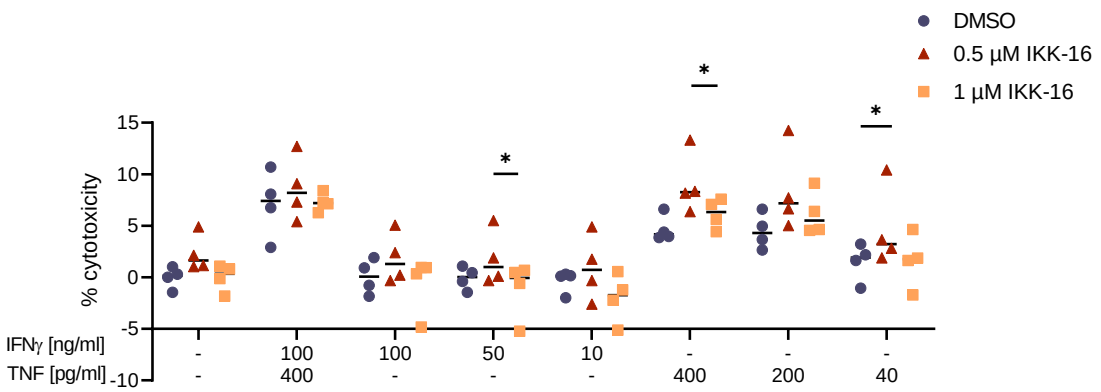

Figure 3.20: LDH cytotoxicity assay shows no differences between the application of 0.5 µM or 1 µM IKK-16 after 24 h. Treatment with IFNγ and TNF leads to increased cytotoxicity in both DMSO and inhibitor-treated cells. Similar results are also observed in the TNF single treatment. In contrast, the medium control and cells treated with IFNγ only do not show any cytotoxic effects. (n=4)

cells to a single cytokine treatment is observed after 72 h of incubation.

After a total incubation time of 96 h, the extinction value of the medium-treated DMSO control increased further up to approx. 1.3 (Figure 3.21d). The medium-treated 1 µM IKK-16-treated cells also increased the extinction value compared to the 72 h, but it is significantly lower than in the DMSO control (extinction value approx. 0.7). The 0.5 µM IKK-16 with an extinction value of approx. 1.0 lies in between; however, it is not significant. Furthermore, in the double cytokine-treated cells the extinction values are the lowest in the crystal violet assay after 96 h (extinction value approx. 0.1) Within this group, no difference can be found. In the IFNγ single-treated cells, the extinction value is on average 0.7. Once again, there is no IFNγ concentration-dependent influence on the extinction value. The extinction value of the 400 pg mL^{-1} TNF DMSO-treated cells is approx. 1.0. With increasing IKK-16 concentration, the extinction values decreases, resulting in an extinction value of approx. 0.4 for 1 µM IKK-16. However, the difference is not significant, which is due to the variability of the single measured values. The negative correlation of the TNF concentration to the extinction value can also be observed after 96 h treatment time.

In summary, the results of Figure 3.20 and Figure 3.21 show that the cytotoxicity for 0.5 µM IKK-16 lies between 1 µM IKK-16 and the DMSO control. Furthermore, 0.5 µM IKK-16 is tolerable for A204 cancer cells. In addition, it could be shown that IKK-16 treatment does not lead to an increased sensitivity to any of the cytokines. Even in the double cytokine-treated cells, no significant difference between the DMSO control and the IKK-16-treated cells was found at any time point.

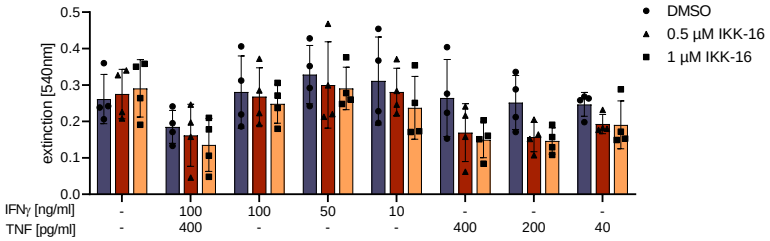

(a) Crystal violet assay after 24 h.

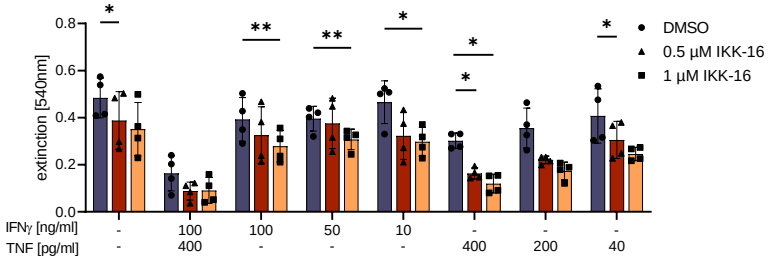

(b) Crystal violet assay after 48 h.

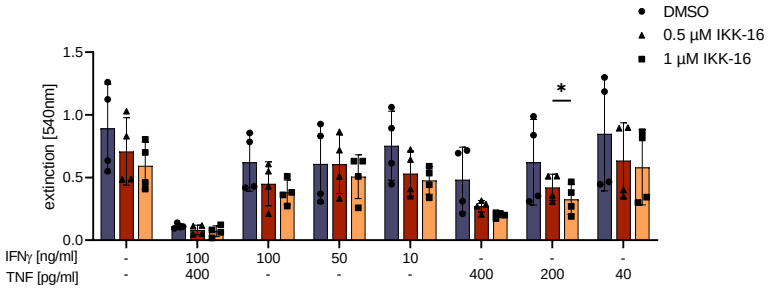

(c) Crystal violet assay after 72 h.

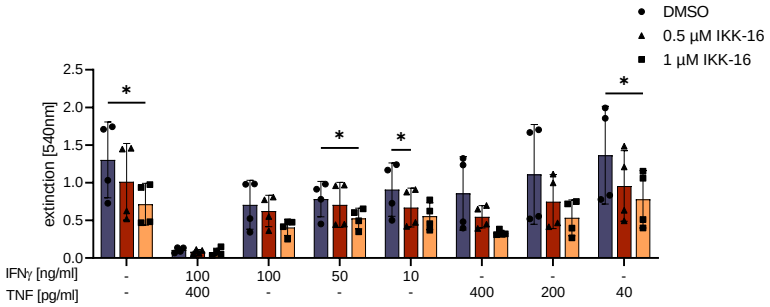

(d) Crystal violet assay after 96 h.

Figure 3.21: Crystal violet assays show moderate cytotoxicity using 0.5 µM IKK-16. Over the course of 96 h, the extinction values increase for all treatments, but stagnate for cells treated with IFNγ and TNF. Also, the use of single cytokine treatment reveals no sensitivity of the inhibitor treatment compared to the DMSO control. (n=4)

The next step was to test whether a concentration of 0.5 µM IKK-16 is sufficient to suppress the NF-κB signaling pathway and thereby reduce the cytokine-dependent expression of JunB. Like in Figure 3.16 and Figure 3.18, A204 cancer cells were treated with declining concentrations of IKK-16 (1 µM, 0.5 µM, and 0.1 µM), either with or without addition of IFNγ and TNF. Cells were harvested after 2 h and 4 h and subsequently analyzed using Western Blot.

As can be seen in Figure 3.22a and Figure 3.23a, the cytokine-treated DMSO control cells display a JunB expression after 2 h of incubation. This expression is reduced by the application of 1 µM IKK-16, as already shown in Figure 3.18. The exposure to 0.5 µM IKK-16 also leads to a decreased JunB protein expression. However, the inhibition is not as strong as after the treatment with 1 µM IKK-16. Yet the inhibition of JunB expression is stronger compared to the use of 0.1 µM IKK-16. Moreover, Figure 3.22b and Figure 3.23b show the expression of IκBα and its phosphorylation, respectively. The cytokine-dependent phosphorylation of IκBα is diminished after the application of IKK-16. More specifically, a concentration of 0.5 µM IKK-16 results in a sufficient inhibition of pIκBα.

After 4 h incubation time, the concentration-dependent effect of IKK-16 is even more evident (Figure 3.22c and Figure 3.23c). Here, the negative correlation between the increasing inhibitor concentration and the decreasing JunB expression and phosphorylation of IκBα, respectively, is clearly visible (Figure 3.22d and Figure 3.23d).

The results of Figure 3.22 and Figure 3.23 demonstrate a sufficient reduction of IκBα phosphorylation and expression of JunB for early time points by using 0.5 µM IKK-16. For the induction of CIS, however, an overall incubation time of 96 h is required. In the following experiment, A204 cancer cells were treated with IKK-16 (0.5 µM and 1 µM) as well as with T_h1 cytokines for the duration of 96 h. After 4 h (early time point), 48 h (mean time point of induction) and 96 h (end of CIS induction) samples were harvested for Western Blot analysis.

Figure 3.24 and Figure 3.25 show the results of the experiment. Similar to Figure 3.22c and Figure 3.23c, JunB cytokine-dependent expression is significantly inhibited after an incubation period of 4 h by the addition of 1 µM and 0.5 µM IKK-16, respectively (Figure 3.24 and Figure 3.25a). After 48 h, the inhibition of JunB expression is still detectable (Figure 3.24 and Figure 3.25b). Even after a total incubation time of 96 h the inhibitor is still effective and reduces the expression of JunB (Figure 3.24 and Figure 3.25c).

In conclusion, the results of this experiment show that the inhibitor IKK-16 remains effective for about 96 h, thereby reducing JunB expression during CIS induction.

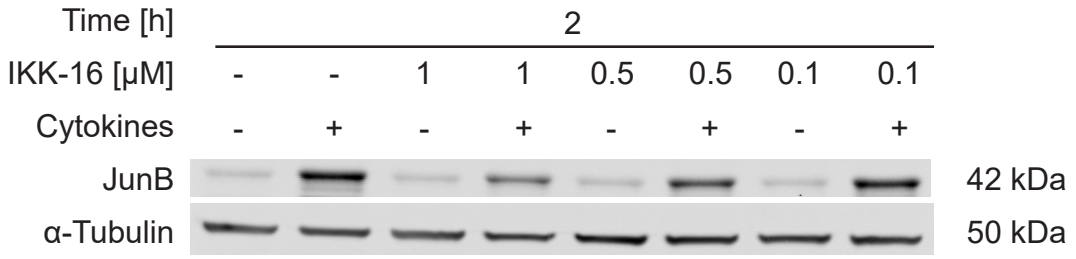

(a) JunB protein expression after 2 h of cytokine treatment.

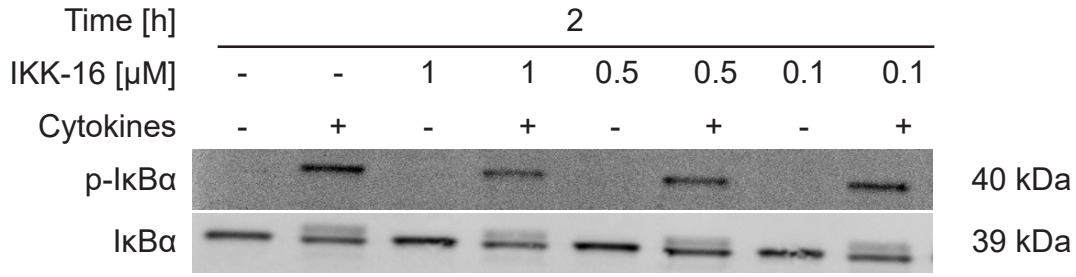

(b) pIκBα and IκBα protein expression after 2 h of cytokine treatment.

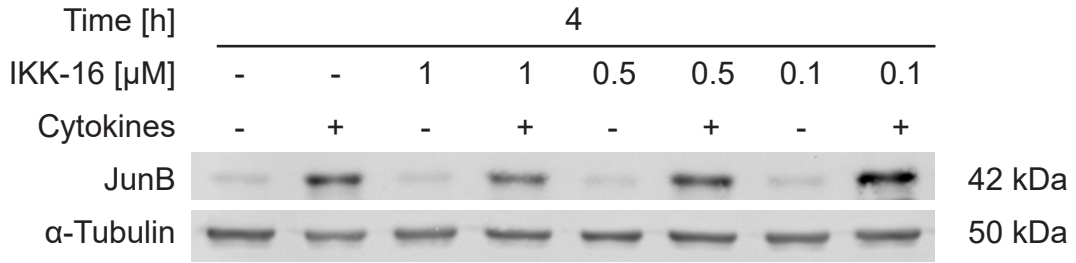

(c) JunB protein expression after 4 h of cytokine treatment.

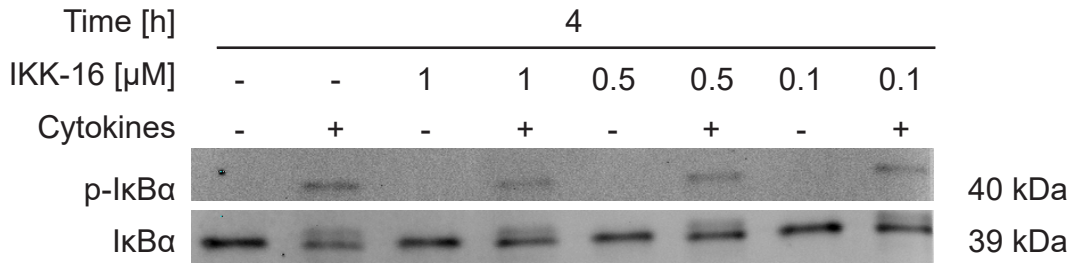

(d) pIκBα and IκBα protein expression after 4 h of cytokine treatment.

Figure 3.22: Using a concentration of 0.5 µM IKK-16 leads to reduced protein levels of JunB or pIκBα. While the cytokine-treated DMSO samples show an increase in JunB expression and phosphorylation of IκBα, IKK-16-treated cells display a decreased level of those proteins. Representative Western Blots are shown. (n=3)

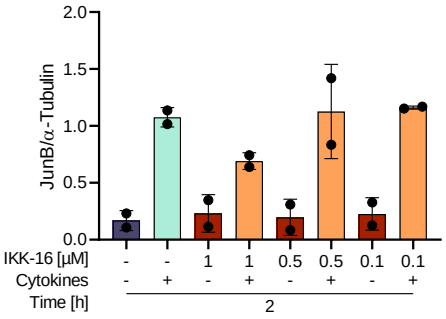

(a) Densiometric quantification of JunB protein expression after 2 h of cytokine treatment.

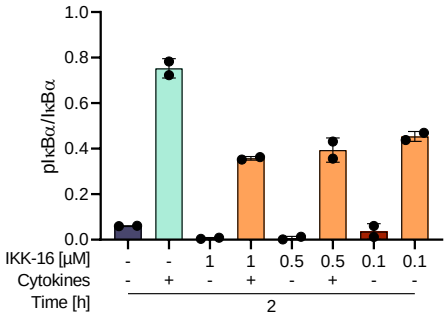

(b) Densiometric quantification of pIκBα protein expression after 2 h of cytokine treatment.

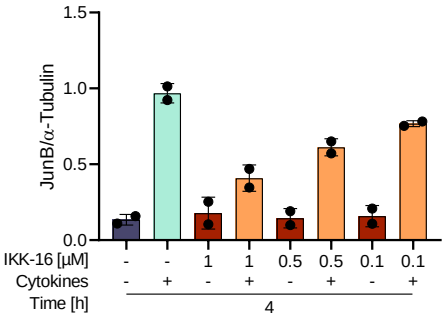

(c) Densiometric quantification of JunB protein expression after 4 h of cytokine treatment.

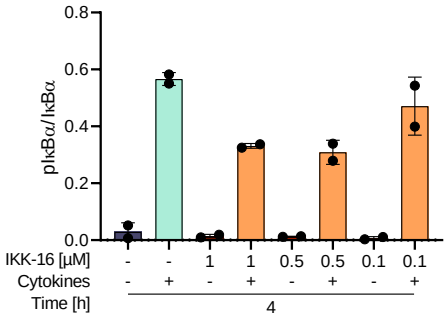

(d) Densiometric quantification of pIκBα protein expression after 4 h of cytokine treatment.

Figure 3.23: Densiometric quantification of JunB protein expression and phosphorylated IκBα. The samples were treated with IKK-16 concentrations of 1 µM, 0.5 µM and 0.1 µM, either alone or in combination with IFNγ and TNF. The samples were harvested after 2 h or 4 h of treatment and subsequently analyzed by Western Blot. (n=2)

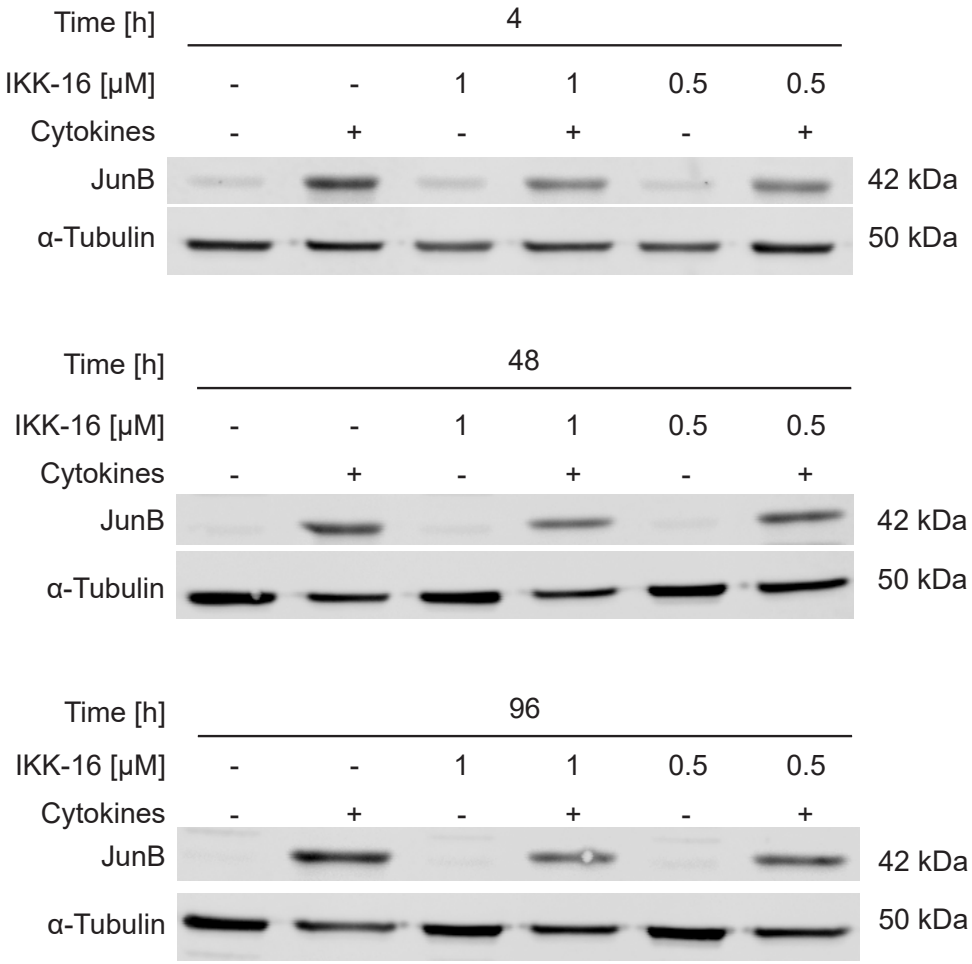

Figure 3.24: Inhibition of the cytokine-dependent expression of JunB is sustained over the course of CIS induction. The use of 1 µM, respectively 0.5 µM, IKK-16 is sufficient to reduce the expression of JunB at early (4 h), middle (48 h), and late (96 h) incubation times. Representative Western Blots are shown. (n=3)

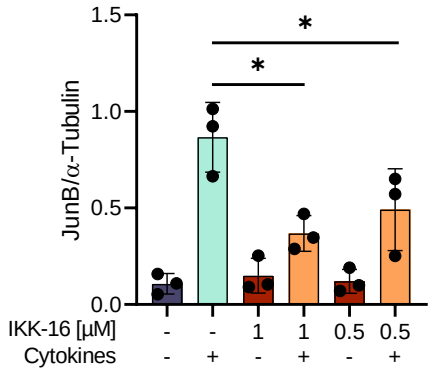

(a) JunB protein expression after 4 h.

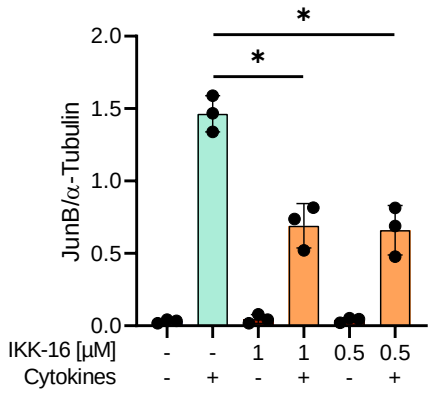

(b) JunB protein expression after 48 h.

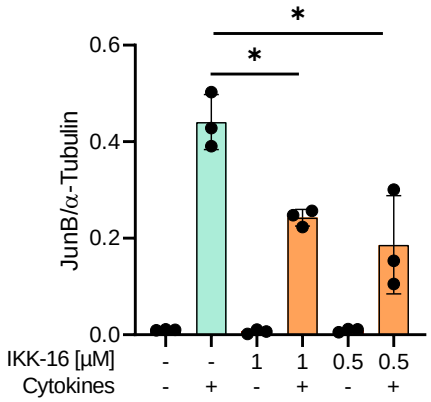

(c) JunB protein expression after 96 h.

Figure 3.25: Densiometric quantification of JunB protein expression during incubation with cytokines and/or IKK-16. The Western Blot analyses (Figure 3.24) show a significant reduction of JunB protein levels for all three time points measured. Moreover, 0.5 µM IKK-16 is sufficient to decrease the cytokine-dependent expression of JunB. (n=3)

3.4 Pharmacological downregulation of JunB does not effect the induction of CIS

In the previous experiments, a tolerable and effective concentration of IKK-16 was found. Furthermore, it was shown that IKK-16 inhibits the cytokine-dependent expression of JunB over a period of 96 h. In the following, the relationship between the reduced JunB expression and the induction of CIS is investigated. For this purpose, a growth arrest assay with A204 cancer cells was performed. Cells were treated for 96 h with medium or the T_h1 cytokines, either in combination with DMSO, 0.5 µM IKK-16, or 1 µM IKK-16 (passage -1). After the first 96 h, the cells were trypsinized, counted, and reseeded in medium without any inhibitor or cytokines present (passage 0). The process was repeated after an additional 96 h of incubation (passage 1). A proliferation index (Equation (2.2)) was calculated from these counts. In Figure 3.26, the results of the growth arrest assay are shown.

In the beginning, 3×10^5 cells per treatment group were seeded (passage -1). After an incubation time of 96 h, an increased cell count is observed in medium-treated DMSO control cells (cell count approx. 1.3×10^6). Similar increases in cell count are found in medium-treated 0.5 µM IKK-16 and 1 µM IKK-16, respectively. However, no difference is observed between these groups at passage 0. In contrast, the application of IFNγ and TNF in the DMSO control cells results in a stagnation of the cell count (cell count approx. 3×10^5). However, as soon as the cells are treated with IKK-16 in addition to the T_h1 cytokines, the cell number decreases further with increasing IKK-16 concentration (0.5 µM IKK-16 cell count approx. 2×10^5, 1 µM IKK-16 cell count approx. 8×10^4). After cells have been reseeded and counted after additional 96 h (passage 1), a further increase of the cell count can be seen in all medium-treated cells (cell count for DMSO, 0.5 µM IKK-16 and 1 µM IKK-16 approx. 7×10^7). At the same time, the cytokine-treated DMSO cells display a slight increase in cell count at passage 1 (cell count about 2×10^6). Similarly, the inhibitor-treated cells show an increase in cell numbers after cytokine treatment (0.5 µM cell count approx. 1×10^6, 1 µM IKK-16 cell count approx. 4×10^5).

In summary, the results show that the application of the IKK-1 and IKK-2-inhibitor IKK-16, which leads to a reduced NF-κB signaling and in consequence to a reduction of the JunB signaling pathway, does not prevent the induction of the cytokine-induced senescence.

3.5 Downregulation of JunB mediated by siRNA does not influence CIS induction

In previous experiments, a downregulation of JunB expression was achieved with the inhibitor IKK-16. However, since it inhibits the kinases IKK-1 and IKK-2, JunB was

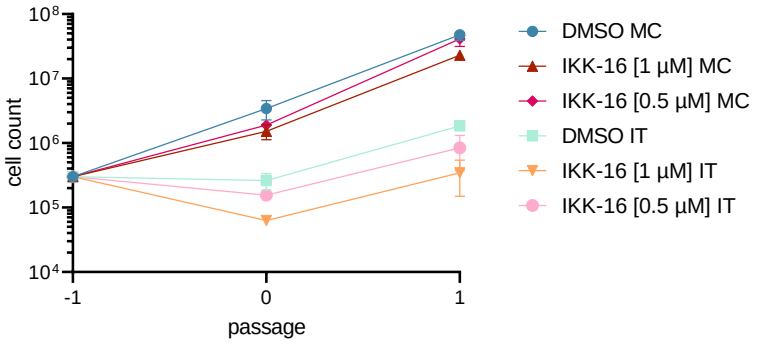

Figure 3.26: Growth arrest induction is not prevented by IKK-16 treatment. Despite the reduced IκBα phosphorylation and therefore decreased JunB expression, CIS induction is observed. (n=3)

Abbreviations: IT (IFNγ + TNF), MC (medium control).

only indirectly regulated. Besides cytotoxic effects, other side effects of the inhibitor treatment cannot be excluded when using the inhibitor. Therefore, the next step was to regulate JunB expression by siRNA. The used pool of siRNA covers five different JunB mRNA sequences (Table 2.6). After transfection, the siRNA is transferred into the RNA-induced silencing complex (RISC), leading to the degradation of the JUNB mRNA. This results in a reduced JunB protein expression in the cells. Results from preliminary experiments showed that 24 h of treatment with siRNA is sufficient to reduce JunB expression (data not shown). Furthermore, these experiments showed that the strongest downregulation of JunB is found 72 h after the start of treatment. In order to test the effect of the reduced JunB expression on the induction of CIS, a treatment scheme was established (Figure 3.27). Here, A204 cancer cells are seeded and treated with siRNA after 24 h. After additional 24 h, the medium is replaced. Cells remain in normal cell culture medium for additional 48 h. After a total incubation time of 72 h, the cells are treated with either medium or the T_h1 cytokines IFNγ and TNF for 96 h. Cells are then counted and reseeded at the original cell count (passage 0). The treatment scheme was repeated two more times (until passage 2). In Figure 3.28, the results of this experiment are displayed. To prove that JunB expression is reduced at the beginning of the senescence induction, a Western Blot was performed. As can be seen in Figure 3.28a, the expression of JunB in siJUNB transfected cells is considerably reduced compared to siCtrl transfected cells after cytokine treatment. The results of the growth arrest assay show that the cytokine-treated siJUNB and siCtrl cells entered a growth arrest at passage 0 (cell count approx. 4×10^4). However, the medium-treated cells grow exponentially throughout the treatment (cell count at passage 0 approx. 8×10^6, passage 1 approx. 5×10^8, passage 2 approx. 8×10^{10}). After a further treatment round (passage 1), the cell count for the cytokine-treated siJUNB and siCtrl increases slightly (cell count approx. 1×10^5). At the end of treatment (passage 2), the cell count for the cytokine-treated siJUNB and siCtrl

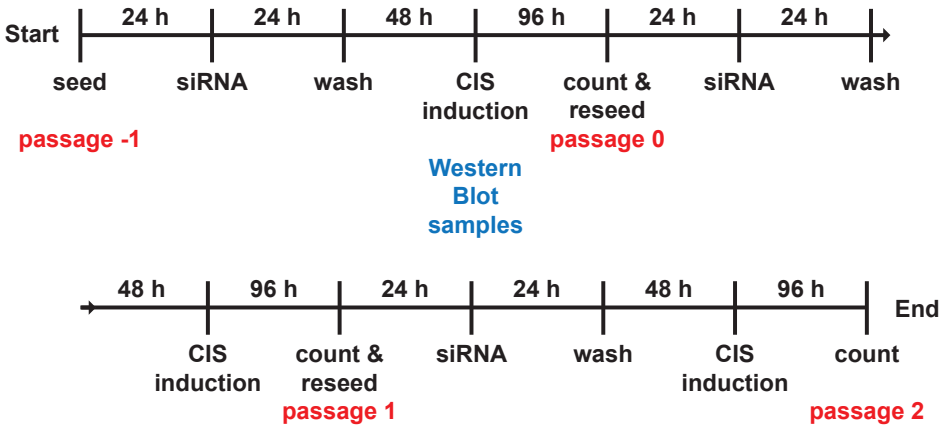

Figure 3.27: Treatment scheme of siRNA growth arrest assay. Initially, 2.5×10^4 cells per treatment group were seeded (passage -1). After 24 h, the cells were treated with siRNA (siCtrl or siJUNB). To avoid cytotoxic effects, the medium was replaced after 24 h (wash), and cells were kept in medium for another 48 h. After a total incubation time of 72 h, cells were treated with IFNγ and TNF for 96 h (CIS induction). In order to show that the JunB expression was downregulated during the initiation of senescence, samples for Western Blot analysis were taken before the start of the 96 h incubation phase. At the end of the senescence induction, cells were counted and reseeded (passage 0). This procedure was repeated until passage 2.

Abbreviations: CIS (cytokine-induced senescence), siRNA (small interfering RNA).

is approx. 2×10^7. In summary, there is no difference between the growth curves of the siJUNB and siCtrl transfected cells. Thus, the downregulation of JunB does not affect the proliferation of A204 cancer cells. No influence on the induction of CIS is observed as well.

3.6 CRISPR/Cas9-mediated knockdown of JunB has no effect on CIS induction

The inhibitor IKK-16 reduced the signal transduction of the TNF signaling pathway pharmacologically, but failed to prevent CIS induction. Moreover, siRNA-mediated reduction of JunB expression could not prevent the induction of CIS as well. Since a residual expression of JunB is still found in both experiments, an attempt was made to create cells with a complete JunB knockout. For this purpose, CRISPR/Cas9 was used in human A204 cancer cells. CRISPR/Cas9 is a tool to specifically excise genes in the genome. The commercially available JunB CRISPR/Cas9 pool from Santa Cruz consists of three CRISPR/Cas9 plasmids, which cover different sequences of the JunB gene with

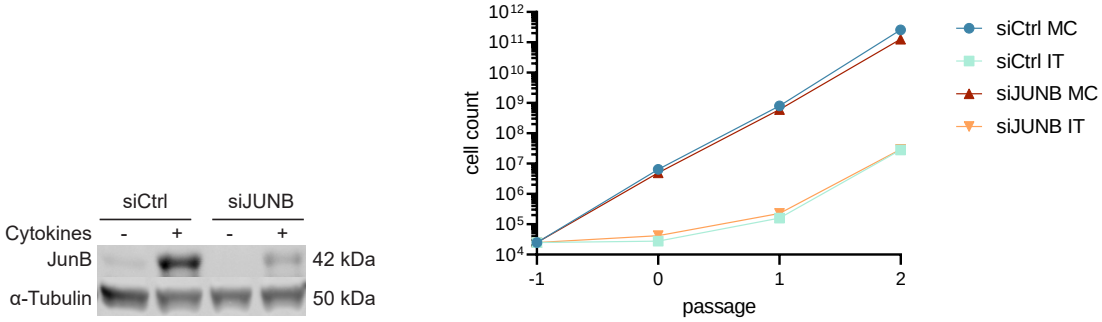

(a) JunB protein expression.

(b) Growth arrest assay.

Figure 3.28: siRNA-mediated downregulation of JunB is not sufficient to prevent CIS induction. Downregulation of JunB is confirmed 72 h after the addition of the siRNA ((a), see also Figure 3.27). The growth arrest assay reveals no difference between the medium and cytokine-treated siCtrl or siJUNB cells (b). Representative Western Blot is shown in (a). (n=3)

Abbreviations: IT (IFNγ + TNF), MC (medium control), siCtrl (control transfected cells), siJUNB (siRNA-mediated JUNB knockdown).

their guide RNA (gRNA). Furthermore, the plasmids contain a GFP transcription site. If the transfection is successful, GFP is produced in the cells, which is used to purify the cells 24 h after transfection using a cell sorter. The GFP^+ cells are pooled and cultured together. Since GFP expression is transient, and no antibiotic resistance was integrated into the genome, the cells cannot be purified again.

In order to confirm a successful JunB knockout, control transfected cells (Ctrl ko) and JUNB knockout (JUNB ko) cells were seeded and treated for 4h with either medium or the T_h1 cytokines IFNγ and TNF. Subsequently, cells were harvested, and protein expression was analyzed by Western Blot. The JUNB mRNA expression was measured via qPCR. The results of the Western Blot are shown in Figure 3.29a and Figure 3.29b. As already known from previous experiments, JunB is not expressed when treated with medium only. Therefore, no or a low JunB protein expression is visible in the medium-treated cells of Ctrl ko and JUNB ko cells. After 4 h incubation with the T_h1 cytokines, an increase in JunB expression is found in the Ctrl ko cells. This also applies for the cytokine-treated JUNB ko cells. However, it is significantly weaker than in the Ctrl ko cells. The analysis of the mRNA confirms the increased JUNB expression after cytokine treatment which was already found for Ctrl ko and JUNB ko cells at the protein level (Figure 3.29c). However, comparing the relative mRNA expression of Ctrl ko to JUNB ko cells, a significant decrease is observed (Ctrl ko rel. mRNA expression 0.03 versus JUNB ko rel. mRNA expression 0.01). For both medium-treated cells, only a minor JUNB expression is found (Ctrl ko and JUNB ko rel. mRNA expression 0.005).

In summary, it was not possible to create a A204-derived JUNB ko cell line. However, JUNB ko cells show a significant reduction of JunB expression in both mRNA and protein expression.

Therefore, a growth arrest assay was performed with the Ctrl ko and JUNB ko cells. For this purpose, 3×10^5 cells per treatment group were seeded (passage -1) and treated with either medium only or the T_h1 cytokines IFNγ and TNF for 96 h. The cells were trypsinized, counted, and reseeded (passage 0). After 96 h, the procedure was repeated (passage 1). Subsequently, after an additional 96 h treatment time, cells were counted once more (passage 2). The results are shown in Figure 3.30.

The number of the medium-treated Ctrl ko cells continuously increases, resulting in cell count of approx. 2×10^6 cells at passage 0, and a cell count of approx. 1×10^7 cells at passage 1. In contrast, the cytokine-treated Ctrl ko cells become growth arrested (cell count at passage 0 approx. 3×10^5). However, the cell count increases slightly at passage 1 (cell count approx. 7×10^5). Like the medium-treated Ctrl ko cells, an exponential cell growth is found in the medium-treated JUNB ko cells (cell count at passage 1 approx. 1×10^7). Overall, the growth curves of medium-treated Ctrl ko and JUNB ko cells are aligned until passage 1. After that, a minor, but not significant, discrepancy is observed. Regarding the growth curve of the cytokine-treated cells, no difference can be seen between the Ctrl ko and JUNB ko cells. In conclusion, the results from Figure 3.29 and Figure 3.30 demonstrate that the CRISPR/Cas9-mediated knockdown of JUNB does not influence the induction of the cytokine-induced senescence.

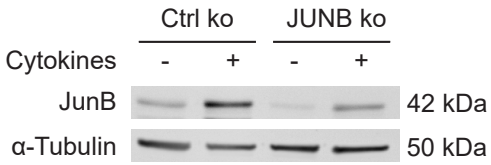

(a) JunB protein expression.

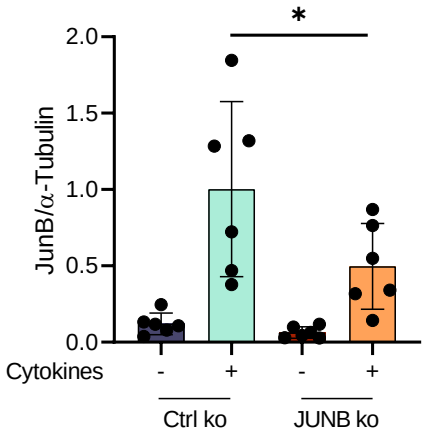

(b) Densiometric quantification of JunB protein expression.

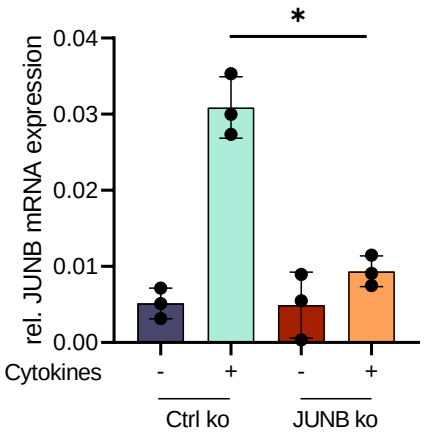

(c) JUNB mRNA expression.

Figure 3.29: CRISPR/Cas9-induced JUNB knockdown in A204 cancer cells. Although a complete knockout of JUNB could not be achieved, JUNB knockout cells show a reduced mRNA level and protein expression after cytokine treatment compared to control transfected cells. Representative Western Blot are shown in (a). ((a) and (b) n=6, (c) n=3)

Abbreviations: Ctrl ko (control transfected cells), JUNB ko (JUNB knockout).

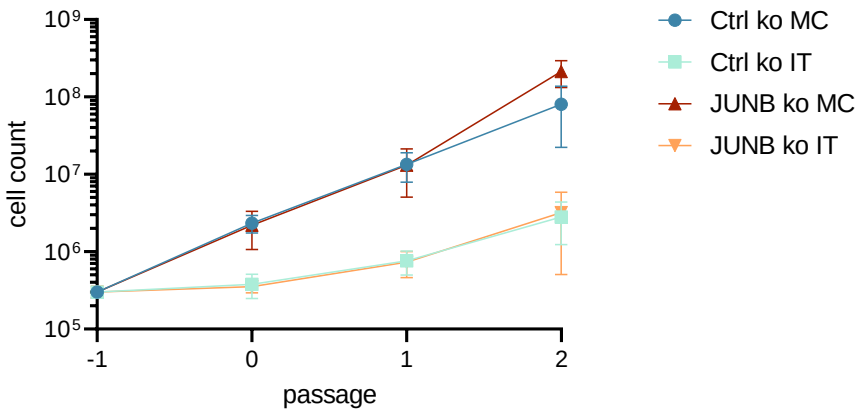

Figure 3.30: Knockdown of JUNB has no impact on cytokine-induced senescence. After 96 h, the cytokine-treated cells of both Ctrl ko and JUNB ko become growth arrested. In contrast, the medium-treated cells (both Ctrl ko and JUNB ko) grow exponentially. Overall, no difference between Ctrl ko and JUNB ko cells is found. (n=3)

Abbreviations: Ctrl ko (control transfected cells), IT (IFNγ + TNF), JUNB ko (JUNB knockout), MC (medium control).

Chapter 4

Discussion

4.1 Chromosomal aberrations in RT2 and RT2xStat1$^{-/-}$ cancer cell lines after *in vitro* cytokine treatment and *in vivo* ICB therapy

4.1.1 No influence on chromosomal aberrations after cytokine treatment in stable RT2 and RIP1-Tag2 x signal transducer and activator of transcription 1$^{-/-}$ cancer cell lines

The aim of the CGH analyses of RT2 tumors was to investigate whether senescence induction with the T_h1 cytokines IFNγ and TNF leads to changes in chromosomal aberration patterns.

The tumors examined in the CGH analyses originated exclusively from the RIP1-Tag2 mouse strain. In these mice, the viral SV40 large T-cell antigen is already embryonically expressed in the insulin-producing β-cells (Hanahan (1985)). This leads to an inhibition of the tumor suppressor p53 in these cells. Without the function of p53 as "guardian of the genome" (Lane (1992)), DNA damages accumulate in the cells, including single nucleotide substitutions and chromosomal aberrations (Bassing and Alt (2004)). In consequence of this loss of genomic integrity, insulinomas develop in the RT2 mice. Although the underlying mechanism of tumor development is the same in all RT2 mice, each mouse, and each tumor accumulates different mutations and chromosomal aberrations. This is also influenced by different environmental conditions that favor specific mutations. As β-cancer cells develop in immunocompetent mice, they are confronted with the immune system. Therefore, mutations that cause a decreased antigen presentation result in a survival advantage for the tumor cell (Leone *et al.* (2013)). In addition, tumor cells that have a higher proliferation rate or are better at exploiting resources (nutrients, oxygen) also have an overall survival benefit (Galmarini *et al.* (2000)). Among all of the acquired mutations, both driver and passenger mutations can be found. While driver mutations enable the survival and proliferation of the tumor cell, passenger mutations come along with the driver mutation but do not offer any advantage or disad-

vantage to the cell (Greaves and Maley (2012)). Although the emergence of mutations is a random process, their establishment is not. During tumor progression, mutations and chromosomal aberrations repeatedly develop (Albertson *et al.* (2003)). If these are beneficial or at least not harmful for survival and progression, the cell continues to proliferate. Through this process, mutations gradually accumulate. However, if the genetic alterations are harmful, the cells could die or become growth-arrested like, for example, in cells with MYC overexpression (Pelengaris *et al.* (2002)).

In the here performed CGH analyses the accumulation of different chromosomal aberrations of the RT2 cancer cell lines 1 and 2 can be seen (Figure 3.2 and Figure 3.3). While in RT2 cancer cell line 1 (Figure 3.2) deletions are present on chromosome 1, 3, 6, 9, and 16, only chromosome 3, 6, and 9 are depleted in RT2 cancer cell line 2 (Figure 3.3). Furthermore, the RT2xStat1$^{-/-}$ cancer cell line in Figure 3.4 displays a partial deletion on chromosome 6 as well. The deletions found for chromosomes 6 and 9 are among those typically found in RT2 tumors (Hodgson *et al.* (2001)). However, most of the deletions present in the different cancer cell lines are unique. Regarding amplification, a partially amplified region is found on chromosome 2 in both RT2 cell lines and in the RT2xStat1$^{-/-}$ cancer cell line (Figure 3.2, Figure 3.3, and Figure 3.4). However, there are also differences in amplification between the cancer cell lines described. Thus, the direct comparison of these primary RT2 and RT2xStat1$^{-/-}$ cancer cell lines reveals that the tumors, although originating from the same genetic background, develop different chromosomal aberrations.

Regarding cytokine treatment, none of the RT2 cancer cell lines from Figure 3.2 and Figure 3.3 show any change in chromosomal aberrations. In the absence of STAT1 (Figure 3.4), there is no difference between the untreated, medium control, and IFNγ and TNF-treated cells as well. Up to this point, none of the RT2 or STAT1 cancer cell lines displayed any change in chromosomal aberrations during T_h1 cytokine treatment.

Therefore, one can conclude that the senescence induction with T_h1 cytokines does not lead to changes in chromosomal aberrations in primary RT2 cancer cell lines. Whether epigenetic modifications, such as histone modifications or DNA methylation, occur instead, cannot be analyzed with the CGH method. Nevertheless, the results of the RT2 cancer cell line 3 present a different picture, which does not necessarily contradict the previous results.

4.1.2 T_h1 cytokine treatment can modify chromosomal aberration in unstable RT2 cancer cell lines

In contrast to RT2 cancer cell line 1, 2, and RT2xStat1$^{-/-}$ cancer cell line, the chromosomal aberrations of the RT2 cancer cell line 3 appear to be altered, after medium as well as after T_h1 cytokine treatment. The CGH analysis in Figure 3.7 shows an increasing loss of the chromosomes 4 and 14 already present in the medium control which is enhanced by the treatment with the T_h1 cytokines. At first it is surprising that, in contrast

to the previous described cancer cell lines, the T_h1 cytokine treatment leads to changes in chromosomal aberrations in this cancer cell line. Nevertheless, since the shift in chromosomes 4 and 14 is observed in the medium control treatment as well, the cytokine treatment alone cannot be responsible for this. Instead, it is more convincing that the CGH analyses captured the time point in which the ratios of the subpopulations in RT2 cancer cell line 3 changed due to selection pressure.

The heterogeneous population of β-cancer cell lines is a result of the generation process of the RT2 cancer cell lines. During preparation, several β-cancer cell tumors from the same mouse are collected and homogenized together. From this cell suspension, the primary cancer cell line is established, i.e., each β-cancer cell line consists of a mixed population of tumors. Besides the above described intertumoral heterogeneity, the intratumoral heterogeneity of RT2 tumors leads to a further increase in genetic diversity (Landau *et al.* (2013), Brenner *et al.* (2020)). The CGH results generated from the primary RT2 cancer cell lines thus show the chromosomal aberrations that dominate within the population. Individual clones or small subpopulations cannot be detected in the CGH used in this thesis. This would require a single cell CGH analysis.

While the RT2 tumor cells are being transferred from an *in vivo* environment to an *in vitro* setting, the cells have to adapt to the altered conditions, such as nutrition availability, O_2 and CO_2 concentrations (Greaves and Maley (2012), Fukumura *et al.* (2010), Brown *et al.* (2001)). It is possible that a cell population that initially represented the main fraction of the RT2 cancer cell line is less adapted to the *in vitro* environment. Thus, an initially smaller but better-adapted cell population can overtake the main population (Shackleton *et al.* (2009)). This was probably the case with RT2 cancer cell line 3. Since the experiment was performed during the transition of this cancer cell line, the RT2 cancer cell line 3 was still responding in a growth arrest assay after T_h1 cytokine treatment. However, with each further cell division, the ratio of the subpopulations changes. This explains the already significant loss of chromosome 4 and 14 in the medium-treated sample (Figure 3.7). As can be seen in the CGH analysis, T_h1 cytokine treatment results in an increased loss of chromosome 4 and 14. Due to the loss of chromosome 4, the tumor suppressor gene Cdkn2a is lost as well (Figure 3.8). Therefore, cells with a loss of chromosome 4, or Cdkn2a respectively, can no longer respond to the Cdkn2a-dependent senescence induction (Mirzayans *et al.* (2012), Rayess *et al.* (2012)). During the experiment, the Cdkn2a negative cells continue to proliferate while the Cdkn2a positive cells are arrested by the cytokine treatment (Braumüller *et al.* (2013)).

4.1.3 *In vivo* selection pressure favors the establishment of a Cdkn2a-negative subpopulation

An even more pronounced alteration of chromosomal aberrations in RT2 cancer cell line 3 is observed after its transfer into four different $CD8^+$-depleted C3HeB/FeJ mice. After tumor attachment, ICB therapy was initiated in these mice. Here, either a combination

therapy with PD-L1 and LAG-3 or PD-1 and CTLA-4 was applied. Contrary to expectations, the growth of the tumors could not be inhibited by ICB therapy. After the tumors had reached a size of >10 mm, they were removed from the mouse and cultivated *in vitro* (mSc cancer cell line #3, #4, #5, and #6). The subsequent growth arrest assay confirmed that the tumor cells do no longer respond to CIS induction as well (experiment performed by Ellen Brenner, data not shown). These four mSc cancer cell lines were then used in an experiment according to the treatment scheme shown in Figure 3.1, and the samples were subsequently used for CGH analysis. The CGH results of the four mSc cancer cell lines are presented in Figure 3.5. When comparing the chromosomal aberrations of the four mSc cell lines directly in the overlay, it is noticeable that they are almost identical. This is even more remarkable as the mSc cancer cell lines grew in different mice, some of which have received different ICB therapies. Nevertheless, the transfer of RT2 cancer cell line 3 into an immunocompetent environment led to the selection of similar chromosomal aberrations. As a result, the amplification of chromosome 15, which was initially slightly indicated in the parental RT2 cancer cell line 3, has developed into a significant amplification in all mSc cancer cell lines. Moreover, the deletions of chromosomes 3, 4, 9, 14, and 16 in the parental RT2 cancer cell line 3 are no longer present in the mSc cancer cell line. Instead, the alterations of theses chromosomes normalized, except for some partial amplifications (chromosome 3) or deletions (chromosome 4).

The fact that the change from *in vitro* to *in vivo* conditions, respectively, altered environmental conditions, influence the formation of chromosomal aberrations does not exclusively apply to the primary RT2 cancer cell lines. In a study comparing the genetic composition of primary breast cancer tumors and their metastases with a CGH analysis, it was shown that 69% of the chromosomal aberrations were almost identical (Kuukasjärvi *et al.* (1997)). In the remaining 31%, however, the metastasis revealed high genetic differences in comparison to their primary tumor tissue. The authors conclude that, although the metastasis originates from the primary tumor, different early stem line clones are formed. These subsequently established different chromosomal aberrations depending on the specific selection pressure of the tissue. With regard to mSc cancer cell lines, it was not the type of ICB therapy that was critical for the establishment of chromosomal aberrations, but the transfer from an *in vitro* to an *in vivo* environment.

A more detailed analysis of chromosome 4 shows that Cdkn2a is significantly deleted in all four mSc cancer cell lines. Consequently, the selection process within the immunocompetent environment has led to the loss of the subpopulation that has a complete deletion of chromosome 4. These cells were probably less adapted to *in vivo* conditions. In contrast, a subpopulation with a specific loss of tumor suppressor Cdkn2a, which functioned as a driver mutation, was able to dominate within the *in vivo* environment. This loss enables the cells to proliferate without being affected by Cdkn2a as a cell cycle inhibitor (Mirzayans *et al.* (2012)). As several studies demonstrated, heterogeneous tumor will give rise to a resistant subpopulation when put under selection pressure (Szerlip *et al.* (2012), Gerlinger *et al.* (2012), Snuderl *et al.* (2011)). In consequence, the resistant subpopulation drives the tumor formation. The punctual, specific aberration found in the

Cdkn2a deficient subpopulations (Figure 3.6) is a phenomenon known mainly from the specific amplifications of oncogenes (Albertson *et al.* (2000), Albertson (2006)). These include epidermal growth factor receptor (EGFR) and mouse double minute 2 homolog (MDM2), for example, since their amplification improves the survival and proliferation of the cancer cells. However, increasing amplifications are associated with decreasing patient survival (Al-Kuraya *et al.* (2004), Blegen *et al.* (2003)).

The absence of Cdkn2a leads to the loss of an important cell cycle control mechanism. Without Cdkn2a, the cell continues to proliferate despite DNA damage, for instance. Thus, the loss of CDKN2A or a mutation of it is a tumor driving mechanism and therefore observed in many different human tumor entities as well (AACR Project GENIE Consortium (2017)). For example, 21.44% of melanoma patients have a mutation, and 11.61% a loss of CDKN2A. In glioblastoma, CDKN2A is mutated in 34.59% of cases and deleted in 32.16%. Furthermore, it could be shown that the increasing loss of CDKN2A expression is associated with increasing malignancy in melanoma (Mihic-Probst *et al.* (2006)).

In summary, the data show that ICB (Figure 3.5) or CIS (Figure 3.7) therapy gives rise to a previously existing minor Cdkn2a-negative subpopulation which eventually drives tumor progression. In contrast to RT2 cancer cell line 1, 2, and RT2xStat1$^{-/-}$ cancer cell line, RT2 cancer cell line 3 did not establish an equilibrium between the different subpopulations when the experiments were performed (Gupta *et al.* (2011)). Therefore, treatment with medium or T_h1 cytokines altered the ratio of cells harboring different chromosomal aberrations within the unstable RT2 cancer cell line 3. Further, the results of the CGH analyses indicate potential problems with therapeutic application of CIS therapy in patients, especially in melanoma. As mentioned before, CDKN2A-deficiency is commonly found in advancing melanoma (AACR Project GENIE Consortium (2017), Wellbrock *et al.* (2004), Dhomen *et al.* (2009)). Therefore, the CIS therapy would only target CDKN2A-positive cells. In consequence, the resistant cells would still grow and drive tumor progression.

Overall, the results of CGH demonstrate how essential the function of Cdkn2a and $p16^{INK4a}$, respectively, is for the induction of CIS and successful ICB therapy. However, it has not yet been deciphered how $p16^{INK4a}$ is expressed after T_h1 cytokine stimulation. The second part of the discussion addresses a potential JunB-dependent expression of $p16^{INK4a}$.

4.2 The role of JunB in CIS

The aim of the investigations of JunB was to find a possible correlation between the AP-1 transcription factor JunB and the $p16^{INK4a}$ induction necessary for the induction of senescence. The overall intention was to replace the TNF addition required for CIS induction in order to avoid the toxicity of TNF.

4.2.1 JunB expression in CIS is TNF-dependent

For all experiments, except those dealing with JunB protein expression, the human rhabdomyosarcoma cell line A204 was used. Although it is more known about senescence induction for the RT2 cancer cells (also *in vivo*), the primary cells display some disadvantages. As it was shown in Section 4.1.2, RT2 cancer cell lines are a heterogeneous population. The composition of the subpopulations can additionally vary under the influence of the T_h1 cytokines (Figure 3.7). Furthermore, it is known that RT2 cancer cells do not respond to CIS induction after being passaged several times and that the morphology of RT2 cancer cells changes as well as the expression of RT2 cancer cell markers (internal laboratory observations). Another obstacle was the limited transfectability of RT2 cells. The attempt to knockout JunB in RT2 cancer cells by CRISPR/Cas9 or to knockdown JunB with shRNA led to a dedifferentiation of these cells. As a result, RT2 cancer cells changed their morphology and the expression of characteristic RT2 cancer cell markers, such as synaptophysin (data not shown). The human cancer cell line A204, on the other hand, is genetically stable during further passage. In addition, replicative senescence, depending on $p16^{INK4a}$ induction, has already been demonstrated in the A204 cancer cells (Chai *et al.* (2005)). Similar to this thesis (Figure 3.10), an increased expression of SA-β-gal could be detected in the A204 cancer cells after senescence induction (Chai *et al.* (2005), Betz *et al.* (2002)). Since no replacement for an antibody used in our laboratory detecting $p16^{INK4a}$ in the Western Blot has been found so far, no $p16^{INK4a}$ protein expression could be shown in this thesis. Nevertheless, the expression of $p16^{INK4a}$ after CIS induction in A204 cancer cells was shown in previous work (Hahn (2017)).

As shown in the results of Figure 3.9, treatment with T_h1 cytokines induces JunB protein expression in murine cancer cells. This expression is independent of the origin of the tumor. Comparable results were found in the results of the A204 cancer cell line (Figure 3.9d). In addition to the elevated protein expression, an increase in JUNB mRNA was also found (Figure 3.12). The induction of JUNB expression occurs rapidly after cytokine addition on mRNA as well as on protein level. A comparably fast dynamic of JunB protein expression has already been shown in several studies (Chalaux *et al.* (1998), Schmid *et al.* (2013)). Despite an increased JunB protein level, the translocation of JunB into the nucleus must take place in order to be able to act as the transcription factor, for example, for $p16^{INK4a}$ (Schmid *et al.* (2013)). This translocation could be demonstrated in Figure 3.13 after T_h1 cytokine addition. To find out whether TNF, IFNγ or the combination of both cytokines is necessary to induce JunB expression, the cytokines

were added to A204 cancer cells individually or in combination (Figure 3.11). The results show that JunB expression occurs within the first 4 h after TNF single treatment or cytokines double treatment. Other experiments which focused on early time points, revealed a JunB protein expression as early as 2 h after cytokine treatment (Figure 3.18a, Figure 3.19a). Surprisingly, the TNF-induced expression of JunB decreases constantly after 24 h and is no longer detectable after 48 h. Thereafter, the JunB expression is only visible in the double treatment. Although JunB can act as a transcription factor for TNF, this cannot be an explanation for the continued expression of JunB in double treatment (Zhang *et al.* (2015), Gomard *et al.* (2010)). Otherwise, JunB expression would occur in all cytokine-treated samples after an initial delay. It is possible that TNF expression is induced by IFNγ treatment in IFNγ as well as IFNγ and TNF treatment. Probably, the extrinsic TNF is exhausted, which results in a decline in JunB expression after 24 h. The IFNγ-induced TNF expression would result in an autocrine TNF stimulation, leading to JunB expression (Vila-del Sol *et al.* (2008)). In fact, a low JunB expression, after initial delay, can be seen in IFNγ single treatment. Moreover, this feedback loop could lead to a stabilization of JunB expression in cytokine double treatment cells, resulting in a more pronounced JunB expression compared to the IFNγ single treatment. Additionally, it cannot be excluded that the IFNγ treatment may inhibit the degradation process of JunB. This unknown mechanism would prevent the degradation of the protein after the initial TNF-dependent induction of JunB. Among the proteins which are known to be involved in JunB degradation are itchy E3 ubiquitin protein ligase (ITCH) and glycogen synthase kinase 3 (GSK3/SCF$^{\text{Fbxw7}}$) (Vartanian *et al.* (2011), Pérez-Benavente *et al.* (2013)). However, these speculations have to be examined in subsequent experiments.

4.2.2 Strong evidence of NF-κB-mediated induction of JunB expression after T_h1 cytokine treatment

The results so far revealed an increase in JunB expression in CIS. However, it is still unclear how the signal transmission of TNF and JunB takes place. Possible candidates for signal transduction between the two factors could be, for example, p38 mitogen-activated protein kinases (p38) (Zhou *et al.* (2006)), c-Jun N-terminal kinases (JNK) (Reinhard *et al.* (1997)), ERK (Textor *et al.* (2006), Kong *et al.* (2017), Staber *et al.* (2007)) and NF-κB (Yin *et al.* (2009), Granet and Miossec (2004), Schmidt *et al.* (2007)). In this thesis, the focus was on a potential signal transmission by NF-κB. To verify this relationship, the A204 cancer cells were treated with the IKK-1 and IKK-2 kinase inhibitor IKK-16. After determination of a tolerable cytotoxicity (Figure 3.15, Figure 3.20, and Figure 3.21), the cells were treated with the both T_h1 cytokines under inhibitor treatment. As the results show, the application of IKK-16 led to an inhibition of the NF-κB signaling pathway (Figure 3.18b, Figure 3.19b, Figure 3.22b, Figure 3.22d, Figure 3.23b, and Figure 3.23d) and subsequently to a reduced cytokine-dependent expression of JunB (Figure 3.16, Figure 3.17, Figure 3.18a, Figure 3.19a, Figure 3.22a, Figure 3.22c, Fig-

ure 3.23a, Figure 3.23c, Figure 3.24, and Figure 3.25). Since other potential signaling pathways were not investigated, it cannot be excluded that JunB expression is also induced by p38, JNK, or ERK.

Nevertheless, the data suggest that signal transduction of TNF is most likely transmitted by NF-κB in CIS induction. Since no specific JunB inhibitor currently exists, the indirect inhibition of JunB expression by blocking the NF-κB signaling was utilized to analyze whether CIS can still be induced in A204 cancer cells. However, the results from Figure 3.26 show no difference between the inhibitor and control-treated groups, independent of cytokine stimulation. Nevertheless, there is a possibility that the remaining expression of JunB is sufficient to induce a growth arrest in the cells. As mentioned above, inhibition of the kinases IKK-1 and IKK-2 is only an indirect way to reduce JunB expression. Further side effects and interference with other downstream signaling pathways resulting from the application of the inhibitor cannot be excluded at this point.

4.2.3 Reduction of JunB expression has no influence on the induction of CIS in A204 cancer cells

To achieve a specific inhibition of JunB expression, siRNA was used (Figure 3.28a (Gurzov *et al.* (2012), Zhang *et al.* (2015), Hyakusoku *et al.* (2016)). From previous experiments it was known that a sufficient reduction of JunB protein expression only occurs 72 h after siRNA treatment (data not shown). With the aim of starting CIS induction with the lowest possible JunB expression, T_h1 cytokines were added 72 h after siRNA treatment (Figure 3.27). Since it was shown in the publication of Konishi *et al.* (2008) that repeated transfection with siJUNB led to a reduction of $p16^{INK4a}$, repeated transfection was performed in this experimental scheme as well. A further reason for the repeated transfection was to overcome the limited efficacy of siRNA (Layzer *et al.* (2004), Morrissey *et al.* (2005)). Despite the reduced JunB expression, no difference in senescence induction or proliferation between the siCtrl and siJUNB group was found (Figure 3.28b). This effect was also independent of cytokine addition.

Since both the pharmacological and siRNA-mediated reduction of JunB expression were not sufficient to observe an effect on the proliferation of A204 cancer cells, CRISPR/Cas9 was used to delete the JUNB transcription site in the genome. However, the use of CRISPR/Cas9 did not lead to a knockout, but only to a knockdown of JunB (Figure 3.29a). The reason is probably the lack of sufficient selection methods after CRISPR/Cas9 transfection. The plasmid used (Table 2.7) leads to GFP expression in successfully transfected cells. These cells were subsequently collected using FACS. Afterward, an additional transfection would have introduced puromycin resistance into the CRISPR/Cas9 site as well as a RFP sequence. However, this step could not be carried out due to a distribution stop of the second plasmid. As a result, successfully transfected cells were cultured as a bulk population, but it was unclear whether a knockout would be successful in all transfected cells. Here, a single cell selection would have been useful

to produce a pure A204 JUNB knockout cell line. Nevertheless, the transfected A204 cancer cells were studied, and reduced expression of JunB in Western Blot analysis was found (Figure 3.29). Once again, a subsequent growth arrest assay showed no influence of the reduced JunB expression on the induction of CIS (Figure 3.30). In order to achieve a stronger reduction of JunB expression, the CRISPR/Cas9 JUNB ko cells were treated with IKK-16. Western Blot analyses revealed that there was only a small additional reduction in JunB expression which had no influence on the induction of CIS (data not shown). In summary, none of the methods used lead to a sufficient or complete reduction of JunB expression. Besides, the JunB reduction had no influence on the CIS induction in A204 cancer cells.

4.2.4 Relationship of JunB and $p16^{INK4a}$ expression in the induction of CIS remains unresolved

The incomplete reduction of JunB expression might still lead to a $p16^{INK4a}$ expression, since the correlation of $p16^{INK4a}$ expression by the transcription factor JunB has been demonstrated in various studies (Yogev *et al.* (2006), Passegué *et al.* (2001)). The dependence of CIS on $p16^{INK4a}$ induction has also been shown numerous times (Braumüller *et al.* (2013), Brenner *et al.* (2020)). Attempts to overexpress JunB and thereby induce a TNF-independent $p16^{INK4a}$ induction failed (data not shown). Furthermore, an attempt was made to prove the physical interaction of JunB in the promoter region of CDKN2A by using chromatin immunoprecipitation (ChIP). The only previously reported evidence of JunB binding to the promoter region of Cdkn2a was shown in the publication of Passegué and Wagner (2000). Here, MEF cells were transfected with a $p16^{INK4a}$ luciferase construct as well as with a JunB expression plasmid. This lead to a strong, JunB-dependent expression of $p16^{INK4a}$. It remains to be shown whether physiologically expressed quantities of JunB lead to binding to the promoter region of native CDKN2A after CIS induction.

4.2.5 The complexity of the AP-1 transcription factor impedes the accurate analysis of JunB in CIS

Another problem is the way AP-1 operates as a transcription factor. Due to the high amount of possible combinations within the different AP-1 members, a high complexity of the AP-1 transcription factors is achieved (Kovary and Bravo (1991), Kovary and Bravo (1992), Malnou *et al.* (2010)). The resulting complexes have different binding affinities (Staber *et al.* (2007)). Furthermore, the composition of the AP-1 transcription factor can also change under the same physiological induction, for example, during the induction of hypoxia in A549 cells (Yadav *et al.* (2017)). It was also shown that the loss of an AP-1 member could be compensated by the expression of another AP-1 protein (Passegué *et al.* (2002)). These facts demonstrate how versatile the possibilities of

complex composition and transcriptional regulation by AP-1 can be.

In this thesis, it cannot be excluded that the reduced expression of JunB was compensated by the expression of another AP-1 member. In order to clarify this question, a co-immunoprecipitation (Co-IP) would be useful to determine the composition of AP-1 complexes in senescence induction. Furthermore, it cannot be excluded that JunB does not play a role in CIS and that another transcriptions factor mediates the signal transduction between TNF and $p16^{INK4a}$. A possible candidate is the transcription factor ETS-1. The expression of ETS-1 can be stimulated by TNF (Goetze *et al.* (2001)) or by IFNγ (Nguyen *et al.* (2012)). In the context of CIS induction, ETS-1 expression was observed in T_h1 cytokine-treated A204 cancer cells (data not shown). Whether this induction is relevant for cytokine-dependent $p16^{INK4a}$ induction has to be evaluated in future experiments.

4.2.6 Deciphering the TNF signaling pathway in CIS will help to identify potential targets

The elucidation of the signaling pathway leading to $p16^{INK4a}$ induction is an important first step towards understanding the molecular mechanisms in CIS. Considering the goal to stimulate the TNF pathway without the addition of TNF, the link between TNF stimulation and $p16^{INK4a}$ expression has to be found first.

However, the regulation of the transcription factor, which is situated between the TNF stimulation and $p16^{INK4a}$ induction, might be problematic. The pharmacological targeting of transcription factors is challenging since a binding site for an inhibitor is difficult to identify using classical methods (Liu and Altman (2014)). The dimerization of many transcription factors, such as AP-1, also raises problems (Fontaine *et al.* (2015)). In the context of AP-1, pharmacological regulation might be particularly difficult, since, as mentioned above, the loss of an AP-1 member can be compensated by other AP-1 proteins (Passegué *et al.* (2002)). Since JunB as a transcription factor also regulates the expression of multiple other target proteins, a therapy at this level of the signaling pathway would probably lead to various side effects (Bakiri *et al.* (2000), Robinson *et al.* (2001), Sreeramaneni *et al.* (2005)). Therefore, if AP-1 proteins play a role in CIS induction, it would be more interesting to target proteins that regulate the activity or degradation of AP-1, such as e.g., ITCH and $GSK3/SCF^{Fbxw7}$.

4.3 Conclusion

In the first part of the thesis, it was shown that in RT2 cancer cell, no change in chromosomal aberration appears after T_h1 cytokine treatment. However, it could be demonstrated that the RT2 cancer cell line consists of different subpopulations. If the heterogeneous RT2 population is still unstable at the time of the experiment, i.e., the different subpopulations are not in an equilibrium, a shift in chromosomal aberrations can occur. This shift of chromosomal aberrations can be enhanced by the treatment with T_h1 cytokines. In the displayed RT2 cancer cell line, an increasing loss of chromosome 4, including Cdkn2a, was most prominent. Moreover, an *in vivo* transfer of such an unstable RT2 cancer cell line further diversifies the appearance of chromosomal aberrations. The selective loss of Cdkn2a was particularly significant here. Due to this driver mutation, the cells were no longer able to respond to ICB therapy and even a subsequent *in vitro* T_h1 cytokine treatment failed to induce CIS. Thus, these results underline the pivotal role of $p16^{INK4a}$ in senescence induction.

The second part of the work aimed to clarify how the expression of $p16^{INK4a}$ is mediated during CIS induction. The results showed that CIS induction lead to increased JunB expression. Furthermore, it could be shown that this expression is TNF-dependent, especially in the early induction phase. At later stages of CIS induction, the TNF-induced expression of JunB decreases. After that, JunB expression is found, to a small extent, in IFNγ-treated cells. However, only the combined T_h1 cytokine treatment resulted in a strong JunB expression. Moreover, it was shown that there is a translocation of the transcription factor JunB from the cytoplasm into the nucleus after T_h1 cytokine treatment. The treatment with the IKK-1 and IKK-2 kinase inhibitor IKK-16 demonstrated that, in CIS induction, a NF-κB-dependent expression of JunB is most likely to occur.

If the signaling pathway hypothesis is correct (Figure 1.11), a loss of JunB would result in a decreased expression of $p16^{INK4a}$. This would eventually prevent the induction of the CIS in A204 cancer cells. However, different approaches leading to a reduced JunB expression (indirectly via NF-κB inhibition, or siRNA knockdown) could not reveal any difference in the induction of CIS. The attempt to completely knockout JUNB using CRISPR/Cas9 was not successful. Again, the reduced expression of JunB in CRISPR/Cas9-transfected A204 cancer cells did not prevent CIS induction in A204 cancer cells. In summary, an induction of JunB is observed in cytokine-induced senescence. Whether this is related to the $p16^{INK4a}$ expression could not be sufficiently clarified in this thesis.

List of Figures

1.1 Hallmarks of cancer 2
1.2 The expression level of p53 determines cell fate 4
1.3 Telomere shortening threatens chromosomal stability 6
1.4 Targeted cancer therapy 7
1.5 Senescence induction 9
1.6 Cell cycle arrest is mediated by p53 and $p16^{INK4a}$ 10
1.7 Divergent effects of the SASP 12
1.8 Structure of the AP-1 transcription factor 15
1.9 JunB is involved in various cellular events 16
1.10 JunB has a dual role in cell cycle regulation 18
1.11 Visualization of the proposed signaling pathway model 20

3.1 CGH treatment scheme 46
3.2 CGH of the RT2 cancer cell line 1 48
3.3 CGH of the RT2 cancer cell line 2 49
3.4 CGH of the RIP1-Tag2 x signal transducer and activator of transcription $1^{-/-}$ cancer cell line 50
3.5 CGH of four subcutaneously transplanted RT2 tumors (mSc) 51
3.6 Specific loss of the $p16^{INK4a}$ gene locus Cdkn2a in all four mSc tumors 52
3.7 The CGH of the RT2 cancer cell line 3 reveals a gradual loss of the chromosomes 4 and 14 53
3.8 Close-up of chromosome 4 shows the progressive loss of the $p16^{INK4a}$ transcription site Cdkn2a 54
3.9 Upregulation of the JunB protein level in various cancer cells lines after stimulation with the T_h1 cytokines 56
3.10 The T_h1 cytokines IFNγ and TNF induce senescence in A204 cancer cells 57
3.11 Treatment with TNF leads to the initial expression of JunB 58
3.12 Increased JUNB expression on mRNA level after cytokine treatment . . 58
3.13 Translocation of JunB into the nucleus during CIS induction 59
3.14 TNF leads to activation of the NF-κB signaling in CIS 60
3.15 Titration of the IKK-1 and IKK-2 inhibitor IKK-16 62
3.16 Incubation of A204 cancer cells with 0.1 µM IKK-16 inhibitor 64
3.17 Application of 0.1 µM IKK-16 is not sufficient to inhibit the expression of JunB 64
3.18 Inhibition of JunB expression after treatment with 1 µM IKK-16 65

3.19 Inhibition of cytokine-dependent phosphorylation of IκBα leads to a significant reduction of JunB protein expression 66
3.20 LDH cytotoxicity assay shows no differences between the application of 0.5 µM or 1 µM IKK-16 after 24 h 68
3.21 Crystal violet assays show moderate cytotoxicity using 0.5 µM IKK-16 . 69
3.22 Using a concentration of 0.5 µM IKK-16 leads to reduced protein levels of JunB or pIκBα 71
3.23 Densiometric quantification of JunB protein expression and phosphorylated IκBα 72
3.24 Inhibition of the cytokine-dependent expression of JunB is sustained over the course of CIS induction 73
3.25 Densiometric quantification of JunB protein expression during incubation with cytokines and/or IKK-16 74
3.26 Growth arrest induction is not prevented by IKK-16 treatment 76
3.27 Treatment scheme of siRNA growth arrest assay 77
3.28 siRNA-mediated downregulation of JunB is not sufficient to prevent CIS induction 78
3.29 CRISPR/Cas9-induced JUNB knockdown in A204 cancer cells 80
3.30 Knockdown of JUNB has no impact on cytokine-induced senescence . . 81

List of Tables

2.1 Equipment 21
2.2 Consumables 22
2.3 Chemicals and Reagents 23
2.4 Buffers and Solutions 25
2.5 Kits 27
2.6 siRNA sequences 29
2.7 Sequences of CRISPR/Cas9 plasmids 29
2.8 Oligonucleotides 29
2.9 Antibodies 30
2.10 Compounds 30
2.11 Software and Websites 31
2.12 Cell Culture medium recipes 32
2.13 PCR master mix recipe 34
2.14 PCR standard program 35
2.15 cDNA synthesis master mix 36
2.16 cDNA synthesis thermocycler program 36
2.17 Recipe for qPCR master mix 37
2.18 qPCR lightcycler program 37
2.19 SDS-PAGE recipe 39
2.20 CGH digestion master mix 42
2.21 CGH labeling master mix 43
2.22 CGH labeling control 43
2.23 CGH hybridization master mix 44

Acronyms

AA	amino acids
AP-1	activator protein 1
APC	antigen-presenting cells
APS	ammonium persulfate
ATF	activating transcription factor
ATF2	activating transcription factor 2
ATF3	activating transcription factor 3
ATM	ataxia telangiectasia mutated
ATR	ataxia telangiectasia and Rad3-related protein
BAX	Bcl-2-associated X protein
BCA	bicinchoninic acid
Bcl-2	B-cell lymphoma 2
Bcl-x_L	B-cell lymphoma-extra large
Bim	Bcl-2-like protein 11
BRAF	B-Raf proto-oncogene
BSA	bovine serum albumin
bZIP	basic leucine zipper
C_t	threshold cycle
c-Jun	Jun proto-oncogene
c-Maf	Maf bZIP transcription factor
c-NHEJ	classical non-homologous end joining
CAR	chimeric antigen receptors
CD20	B-lymphocyte antigen CD20
CD30	TNF receptor superfamily member 8
CD4	cluster of differentiation 4
CD80	cluster of differentiation 80, B7-1
CD86	cluster of differentiation 86, B7-2
$CD8^+$	cytotoxic T cell
CDK2	cyclin-dependent kinase 2

CDK4/6	cyclin-dependent kinase 4/6
CDK9	cyclin-dependent kinase 9
CDKN2A	cyclin-dependent kinase inhibitor 2A
Cdkn2a	cyclin-dependent kinase inhibitor 2A
cDNA	complementary DNA
CGH	array comparative genomic hybridization
ChIP	chromatin immunoprecipitation
CHK1	checkpoint kinase 1
CHK2	checkpoint kinase 2
CIS	cytokine-induced senescence
CLL	chronic lymphatic leukemia
Co-IP	co-immunoprecipitation
CRE	cAMP response element
CRISPR/Cas9	clustered regularly interspaced short palindromic repeats/crispr associated protein 9
CT26	murine colon cancer
CTLA-4	cytotoxic T-lymphocyte-associated protein 4
Ctrl ko	control transfected cells
Cy3	cyanine 3
Cy5	cyanine 5
DAPI	4,6-diamidino-2-phenylindole
DDR	DNA damage response
DMEM	dulbecco's modified eagle's medium
DMSO	dimethyl sulfoxide
DNA	deoxyribonucleic acid
DSBs	double strand breaks
dUTP	deoxyuridine triphosphate
E2F	E2F transcription factor
EDTA	ethylenediamine tetraacetic acid disodium salt dihydrate
EGFR	epidermal growth factor receptor
EMT	epithelial-mesenchymal transition
ER	endoplasmic reticulum
ERK	extracellular signal-regulated kinase
ETS-1	protein C-ets-1

FACS	fluorescence activated cell sorter
Fas receptor	tumor necrosis factor receptor superfamily member 6
FCS	fetal bovine serum
FDA	Food and Drug Administration
FISH	fluorescent DNA *in situ* hybridization
FOS	Fos proto-oncogenee
FOSB	FosB proto-oncogene
FOSL1	Fos-related antigen 1
FOSL2	Fos-related antigen 2
GAPDH	glyceraldehyde 3-phosphate dehydrogenase
gDNA	genomic deoxyribonucleic acid
GFP	green fluorescent protein
GOI	gene of interest
gRNA	guide RNA
GSK3/SCF^{Fbxw7}	glycogen synthase kinase 3
HBP1	HMG-box transcription factor 1
HEPES	4-(2-hydroxyethyl)-1-piperazineethanesulfonic acid
HIF	hypoxia-inducible factors
HNSCC	head and neck squamous cell carcinoma
HR	homologous recombination
IκBα	nuclear factor of kappa light polypeptide gene enhancer in B-cells inhibitor, alpha
i.e.	id est, this is to say
ICB	immune checkpoint blockade
IFNα	interferon alpha
IFNγ	interferon gamma
IL-6	interleukin 6
IL-8	interleukin 8
iNOS	inducible nitric oxide synthase
INT	tetrazolium salt
IT	IFNγ + TNF
ITCH	itchy E3 ubiquitin protein ligase

JNK	c-Jun N-terminal kinases
JunB	JunB proto-oncogene
JunD	JunD proto-oncogene
kb	kilo base
kDa	kilo Dalton
Ki67	marker of proliferation Ki67
ko	knockout
LAG-3	lymphocyte-activation gene 3
LDH	lactate dehydrogenase
LLC	lewis lung carcinoma
MafA	transcription factor MafA
MAPK	mitogen-activated protein kinase
MC	medium control
MDM2	mouse double minute 2 homolog
MEF	mouse embryonic fibroblasts
MEK	mitogen-activated protein kinase kinase
MHC class II	major histocompatibility complex class II
MMP-2, MMP-4, MMP-9	matrix metallopeptidase-2, -4, -9
mRNA	messenger RNA
mSc	mouse subcutaneous cell line
mTOR	mammalian target of rapamycin
MYC	cellular myelocytomatosis
NF-κB	nuclear factor kappa-light-chain-enhancer of activated B-cells
NP-40	polyethylene glycol p-(1,1,3,3-tetramethylbutyl)-phenyl ether
NSCLC	non-small-cell lung carcinoma
NTP	nucleoside triphosphate
o/n	over night
P/S	penicillin/streptavidin
$p16^{INK4a}$	cyclin-dependent kinase inhibitor 2A

p21	cyclin-dependent kinase inhibitor 1
p38	p38 mitogen-activated protein kinases
p53	tumor suppressor protein p53
PBS	phosphate-buffered saline
PCR	polymerase chain reaction
PD-1	programmed cell death protein 1
PD-L1	programmed cell death protein 1 ligand
PI	protease inhibitor
PS	phospho stop
PUMA	p53 upregulated modulator of apoptosis
PVDF	polyvinylidene fluoride
qPCR	quantitative polymerase chain reaction
RAF	rapidly accelerated fibrosarcoma
RAS	rat sarcoma
Rb	retinoblastoma protein
RFP	red fluorescent protein
RIP	rat insulin promoter
RIPA	radio immuno precipitation assay buffer
RISC	RNA-induced silencing complex
RNA	ribonucleic acid
ROS	reactive oxygene species
rpm	revolutions per minute
RPMI	roswell park memorial institute medium
RT	room temperature
RT2	RIP1-Tag2
RT2xStat1$^{-/-}$	RIP1-Tag2 x signal transducer and activator of transcription 1$^{-/-}$
RT2xTNFR1$^{-/-}$	RIP1-Tag2 x tumor necrosis factor receptor 1$^{-/-}$
RTK	receptor tyrosine kinases
SA-β-gal	senescence-associated β-galactosidase
SAHF	senescence-associated heterochromatin foci
SASP	senescence-associated secretory phenotype
SDS	sodium dodecyl sulfate
SDS-PAGE	sodium dodecyl sulfate – polyacrylamide gel electrophoresis

shRNA	small hairpin RNA
siRNA	small interfering RNA
SLE	systemic lupus erythematosus
Snail	zinc finger protein SNAI1
STAT1	signal transducer and activator of transcription 1
STAT3	signal transducer and activator of transcription 3
T_h1	$CD4^+$ T-helper cell 1
TAG2	SV40 large T-cell antigen
TCR	T-cell receptor
TEMED	tetramethylethylenediamine
TNF	tumor necrosis factor
TPA	12-*O*-tetradecanoylphorbol 13-acetate
Twist	twist-related protein 1
UPR	unfolded protein response
UV	ultraviolet
v-maf	transforming protein Maf
v/v	volume per volume
VEGF	vascular endothelial growth factor
w/v	weight per volume

Bibliography

AACR Project GENIE Consortium (2017). AACR Project GENIE: Powering Precision Medicine through an International Consortium. *Cancer Discovery*, **7**(8), 818–831.

Abken, H. (2017). Driving CARs on the Highway to Solid Cancer: Some Considerations on the Adoptive Therapy with CAR T Cells. *Human Gene Therapy*, **28**(11), 1047–1060.

Acosta, J. C., Banito, A., Wuestefeld, T., Georgilis, A., Janich, P., Morton, J. P., Athineos, D., Kang, T.-W., Lasitschka, F., Andrulis, M., Pascual, G., Morris, K. J., Khan, S., Jin, H., Dharmalingam, G., Snijders, A. P., Carroll, T., Capper, D., Pritchard, C., Inman, G. J., Longerich, T., Sansom, O. J., Benitah, S. A., Zender, L., and Gil, J. (2013). A complex secretory program orchestrated by the inflammasome controls paracrine senescence. *Nature Cell Biology*, **15**(8), 978–90.

Al-Kuraya, K., Schraml, P., Torhorst, J., Tapia, C., Zaharieva, B., Novotny, H., Spichtin, H., Maurer, R., Mirlacher, M., Köchli, O., Zuber, M., Dieterich, H., Mross, F., Wilber, K., Simon, R., and Sauter, G. (2004). Prognostic relevance of gene amplifications and coamplifications in breast cancer. *Cancer Research*, **64**(23), 8534–8540.

Albertson, D. G. (2006). Gene amplification in cancer. *Trends in Genetics*, **22**(8), 447–55.

Albertson, D. G., Ylstra, B., Segraves, R., Collins, C., Dairkee, S. H., Kowbel, D., Kuo, W. L., Gray, J. W., and Pinkel, D. (2000). Quantitative mapping of amplicon structure by array CGH identifies CYP24 as a candidate oncogene. *Nature Genetics*, **25**(2), 144–146.

Albertson, D. G., Collins, C., McCormick, F., and Gray, J. W. (2003). Chromosome aberrations in solid tumors. *Nature Genetics*, **34**(4), 369–376.

Alcorta, D. A., Xiong, Y., Phelps, D., Hannon, G., Beach, D., and Barrett, J. C. (1996). Involvement of the cyclin-dependent kinase inhibitor p16 (INK4a) in replicative senescence of normal human fibroblasts. *Proceedings of the National Academy of Sciences of the United States of America*, **93**(24), 13742–13747.

Alpert, S., Hanahan, D., and Teitelman, G. (1988). Hybrid insulin genes reveal a developmental lineage for pancreatic endocrine cells and imply a relationship with neurons. *Cell*, **53**(2), 295–308.

Amit, I., Citri, A., Shay, T., Lu, Y., Katz, M., Zhang, F., Tarcic, G., Siwak, D., Lahad, J., Jacob-Hirsch, J., Amariglio, N., Vaisman, N., Segal, E., Rechavi, G., Alon, U., Mills, G. B., Domany, E., and Yarden, Y. (2007). A module of negative feedback regulators defines growth factor signaling. *Nature Genetics*, **39**(4), 503–512.

Andrecht, S., Kolbus, A., Hartenstein, B., Angel, P., and Schorpp-Kistner, M. (2002). Cell cycle promoting activity of JunB through cyclin A activation. *The Journal of Biological Chemistry*, **277**(39), 35961–8.

Angel, P., Imagawa, M., Chiu, R., Stein, B., Imbra, R. J., Rahmsdorf, H. J., Jonat, C., Herrlich, P., and Karin, M. (1987). Phorbol ester-inducible genes contain a common cis element recognized by a TPA-modulated trans-acting factor. *Cell*, **49**(6), 729–739.

Artandi, S. E. and DePinho, R. A. (2010). Telomeres and telomerase in cancer. *Carcinogenesis*, **31**(1), 9–18.

Artandi, S. E., Chang, S., Lee, S. L., Alson, S., Gottlieb, G. J., Chin, L., and DePinho, R. A. (2000). Telomere dysfunction promotes non-reciprocal translocations and epithelial cancers in mice. *Nature*, **406**(6796), 641–5.

Ascierto, P. A., Kirkwood, J. M., Grob, J.-J., Simeone, E., Grimaldi, A. M., Maio, M., Palmieri, G., Testori, A., Marincola, F. M., and Mozzillo, N. (2012). The role of BRAF V600 mutation in melanoma. *Journal of Translational Medicine*, **10**(1), 85.

Baixeras, E., Huard, B., Miossec, C., Jitsukawa, S., Martin, M., Hercend, T., Auffray, C., Triebel, F., and Piatier-Tonneau, D. (1992). Characterization of the lymphocyte activation gene 3-encoded protein. A new ligand for human leukocyte antigen class II antigens. *Journal of Experimental Medicine*, **176**(2), 327–337.

Bakin, A. V. and Curran, T. (1999). Role of DNA 5-Methylcytosine Transferase in Cell Transformation by fos. *Science*, **283**(5400), 387–390.

Bakiri, L., Lallemand, D., Bossy-Wetzel, E., and Yaniv, M. (2000). Cell cycle-dependent variations in c-Jun and JunB phosphorylation: a role in the control of cyclin D1 expression. *The EMBO Journal*, **19**(9), 2056–68.

Bartkova, J., Horejsí, Z., Koed, K., Krämer, A., Tort, F., Zieger, K., Guldberg, P., Sehested, M., Nesland, J. M., Lukas, C., Ørntoft, T., Lukas, J., and Bartek, J. (2005). DNA damage response as a candidate anti-cancer barrier in early human tumorigenesis. *Nature*, **434**(7035), 864–70.

Bassing, C. H. and Alt, F. W. (2004). The cellular response to general and programmed DNA double strand breaks. *DNA Repair*, **3**(8-9), 781–96.

Bauer, A., Kirschnek, S., and Häcker, G. (2007). Inhibition of apoptosis can be accompanied by increased Bim levels in T lymphocytes and neutrophil granulocytes [2]. *Cell Death & Differentiation*, **14**(9), 1714–1716.

Berx, G. and van Roy, F. (2009). Involvement of members of the cadherin superfamily in cancer. *Cold Spring Harbor Perspectives in Biology*, **1**(6).

Betz, B. L., Strobeck, M. W., Reisman, D. N., Knudsen, E. S., and Weissman, B. E. (2002). Re-expression of hSNF5/INI1/BAF47 in pediatric tumor cells leads to G1 arrest associated with induction of p16ink4a and activation of RB. *Oncogene*, **21**(34), 5193–5203.

Blegen, H., Will, J. S., Ghadimi, B. M., Nash, H.-P., Zetterberg, A., Auer, G., and Ried, T. (2003). DNA amplifications and aneuploidy, high proliferative activity and impaired cell cycle control characterize breast carcinomas with poor prognosis. *Analytical Cellular Pathology*, **25**(3), 103–14.

Braumüller, H., Wieder, T., Brenner, E., Aßmann, S., Hahn, M., Alkhaled, M., Schilbach, K., Essmann, F., Kneilling, M., Griessinger, C., Ranta, F., Ullrich, S., Mocikat, R., Braungart, K., Mehra, T., Fehrenbacher, B., Berdel, J., Niessner, H., Meier, F., van den Broek, M., Häring, H.-U., Handgretinger, R., Quintanilla-Martinez, L., Fend, F., Pesic, M., Bauer, J., Zender, L., Schaller, M., Schulze-Osthoff, K., and Röcken, M. (2013). T-helper-1-cell cytokines drive cancer into senescence. *Nature*, **494**(7437), 361–365.

Brenner, E., Schörg, B. F., Ahmetlić, F., Wieder, T., Hilke, F. J., **Simon, Nadine**, Schroeder, C., Demidov, G., Riedel, T., Fehrenbacher, B., Schaller, M., Forschner, A., Eigentler, T., Niessner, H., Sinnberg, T., Böhm, K. S., Hömberg, N., Braumüller, H., Dauch, D., Zwirner, S., Zender, L., Sonanini, D., Geishauser, A., Bauer, J., Eichner, M., Jarick, K. J., Beilhack, A., Biskup, S., Döcker, D., Schadendorf, D., Quintanilla-Martinez, L., Pichler, B. J., Kneilling, M., Mocikat, R., and Röcken, M. (2020). Cancer immune control needs senescence induction by interferon-dependent cell cycle regulator pathways in tumours. *Nature Communications*, **11**(1), 1335.

Brentjens, R. J., Rivière, I., Park, J. H., Davila, M. L., Wang, X., Stefanski, J., Taylor, C., Yeh, R., Bartido, S., Borquez-Ojeda, O., Olszewska, M., Bernal, Y., Pegram, H., Przybylowski, M., Hollyman, D., Usachenko, Y., Pirraglia, D., Hosey, J., Santos, E., Halton, E., Maslak, P., Scheinberg, D., Jurcic, J., Heaney, M., Heller, G., Frattini, M., and Sadelain, M. (2011). Safety and persistence of adoptively transferred autologous CD19-targeted T cells in patients with relapsed or chemotherapy refractory B-cell leukemias. *Blood*, **118**(18), 4817–4828.

Brown, C. E. and Mackall, C. L. (2019). CAR T cell therapy: inroads to response and resistance. *Nature Reviews Immunology*, **19**(2), 73–74.

Brown, E. B., Campbell, R. B., Tsuzuki, Y., Xu, L., Carmeliet, P., Fukumura, D., and Jain, R. K. (2001). In vivo measurement of gene expression, angiogenesis and physiological function in tumors using multiphoton laser scanning microscopy. *Nature Medicine*, **7**(7), 864–868.

Brudno, J. N. and Kochenderfer, J. N. (2016). Toxicities of chimeric antigen receptor T cells: recognition and management. *Blood*, **127**(26), 3321–30.

Bruhn, H. D., Fölsch, U. R., Kneba, M., and Löffler, H. (2003). *Onkologische Therapie*. Schattauer.

Carmeliet, P. (2005). VEGF as a key mediator of angiogenesis in cancer. *Oncology*, **69**(SUPPL. 3), 4–10.

Carter, L. L., Fouser, L. A., Jussif, J., Fitz, L., Deng, B., Wood, C. R., Collins, M., Honjo, T., Freeman, G. J., and Carreno, B. M. (2002). PD-1:PD-L inhibitory pathway affects both CD4+ and CD8+ T cells and is overcome by IL-2. *European Journal of Immunology*, **32**(3), 634–643.

Ceccaldi, R., Rondinelli, B., and D'Andrea, A. D. (2016). Repair Pathway Choices and Consequences at the Double-Strand Break. *Trends in Cell Biology*, **26**(1), 52–64.

Chai, J., Charboneau, A. L., Betz, B. L., and Weissman, B. E. (2005). Loss of the hSNF5 gene concomitantly inactivates p21CIP/WAF1 and p16INK4a activity associated with replicative senescence in A204 rhabdoid tumor cells. *Cancer Research*, **65**(22), 10192–10198.

Chalaux, E., López-Rovira, T., Rosa, J. L., Bartrons, R., and Ventura, F. (1998). JunB is involved in the inhibition of myogenic differentiation by bone morphogenetic protein-2. *The Journal of Biological Chemistry*, **273**(1), 537–43.

Chen, Q. and Ames, B. N. (1994). Senescence-like growth arrest induced by hydrogen peroxide in human diploid fibroblast F65 cells. *Proceedings of the National Academy of Sciences of the United States of America*, **91**(10), 4130–4134.

Chiruvella, K. K., Liang, Z., and Wilson, T. E. (2013). Repair of double-strand breaks by end joining. *Cold Spring Harbor Perspectives in Biology*, **5**(5), a012757.

Coppé, J.-P., Patil, C. K., Rodier, F., Sun, Y., Muñoz, D. P., Goldstein, J., Nelson, P. S., Desprez, P.-Y., and Campisi, J. (2008). Senescence-Associated Secretory Phenotypes Reveal Cell-Nonautonomous Functions of Oncogenic RAS and the p53 Tumor Suppressor. *PLoS Biology*, **6**(12), 2853–68.

Curran, T. and Franza, B. R. (1988). Fos and Jun: the AP-1 connection. *Cell*, **55**(3), 395–7.

Curtin, J. A., Fridlyand, J., Kageshita, T., Patel, H. N., Busam, K. J., Kutzner, H., Cho, K. H., Aiba, S., Bröcker, E. B., LeBoit, P. E., Pinkel, D., and Bastian, B. C. (2005). Distinct sets of genetic alterations in melanoma. *New England Journal of Medicine*, **353**(20), 2135–2147.

Davies, H., Bignell, G. R., Cox, C., Stephens, P., Edkins, S., Clegg, S., Teague, J., Woffendin, H., Garnett, M. J., Bottomley, W., Davis, N., Dicks, E., Ewing, R., Floyd, Y., Gray, K., Hall, S., Hawes, R., Hughes, J., Kosmidou, V., Menzies, A., Mould, C., Parker, A., Stevens, C., Watt, S., Hooper, S., Jayatilake, H., Gusterson, B. A., Cooper, C., Shipley, J., Hargrave, D., Pritchard-Jones, K., Maitland, N., Chenevix-Trench, G., Riggins, G. J., Bigner, D. D., Palmieri, G., Cossu, A., Flanagan, A., Nicholson, A., Ho, J. W., Leung, S. Y., Yuen, S. T., Weber, B. L., Seigler, H. F., Darrow, T. L., Paterson, H., Wooster, R., Wooster, R., Stratton, M. R., and Futreal, P. A. (2002). Mutations of the BRAF gene in human cancer. *Nature*, **417**(6892), 949–954.

De Cecco, M., Criscione, S. W., Peckham, E. J., Hillenmeyer, S., Hamm, E. A., Manivannan, J., Peterson, A. L., Kreiling, J. A., Neretti, N., and Sedivy, J. M. (2013). Genomes of replicatively senescent cells undergo global epigenetic changes leading to gene silencing and activation of transposable elements. *Aging Cell*, **12**(2), 247–256.

de Lange, T. (2005). Shelterin: the protein complex that shapes and safeguards human telomeres. *Genes & Development*, **19**(18), 2100–10.

Deng, C., Zhang, P., Wade Harper, J., Elledge, S. J., and Leder, P. (1995). Mice Lacking p21 CIP1/WAF1 undergo normal development, but are defective in G1 checkpoint control. *Cell*, **82**(4), 675–684.

Deng, T. and Karin, M. (1993). JunB differs from c-Jun in its DNA-binding and dimerization domains, and represses c-Jun by formation of inactive heterodimers. *Genes & Development*, **7**(3), 479–90.

Denoyelle, C., Abou-Rjaily, G., Bezrookove, V., Verhaegen, M., Johnson, T. M., Fullen, D. R., Pointer, J. N., Gruber, S. B., Su, L. D., Nikiforov, M. A., Kaufman, R. J., Bastian, B. C., and Soengas, M. S. (2006). Anti-oncogenic role of the endoplasmic reticulum differentially activated by mutations in the MAPK pathway. *Nature Cell Biology*, **8**(10), 1053–1063.

Dhomen, N., Reis-Filho, J. S., da Rocha Dias, S., Hayward, R., Savage, K., Delmas, V., Larue, L., Pritchard, C., and Marais, R. (2009). Oncogenic Braf induces melanocyte senescence and melanoma in mice. *Cancer Cell*, **15**(4), 294–303.

Difilippantonio, M. J., Zhu, J., Chen, H. T., Meffre, E., Nussenzweig, M. C., Max, E. E., Ried, T., and Nussenzweig, A. (2000). DNA repair protein Ku80 suppresses chromosomal aberrations and malignant transformation. *Nature*, **404**(6777), 510–4.

Dimri, G. P., Lee, X., Basile, G., Acosta, M., Scott, G., Roskelley, C., Medrano, E. E., Linskens, M., Rubelj, I., Pereira-Smith, O., Peacocke, M., and Campisi, J. (1995). A biomarker that identifies senescent human cells in culture and in aging skin in vivo. *Proceedings of the National Academy of Sciences of the United States of America*, **92**(20), 9363–9367.

Donehower, L. A. and Lozano, G. (2009). 20 years studying p53 functions in genetically engineered mice. *Nature Reviews Cancer*, **9**(11), 831–841.

Dulić, V., Kaufmann, W. K., Wilson, S. J., Tisty, T. D., Lees, E., Harper, J., Elledge, S. J., and Reed, S. I. (1994). p53-dependent inhibition of cyclin-dependent kinase activities in human fibroblasts during radiation-induced G1 arrest. *Cell*, **76**(6), 1013–1023.

Eferl, R. and Wagner, E. F. (2003). AP-1: a double-edged sword in tumorigenesis. *Nature Reviews Cancer*, **3**(11), 859–868.

Eferl, R., Ricci, R., Kenner, L., Zenz, R., David, J.-P., Rath, M., and Wagner, E. F. (2003). Liver tumor development. c-Jun antagonizes the proapoptotic activity of p53. *Cell*, **112**(2), 181–92.

Eischen, C. M., Woo, D., Roussel, M. F., and Cleveland, J. L. (2001). Apoptosis triggered by Myc-induced suppression of Bcl-X(L) or Bcl-2 is bypassed during lymphomagenesis. *Molecular and Cellular Biology*, **21**(15), 5063–70.

El-Deiry, W. S., Tokino, T., Velculescu, V. E., Levy, D. B., Parsons, R., Trent, J. M., Lin, D., Mercer, W., Kinzler, K. W., and Vogelstein, B. (1993). WAF1, a potential mediator of p53 tumor suppression. *Cell*, **75**(4), 817–825.

Eppihimer, M. J., Gunn, J., Freeman, G. J., Greenfield, E. A., Chernova, T., Erickson, J., and Leonard, J. P. (2002). Expression and regulation of the PD-L1 immunoinhibitory molecule on microvascular endothelial cells. *Microcirculation*, **9**(2), 133–45.

Fan, F., Bashari, M. H., Morelli, E., Tonon, G., Malvestiti, S., Vallet, S., Jarahian, M., Seckinger, A., Hose, D., Bakiri, L., Sun, C., Hu, Y., Ball, C. R., Glimm, H., Sattler, M., Goldschmidt, H., Wagner, E. F., Tassone, P., Jaeger, D., and Podar, K. (2017). The AP-1 transcription factor JunB is essential for multiple myeloma cell proliferation and drug resistance in the bone marrow microenvironment. *Leukemia*, **31**(7), 1570–1581.

Feldser, D. M. and Greider, C. W. (2007). Short telomeres limit tumor progression in vivo by inducing senescence. *Cancer Cell*, **11**(5), 461–9.

Finn, R. S., Dering, J., Conklin, D., Kalous, O., Cohen, D. J., Desai, A. J., Ginther, C., Atefi, M., Chen, I., Fowst, C., Los, G., and Slamon, D. J. (2009). PD 0332991, a selective cyclin D kinase 4/6 inhibitor, preferentially inhibits proliferation of luminal estrogen receptor-positive human breast cancer cell lines in vitro. *Breast Cancer Research*, **11**(5).

Flaherty, K. T., Puzanov, I., Kim, K. B., Ribas, A., McArthur, G. A., Sosman, J. A., O'Dwyer, P. J., Lee, R. J., Grippo, J. F., Nolop, K., and Chapman, P. B. (2010). Inhibition of mutated, activated BRAF in metastatic melanoma. *New England Journal of Medicine*, **363**(9), 809–819.

Folkman, J., Watson, K., Ingber, D., and Hanahan, D. (1989). Induction of angiogenesis during the transition from hyperplasia to neoplasia. *Nature*, **339**(6219), 58–61.

Fontaine, F., Overman, J., and François, M. (2015). Pharmacological manipulation of transcription factor protein-protein interactions: opportunities and obstacles. *Cell Regeneration*, **4**(1), 2.

Freeman, G. J., Long, A. J., Iwai, Y., Bourque, K., Chernova, T., Nishimura, H., Fitz, L. J., Malenkovich, N., Okazaki, T., Byrne, M. C., Horton, H. F., Fouser, L., Carter, L., Ling, V., Bowman, M. R., Carreno, B. M., Collins, M., Wood, C. R., and Honjo, T. (2000). Engagement of the PD-1 immunoinhibitory receptor by a novel B7 family member leads to negative regulation of lymphocyte activation. *Journal of Experimental Medicine*, **192**(7), 1027–1034.

Fukumura, D., Duda, D. G., Munn, L. L., and Jain, R. K. (2010). Tumor microvasculature and microenvironment: novel insights through intravital imaging in pre-clinical models. *Microcirculation*, **17**(3), 206–25.

Galmarini, F. C., Galmarini, C. M., Sarchi, M. I., Abulafia, J., and Galmarini, D. (2000). Heterogeneous distribution of tumor blood supply affects the response to chemotherapy in patients with head and neck cancer. *Microcirculation*, **7**(6 Pt 1), 405–10.

Gerlinger, M., Rowan, A. J., Horswell, S., Larkin, J., Endesfelder, D., Gronroos, E., Martinez, P., Matthews, N., Stewart, A., Tarpey, P., Varela, I., Phillimore, B., Begum, S., McDonald, N. Q., Butler, A., Jones, D., Raine, K., Latimer, C., Santos, C. R., Nohadani, M., Eklund, A. C., Spencer-Dene, B., Clark, G., Pickering, L., Stamp, G., Gore, M., Szallasi, Z., Downward, J., Futreal, P. A., and Swanton, C. (2012). Intratumor heterogeneity and branched evolution revealed by multiregion sequencing. *New England Journal of Medicine*, **366**(10), 883–892.

Giard, D. J., Aaronson, S. A., Todaro, G. J., Arnstein, P., Kersey, J. H., Dosik, H., and Parks, W. P. (1973). In vitro cultivation of human tumors: establishment of cell lines derived from a series of solid tumors. *Journal of the National Cancer Institute*, **51**(5), 1417–23.

Goetze, S., Kintscher, U., Kaneshiro, K., Meehan, W. P., Collins, A., Fleck, E., Hsueh, W. A., and Law, R. E. (2001). TNFalpha induces expression of transcription factors c-fos, Egr-1, and Ets-1 in vascular lesions through extracellular signal-regulated kinases 1/2. *Atherosclerosis*, **159**(1), 93–101.

Gomard, T., Michaud, H.-A., Tempé, D., Thiolon, K., Pelegrin, M., and Piechaczyk, M. (2010). An NF-kappaB-dependent role for JunB in the induction of proinflammatory cytokines in LPS-activated bone marrow-derived dendritic cells. *PLoS One*, **5**(3), e9585.

Gong, C., Shen, J., Fang, Z., Qiao, L., Feng, R., Lin, X., and Li, S. (2018). Abnormally expressed JunB transactivated by IL-6/STAT3 signaling promotes uveal melanoma aggressiveness via epithelial-mesenchymal transition. *Bioscience Reports*, **38**(4).

Graña, X., Garriga, J., and Mayol, X. (1998). Role of the retinoblastoma protein family, pRB, p107 and p130 in the negative control of cell growth. *Oncogene*, **17**(25), 3365–3383.

Granet, C. and Miossec, P. (2004). Combination of the pro-inflammatory cytokines IL-1, TNF-alpha and IL-17 leads to enhanced expression and additional recruitment of AP-1 family members, Egr-1 and NF-kappaB in osteoblast-like cells. *Cytokine*, **26**(4), 169–77.

Greaves, M. and Maley, C. C. (2012). Clonal evolution in cancer. *Nature*, **481**(7381), 306–313.

Greider, C. and Blackburn, E. (1996). Telomeres, Telomerase and Cancer. *Scientific American*, **274**(2), 92–97.

Gupta, P. B., Fillmore, C. M., Jiang, G., Shapira, S. D., Tao, K., Kuperwasser, C., and Lander, E. S. (2011). Stochastic state transitions give rise to phenotypic equilibrium in populations of cancer cells. *Cell*, **146**(4), 633–44.

Gurzov, E. N., Ortis, F., Bakiri, L., Wagner, E. F., and Eizirik, D. L. (2008). JunB Inhibits ER Stress and Apoptosis in Pancreatic Beta Cells. *PLoS One*, **3**(8), e3030.

Gurzov, E. N., Barthson, J., Marhfour, I., Ortis, F., Naamane, N., Igoillo-Esteve, M., Gysemans, C., Mathieu, C., Kitajima, S., Marchetti, P., Ørntoft, T. F., Bakiri, L., Wagner, E. F., and Eizirik, D. L. (2012). Pancreatic β-cells activate a JunB/ATF3-dependent survival pathway during inflammation. *Oncogene*, **31**(13), 1723–32.

Hahn, M. S. (2017). *Die Rolle p16INK4a-gesteuerter Signalwege in der Zytokin-induzierten Seneszenz*. Ph.D. thesis, Eberhard Karls Universität Tübingen.

Hai, T. and Curran, T. (1991). Cross-family dimerization of transcription factors Fos/Jun and ATF/CREB alters DNA binding specificity. *Proceedings of the National Academy of Sciences of the United States of America*, **88**(9), 3720–4.

Halazonetis, T. D., Georgopoulos, K., Greenberg, M. E., and Leder, P. (1988). c-Jun dimerizes with itself and with c-Fos, forming complexes of different DNA binding affinities. *Cell*, **55**(5), 917–24.

Han, Z., Wei, W., Dunaway, S., Darnowski, J. W., Calabresi, P., Sedivy, J., Hendrickson, E. A., Balan, K. V., Pantazis, P., and Wyche, J. H. (2002). Role of p21 in apoptosis and senescence of human colon cancer cells treated with camptothecin. *The Journal of Biological Chemistry*, **277**(19), 17154–17160.

Hanahan, D. (1985). Heritable formation of pancreatic β-cell tumours in transgenic mice expressing recombinant insulin/simian virus 40 oncogenes. *Nature*, **315**(6015), 115–122.

Hanahan, D. and Weinberg, R. A. (2011). Hallmarks of cancer: The next generation. *Cell*, **144**(5), 646–674.

Hara, E., Tsurui, H., Shinozaki, A., Nakada, S., and Oda, K. (1991). Cooperative effect of antisense-Rb and antisense-p53 oligomers on the extension of life span in human diploid fibroblasts, TIG-1. *Biochemical and Biophysical Research Communications*, **179**(1), 528–534.

Hay, K. A., Hanafi, L. A., Li, D., Gust, J., Liles, W. C., Wurfel, M. M., López, J. A., Chen, J., Chung, D., Harju-Baker, S., Cherian, S., Chen, X., Riddell, S. R., Maloney, D. G., and Turtle, C. J. (2017). Kinetics and biomarkers of severe cytokine release syndrome after CD19 chimeric antigen receptor–modified T-cell therapy. *Blood*, **130**(21), 2295–2306.

Hayflick, L. and Moorhead, P. S. (1961). The serial cultivation of human diploid cell strains. *Experimental Cell Research*, **25**(3), 585–621.

Hicks, M., Hu, Q., Macrae, E., and DeWille, J. (2014). JUNB promotes the survival of Flavopiridol treated human breast cancer cells. *Biochemical and Biophysical Research Communications*, **450**(1), 19–24.

Hinds, P. W., Mittnacht, S., Dulic, V., Arnold, A., Reed, S. I., and Weinberg, R. A. (1992). Regulation of retinoblastoma protein functions by ectopic expression of human cyclins. *Cell*, **70**(6), 993–1006.

Hirai, S. and Yaniv, M. (1989). Jun DNA-binding is modulated by mutations between the leucines or by direct interaction of fos with the TGACTCA sequence. *The New Biologist*, **1**(2), 181–91.

Hodgson, G., Hager, J. H., Volik, S., Hariono, S., Wernick, M., Moore, D., Nowak, N., Albertson, D. G., Pinkel, D., Collins, C., Hanahan, D., and Gray, J. W. (2001). Genome scanning with array CGH delineates regional alterations in mouse islet carcinomas. *Nature Genetics*, **29**(4), 459–64.

Hoelder, S., Clarke, P. A., and Workman, P. (2012). Discovery of small molecule cancer drugs: Successes, challenges and opportunities. *Molecular Oncology*, **6**(2), 155–176.

Hyakusoku, H., Sano, D., Takahashi, H., Hatano, T., Isono, Y., Shimada, S., Ito, Y., Myers, J. N., and Oridate, N. (2016). JunB promotes cell invasion, migration and distant metastasis of head and neck squamous cell carcinoma. *Journal of Experimental & Clinical Cancer Research*, **35**, 6.

Ismail, I. H., Nyström, S., Nygren, J., and Hammarsten, O. (2005). Activation of ataxia telangiectasia mutated by DNA strand break-inducing agents correlates closely with the number of DNA double strand breaks. *The Journal of Biological Chemistry*, **280**(6), 4649–55.

Janku, F., Garrido-Laguna, I., Petruzelka, L. B., Stewart, D. J., and Kurzrock, R. (2011). Novel Therapeutic Targets in Non-small Cell Lung Cancer. *Journal of Thoracic Oncology*, **6**(9), 1601–1612.

Juarez, J. C., Manuia, M., Burnett, M. E., Betancourt, O., Boivin, B., Shaw, D. E., Tonks, N. K., Mazar, A. P., and Doñate, F. (2008). Superoxide dismutase 1 (SOD1) is essential for H2O2-mediated oxidation and inactivation of phosphatases in growth factor signaling. *Proceedings of the National Academy of Sciences of the United States of America*, **105**(20), 7147–52.

Kalos, M., Levine, B. L., Porter, D. L., Katz, S., Grupp, S. A., Bagg, A., and June, C. H. (2011). T cells with chimeric antigen receptors have potent antitumor effects and can establish memory in patients with advanced leukemia. *Science Translational Medicine*, **3**(95).

Karanam, K., Kafri, R., Loewer, A., and Lahav, G. (2012). Quantitative live cell imaging reveals a gradual shift between DNA repair mechanisms and a maximal use of HR in mid S phase. *Molecular Cell*, **47**(2), 320–9.

Kasibhatla, S., Brunner, T., Genestier, L., Echeverri, F., Mahboubi, A., and Green, D. R. (1998). DNA Damaging Agents Induce Expression of Fas Ligand and Subsequent Apoptosis in T Lymphocytes via the Activation of NF-κB and AP-1. *Molecular Cell*, **1**(4), 543–551.

Kataoka, K., Fujiwara, K. T., Noda, M., and Nishizawa, M. (1994). MafB, a new Maf family transcription activator that can associate with Maf and Fos but not with Jun. *Molecular and Cellular Biology*, **14**(11), 7581–91.

Kawakami, Z., Kitabayashi, I., Matsuoka, T., Gachelin, G., and Yokoyama, K. (1992). Conserved structural motifs among mammalian junB genes. *Nucleic Acids Research*, **20**(4), 914.

Keir, M. E., Francisco, L. M., and Sharpe, A. H. (2007). PD-1 and its ligands in T-cell immunity. *Current Opinion in Immunology*, **19**(3), 309–314.

Kerppola, T. K. and Curran, T. (1994a). A conserved region adjacent to the basic domain is required for recognition of an extended DNA binding site by Maf/Nrl family proteins. *Oncogene*, **9**(11), 3149–58.

Kerppola, T. K. and Curran, T. (1994b). Maf and Nrl can bind to AP-1 sites and form heterodimers with Fos and Jun. *Oncogene*, **9**(3), 675–84.

Kleffel, S., Posch, C., Barthel, S. R., Mueller, H., Schlapbach, C., Guenova, E., Elco, C. P., Lee, N., Juneja, V. R., Zhan, Q., Lian, C. G., Thomi, R., Hoetzenecker, W., Cozzio, A., Dummer, R., Mihm, M. C., Flaherty, K. T., Frank, M. H., Murphy, G. F., Sharpe, A. H., Kupper, T. S., and Schatton, T. (2015). Melanoma Cell-Intrinsic PD-1 Receptor Functions Promote Tumor Growth. *Cell*, **162**(6), 1242–1256.

Kobayashi, M., Sonobe, M., Takahashi, T., Yoshizawa, A., Ishikawa, M., Kikuchi, R., Okubo, K., Huang, C.-L., and Date, H. (2011). Clinical significance of BRAF gene mutations in patients with non-small cell lung cancer. *Anticancer Research*, **31**(12), 4619–23.

Kochenderfer, J. N., Wilson, W. H., Janik, J. E., Dudley, M. E., Stetler-Stevenson, M., Feldman, S. A., Maric, I., Raffeld, M., Nathan, D. A. N., Lanier, B. J., Morgan, R. A., and Rosenberg, S. A. (2010). Eradication of B-lineage cells and regression of lymphoma in a patient treated with autologous T cells genetically engineered to recognize CD19. *Blood*, **116**(20), 4099–4102.

Kong, X., Kuilman, T., Shahrabi, A., Boshuizen, J., Kemper, K., Song, J.-Y., Niessen, H. W. M., Rozeman, E. A., Geukes Foppen, M. H., Blank, C. U., and Peeper, D. S. (2017). Cancer drug addiction is relayed by an ERK2-dependent phenotype switch. *Nature*, **550**(7675), 270–274.

Konishi, N., Shimada, K., Nakamura, M., Ishida, E., Ota, I., Tanaka, N., and Fujimoto, K. (2008). Function of JunB in transient amplifying cell senescence and progression of human prostate cancer. *Clinical Cancer Research*, **14**(14), 4408–16.

Kovary, K. and Bravo, R. (1991). Expression of different Jun and Fos proteins during the G0-to-G1 transition in mouse fibroblasts: in vitro and in vivo associations. *Molecular and Cellular Biology*, **11**(5), 2451–9.

Kovary, K. and Bravo, R. (1992). Existence of different Fos/Jun complexes during the G0-to-G1 transition and during exponential growth in mouse fibroblasts: differential role of Fos proteins. *Molecular and Cellular Biology*, **12**(11), 5015–23.

Krishnamurthy, J., Torrice, C., Ramsey, M. R., Kovalev, G. I., Al-Regaiey, K., Su, L., and Sharpless, N. E. (2004). Ink4a/Arf expression is a biomarker of aging. *Journal of Clinical Investigation*, **114**(9), 1299–307.

Krizhanovsky, V., Yon, M., Dickins, R. A., Hearn, S., Simon, J., Miething, C., Yee, H., Zender, L., and Lowe, S. W. (2008). Senescence of Activated Stellate Cells Limits Liver Fibrosis. *Cell*, **134**(4), 657–667.

Kroner, A., Mehling, M., Hemmer, B., Rieckmann, P., Toyka, K. V., Mäurer, M., and Wiendl, H. (2005). A PD-1 polymorphism is associated with disease progression in multiple sclerosis. *Annals of Neurology*, **58**(1), 50–57.

Krummel, M. F. and Allison, J. P. (2011). Pillars Article: CD28 and CTLA-4 Have Opposing Effects on the Response of T Cells to Stimulation. The Journal of Experimental Medicine. 1995. 182: 459–465. *The Journal of Immunology*, **187**(7), 3459–3465.

Kurzrock, R., Kantarjian, H. M., Druker, B. J., and Talpaz, M. (2003). Philadelphia ChromosomePositive Leukemias: From Basic Mechanisms to Molecular Therapeutics. *Annals of Internal Medicine*, **138**(10), 819.

Kuukasjärvi, T., Karhu, R., Tanner, M., Kähkönen, M., Schäffer, A., Nupponen, N., Pennanen, S., Kallioniemi, A., Kallioniemi, O. P., and Isola, J. (1997). Genetic heterogeneity and clonal evolution underlying development of asynchronous metastasis in human breast cancer. *Cancer Research*, **57**(8), 1597–604.

Landau, D. A., Carter, S. L., Stojanov, P., McKenna, A., Stevenson, K., Lawrence, M. S., Sougnez, C., Stewart, C., Sivachenko, A., Wang, L., Wan, Y., Zhang, W., Shukla, S. A., Vartanov, A., Fernandes, S. M., Saksena, G., Cibulskis, K., Tesar, B., Gabriel, S., Hacohen, N., Meyerson, M., Lander, E. S., Neuberg, D., Brown, J. R., Getz, G., and Wu, C. J. (2013). Evolution and impact of subclonal mutations in chronic lymphocytic leukemia. *Cell*, **152**(4), 714–26.

Lane, D. P. (1992). p53, guardian of the genome. *Nature*, **358**(6381), 15–16.

Latchman, Y., Wood, C. R., Chernova, T., Chaudhary, D., Borde, M., Chernova, I., Iwai, Y., Long, A. J., Brown, J. A., Nunes, R., Greenfield, E. A., Bourque, K., Boussiotis, V. A., Carter, L. L., Carreno, B. M., Malenkovich, N., Nishimura, H., Okazaki, T., Honjo, T., Sharpe, A. H., and Freeman, G. J. (2001). PD-L2 is a second ligand for PD-1 and inhibits T cell activation. *Nature Immunology*, **2**(3), 261–268.

Latchman, Y. E., Liang, S. C., Wu, Y., Chernova, T., Sobel, R. A., Klemm, M., Kuchroo, V. K., Freman, G. J., and Sharpe, A. H. (2004). PD-L1-deficient mice show that PD-L1 on T cells, antigen-presenting cells, and host tissues negatively regulates T cells. *Proceedings of the National Academy of Sciences of the United States of America*, **101**(29), 10691–10696.

Lawless, C., Wang, C., Jurk, D., Merz, A., von Zglinicki, T., and Passos, J. F. (2010). Quantitative assessment of markers for cell senescence. *Experimental Gerontology*, **45**(10), 772–778.

Lawlor, E. R., Soucek, L., Brown-Swigart, L., Shchors, K., Bialucha, C. U., and Evan, G. I. (2006). Reversible kinetic analysis of Myc targets in vivo provides novel insights into Myc-mediated tumorigenesis. *Cancer Research*, **66**(9), 4591–601.

Layzer, J. M., McCaffrey, A. P., Tanner, A. K., Huang, Z., Kay, M. A., and Sullenger, B. A. (2004). In vivo activity of nuclease-resistant siRNAs. *RNA*, **10**(5), 766–71.

Lecot, P., Alimirah, F., Desprez, P. Y., Campisi, J., and Wiley, C. (2016). Context-dependent effects of cellular senescence in cancer development. *British Journal of Cancer*, **114**(11), 1180–1184.

Ledford, H. (2007). Minimum telomere length defined for healthy cells. *Nature*, **449**(7162), 515.

Lee, B. Y., Han, J. A., Im, J. S., Morrone, A., Johung, K., Goodwin, E. C., Kleijer, W. J., DiMaio, D., and Hwang, E. S. (2006). Senescence-associated β-galactosidase is lysosomal β-galactosidase. *Aging Cell*, **5**(2), 187–195.

Lee, W., Mitchell, P., and Tjian, R. (1987). Purified transcription factor AP-1 interacts with TPA-inducible enhancer elements. *Cell*, **49**(6), 741–52.

Leone, P., Shin, E.-C., Perosa, F., Vacca, A., Dammacco, F., and Racanelli, V. (2013). MHC class I antigen processing and presenting machinery: organization, function, and defects in tumor cells. *Journal of the National Cancer Institute*, **105**(16), 1172–87.

Lim, J. S. J. and Soo, R. A. (2016). Nivolumab in the treatment of metastatic squamous non-small cell lung cancer: a review of the evidence. *Therapeutic Advances in Respiratory Disease*, **10**(5), 444–54.

Lin, A. W., Barradas, M., Stone, J. C., van Aelst, L., Serrano, M., and Lowe, S. W. (1998). Premature senescence involving p53 and p16 is activated in response to constitutive MEK/MAPK mitogenic signaling. *Genes & Development*, **12**(19), 3008–3019.

Liu, T. and Altman, R. B. (2014). Identifying druggable targets by protein microenvironments matching: application to transcription factors. *CPT: Pharmacometrics & Systems Pharmacology*, **3**(1), e93.

Malnou, C. E., Brockly, F., Favard, C., Moquet-Torcy, G., Piechaczyk, M., and Jariel-Encontre, I. (2010). Heterodimerization with different Jun proteins controls c-Fos intranuclear dynamics and distribution. *The Journal of Biological Chemistry*, **285**(9), 6552–62.

Malumbres, M. and Pellicer, A. (1998). RAS pathways to cell cycle control and cell transformation. *Frontiers in Bioscience*, **3**, d887–912.

Marconcini, L., Marchio, S., Morbidelli, L., Cartocci, E., Albini, A., Ziche, M., Bussolino, F., and Oliviero, S. (1999). c-fos-induced growth factor/vascular endothelial growth factor D induces angiogenesis in vivo and in vitro. *Proceedings of the National Academy of Sciences of the United States of America*, **96**(17), 9671–6.

Mccurrach, M. E., Connor, T. M., Knudson, C. M., Korsmeyer, S. J., and Lowe, S. W. (1997). bax-deficiency promotes drug resistance and oncogenic transformation by attenuating p53-dependent apoptosis. *Proceedings of the National Academy of Sciences of the United States of America*, **94**(6), 2345–2349.

Michaloglou, C., Vredeveld, L. C. W., Soengas, M. S., Denoyelle, C., Kuilman, T., van der Horst, C. M. A. M., Majoor, D. M., Shay, J. W., Mooi, W. J., and Peeper, D. S. (2005). BRAFE600-associated senescence-like cell cycle arrest of human naevi. *Nature*, **436**(7051), 720–724.

Mihic-Probst, D., Mnich, C. D., Oberholzer, P. A., Seifert, B., Sasse, B., Moch, H., and Dummer, R. (2006). p16 expression in primary malignant melanoma is associated with prognosis and lymph node status. *International Journal of Cancer*, **118**(9), 2262–8.

Mirzayans, R., Andrais, B., Hansen, G., and Murray, D. (2012). Role of p16(INK4A) in Replicative Senescence and DNA Damage-Induced Premature Senescence in p53-Deficient Human Cells. *Biochemistry Research International*, **2012**, 951574.

Morgan, R. A., Yang, J. C., Kitano, M., Dudley, M. E., Laurencot, C. M., and Rosenberg, S. A. (2010). Case report of a serious adverse event following the administration of t cells transduced with a chimeric antigen receptor recognizing ERBB2. *Molecular Therapy*, **18**(4), 843–851.

Morrissey, D. V., Blanchard, K., Shaw, L., Jensen, K., Lockridge, J. A., Dickinson, B., McSwiggen, J. A., Vargeese, C., Bowman, K., Shaffer, C. S., Polisky, B. A., and Zinnen, S. (2005). Activity of stabilized short interfering RNA in a mouse model of hepatitis B virus replication. *Hepatology*, **41**(6), 1349–56.

Murphy, D. J., Junttila, M. R., Pouyet, L., Karnezis, A., Shchors, K., Bui, D. A., Brown-Swigart, L., Johnson, L., and Evan, G. I. (2008). Distinct thresholds govern Myc's biological output in vivo. *Cancer Cell*, **14**(6), 447–57.

Naik, P., Karrim, J., and Hanahan, D. (1996). The rise and fall of apoptosis during multistage tumorigenesis: Down-modulation contributes to tumor progression from angiogenic progenitors. *Genes and Development*, **10**(17), 2105–2116.

Nakano, K. and Vousden, K. H. (2001). PUMA, a Novel Proapoptotic Gene, Is Induced by p53. *Molecular Cell*, **7**(3), 683–694.

Narita, M., Nũnez, S., Heard, E., Narita, M., Lin, A. W., Hearn, S. A., Spector, D. L., Hannon, G. J., and Lowe, S. W. (2003). Rb-mediated heterochromatin formation and silencing of E2F target genes during cellular senescence. *Cell*, **113**(6), 703–716.

National Center for Biotechnology Information, U. N. L. o. M. (2019a). JunB proto-oncogene [Homo sapiens (human)]. https://www.ncbi.nlm.nih.gov/gene/3726.

National Center for Biotechnology Information, U. N. L. o. M. (2019b). JunB proto-oncogene [Mus musculus (house mouse)]. https://www.ncbi.nlm.nih.gov/gene/16477.

Nguyen, H. V., Mouly, E., Chemin, K., Luinaud, R., Despres, R., Fermand, J.-P., Arnulf, B., and Bories, J.-C. (2012). The Ets-1 transcription factor is required for Stat1-mediated T-bet expression and IgG2a class switching in mouse B cells. *Blood*, **119**(18), 4174–81.

Nishimura, H., Nose, M., Hiai, H., Minato, N., and Honjo, T. (1999). Development of lupus-like autoimmune diseases by disruption of the PD-1 gene encoding an ITIM motif-carrying immunoreceptor. *Immunity*, **11**(2), 141–151.

Ohtani, N., Zebedee, Z., Huot, T. J. G., Stinson, J. A., Sugimoto, M., Ohashi, Y., Sharrocks, A. D., Peters, G., and Hara, E. (2001). Opposing effects of Ets and Id proteins on p16INK4a expression during cellular senescence. *Nature*, **409**(6823), 1067–1070.

Okazaki, T., Tanaka, Y., Nishio, R., Mitsuiye, T., Mizoguchi, A., Wang, J., Ishida, M., Hiai, H., Matsumori, A., Minato, N., and Honjo, T. (2003). Autoantibodies against cardiac troponin I are responsible for dilated cardiomyopathy in PD-1-deficient mice. *Nature Medicine*, **9**(12), 1477–1483.

Paris, P. L., Andaya, A., Fridlyand, J., Jain, A. N., Weinberg, V., Kowbel, D., Brebner, J. H., Simko, J., Watson, J. V., Volik, S., Albertson, D. G., Pinkel, D., Alers, J. C., van der Kwast, T. H., Vissers, K. J., Schroder, F. H., Wildhagen, M. F., Febbo, P. G., Chinnaiyan, A. M., Pienta, K. J., Carroll, P. R., Rubin, M. A., Collins, C., and van Dekken, H. (2004). Whole genome scanning identifies genotypes associated with recurrence and metastasis in prostate tumors. *Human Molecular Genetics*, **13**(13), 1303–1313.

Park, J. I., Jeong, J. S., Han, J. Y., Kim, D. I., Gao, Y. H., Park, S. C., Rodgers, G. P., and Kim, I. H. (2000). Hydroxyurea induces a senescence-like change of K562 human erythroleukemia cell. *Journal of Cancer Research and Clinical Oncology*, **126**(8), 455–60.

Passegué, E. and Wagner, E. F. (2000). JunB suppresses cell proliferation by transcriptional activation of p16INK4a expression. *The EMBO Journal*, **19**(12), 2969–2979.

Passegué, E., Jochum, W., Schorpp-Kistner, M., Möhle-Steinlein, U., and Wagner, E. F. (2001). Chronic myeloid leukemia with increased granulocyte progenitors in mice lacking junB expression in the myeloid lineage. *Cell*, **104**(1), 21–32.

Passegué, E., Jochum, W., Behrens, A., Ricci, R., and Wagner, E. F. (2002). JunB can substitute for Jun in mouse development and cell proliferation. *Nature Genetics*, **30**(2), 158–66.

Paulson, T. G., Almasan, A., Brody, L. L., and Wahl, G. M. (1998). Gene Amplification in a p53-Deficient Cell Line Requires Cell Cycle Progression under Conditions That Generate DNA Breakage. *Molecular and Cellular Biology*, **18**(5), 3089–3100.

Pelengaris, S., Khan, M., and Evan, G. I. (2002). Suppression of Myc-induced apoptosis in beta cells exposes multiple oncogenic properties of Myc and triggers carcinogenic progression. *Cell*, **109**(3), 321–34.

Pérez-Benavente, B., García, J. L., Rodríguez, M. S., Pineda-Lucena, A., Piechaczyk, M., Font de Mora, J., and Farràs, R. (2013). GSK3-SCF(FBXW7) targets JunB for degradation in G2 to preserve chromatid cohesion before anaphase. *Oncogene*, **32**(17), 2189–99.

Pfarr, C. M., Mechta, F., Spyrou, G., Lallemand, D., Carillo, S., and Yaniv, M. (1994). Mouse JunD negatively regulates fibroblast growth and antagonizes transformation by ras. *Cell*, **76**(4), 747–60.

Pflegerl, P., Vesely, P., Hantusch, B., Schlederer, M., Zenz, R., Janig, E., Steiner, G., Meixner, A., Petzelbauer, P., Wolf, P., Soleiman, A., Egger, G., Moriggl, R., Kishimoto, T., Wagner, E. F., and Kenner, L. (2009). Epidermal loss of JunB leads to a SLE phenotype due to hyper IL-6 signaling. *Proceedings of the National Academy of Sciences of the United States of America*, **106**(48), 20423–20428.

Piechaczyk, M. and Farràs, R. (2008). Regulation and function of JunB in cell proliferation. *Biochemical Society Transactions*, **36**(Pt 5), 864–7.

Pietsch, E. C., Sykes, S. M., McMahon, S. B., and Murphy, M. E. (2008). The p53 family and programmed cell death. *Oncogene*, **27**(50), 6507–21.

Pipiras, E., Coquelle, A., Bieth, A., and Debatisse, M. (1998). Interstitial deletions and intrachromosomal amplification initiated from a double-strand break targeted to a mammalian chromosome. *The EMBO Journal*, **17**(1), 325–33.

Pollock, P. M., Harper, U. L., Hansen, K. S., Yudt, L. M., Stark, M., Robbins, C. M., Moses, T. Y., Hostetter, G., Wagner, U., Kakareka, J., Salem, G., Pohida, T., Heenan, P., Duray, P., Kallioniemi, O., Hayward, N. K., Trent, J. M., and Meltzer, P. S. (2003). High frequency of BRAF mutations in nevi. *Nature Genetics*, **33**(1), 19–20.

Porter, D. L., Levine, B. L., Kalos, M., Bagg, A., and June, C. H. (2011). Chimeric antigen receptor-modified T cells in chronic lymphoid leukemia. *New England Journal of Medicine*, **365**(8), 725–733.

Rauscher, F. J., Voulalas, P. J., Franza, B. R., and Curran, T. (1988). Fos and Jun bind cooperatively to the AP-1 site: reconstitution in vitro. *Genes & Development*, **2**(12B), 1687–99.

Rayess, H., Wang, M. B., and Srivatsan, E. S. (2012). Cellular senescence and tumor suppressor gene p16. *International Journal of Cancer*, **130**(8), 1715–25.

Reinhard, C., Shamoon, B., Shyamala, V., and Williams, L. T. (1997). Tumor necrosis factor alpha-induced activation of c-jun N-terminal kinase is mediated by TRAF2. *The EMBO Journal*, **16**(5), 1080–92.

Robinson, C. M., Prime, S. S., Huntley, S., Stone, A. M., Davies, M., Eveson, J. W., and Paterson, I. C. (2001). Overexpression of JunB in undifferentiated malignant rat oral keratinocytes enhances the malignant phenotype in vitro without altering cellular differentiation. *International Journal of Cancer*, **91**(5), 625–30.

Roos, W., Baumgartner, M., and Kaina, B. (2004). Apoptosis triggered by DNA damage O6-methylguanine in human lymphocytes requires DNA replication and is mediated by p53 and Fas/CD95/Apo-1. *Oncogene*, **23**(2), 359–367.

Roos, W. P. and Kaina, B. (2006). DNA damage-induced cell death by apoptosis. *Trends in Molecular Medicine*, **12**(9), 440–450.

Ryseck, R. P. and Bravo, R. (1991). c-JUN, JUN B, and JUN D differ in their binding affinities to AP-1 and CRE consensus sequences: Effect of FOS proteins. *Oncogene*, **6**(4), 533–542.

Sachdeva, U. M. and O'Brien, J. M. (2012). Understanding pRb: toward the necessary development of targeted treatments for retinoblastoma. *Journal of Clinical Investigation*, **122**(2), 425–434.

Sacher, A. G. and Gandhi, L. (2016). Biomarkers for the clinical use of PD-1/PD-L1 inhibitors in non-small-cell lung cancer: A review. *JAMA Oncology*, **2**(9), 1217–1222.

Sarkisian, C. J., Keister, B. A., Stairs, D. B., Boxer, R. B., Moody, S. E., and Chodosh, L. A. (2007). Dose-dependent oncogene-induced senescence in vivo and its evasion during mammary tumorigenesis. *Nature Cell Biology*, **9**(5), 493–505.

Savoldo, B., Ramos, C. A., Liu, E., Mims, M. P., Keating, M. J., Carrum, G., Kamble, R. T., Bollard, C. M., Gee, A. P., Mei, Z., Liu, H., Grilley, B., Rooney, C. M., Heslop, H. E., Brenner, M. K., and Dotti, G. (2011). CD28 costimulation improves expansion

and persistence of chimeric antigen receptor-modified T cells in lymphoma patients. *Journal of Clinical Investigation*, **121**(5), 1822–1826.

Schmid, D. I., Schwertz, H., Jiang, H., Campbell, R. A., Weyrich, A. S., McIntyre, T. M., Zimmerman, G. A., and Kraiss, L. W. (2013). Translational control of JunB, an AP-1 transcription factor, in activated human endothelial cells. *Journal of Cellular Biochemistry*, **114**(7), 1519–28.

Schmidt, D., Textor, B., Pein, O. T., Licht, A. H., Andrecht, S., Sator-Schmitt, M., Fusenig, N. E., Angel, P., and Schorpp-Kistner, M. (2007). Critical role for NF-κB-induced JunB in VEGF regulation and tumor angiogenesis. *The EMBO Journal*, **26**(3), 710–719.

Schorpp-Kistner, M., Wang, Z. Q., Angel, P., and Wagner, E. F. (1999). JunB is essential for mammalian placentation. *The EMBO Journal*, **18**(4), 934–48.

Serrano, M., Lin, A. W., McCurrach, M. E., Beach, D., and Lowe, S. W. (1997). Oncogenic ras provokes premature cell senescence associated with accumulation of p53 and p16INK4a. *Cell*, **88**(5), 593–602.

Sewing, A., Wiseman, B., Lloyd, A. C., and Land, H. (1997). High-intensity Raf signal causes cell cycle arrest mediated by p21Cip1. *Molecular and Cellular Biology*, **17**(9), 5588–97.

Shackleton, M., Quintana, E., Fearon, E. R., and Morrison, S. J. (2009). Heterogeneity in cancer: cancer stem cells versus clonal evolution. *Cell*, **138**(5), 822–9.

Sharpe, A. H. and Freeman, G. J. (2002). The B7-CD28 superfamily. *Nature Reviews Immunology*, **2**(2), 116–126.

Sharpless, N. E. and Sherr, C. J. (2015). Forging a signature of in vivo senescence. *Nature Reviews Cancer*, **15**(7), 397–408.

Shay, J. W. and Wright, W. E. (2000). Hayflick, his limit, and cellular ageing. *Nature Reviews Molecular Cell Biology*, **1**(1), 72–76.

Shay, J. W., Pereira-Smith, O. M., and Wright, W. E. (1991). A role for both RB and p53 in the regulation of human cellular senescence. *Experimental Cell Research*, **196**(1), 33–39.

Snuderl, M., Fazlollahi, L., Le, L. P., Nitta, M., Zhelyazkova, B. H., Davidson, C. J., Akhavanfard, S., Cahill, D. P., Aldape, K. D., Betensky, R. A., Louis, D. N., and Iafrate, A. J. (2011). Mosaic amplification of multiple receptor tyrosine kinase genes in glioblastoma. *Cancer Cell*, **20**(6), 810–817.

Son, Y.-O., Heo, J.-S., Kim, T.-G., Jeon, Y.-M., Kim, J.-G., and Lee, J.-C. (2010). Overexpression of JunB inhibits mitochondrial stress and cytotoxicity in human lymphoma cells exposed to chronic oxidative stress. *BMB Reports*, **43**(1), 57–61.

Sosa, V., Moliné, T., Somoza, R., Paciucci, R., Kondoh, H., and LLeonart, M. E. (2013). Oxidative stress and cancer: An overview. *Ageing Research Reviews*, **12**(1), 376–390.

Sreeramaneni, R., Chaudhry, A., McMahon, M., Sherr, C. J., and Inoue, K. (2005). Ras-Raf-Arf Signaling Critically Depends on the Dmp1 Transcription Factor. *Molecular and Cellular Biology*, **25**(1), 220–232.

Staber, P. B., Vesely, P., Haq, N., Ott, R. G., Funato, K., Bambach, I., Fuchs, C., Schauer, S., Linkesch, W., Hrzenjak, A., Dirks, W. G., Sexl, V., Bergler, H., Kadin, M. E., Sternberg, D. W., Kenner, L., and Hoefler, G. (2007). The oncoprotein NPM-ALK of anaplastic large-cell lymphoma induces JUNB transcription via ERK1/2 and JunB translation via mTOR signaling. *Blood*, **110**(9), 3374–3383.

Strickland, K. C., Howitt, B. E., Shukla, S. A., Rodig, S., Ritterhouse, L. L., Liu, J. F., Garber, J. E., Chowdhury, D., Wu, C. J., D'Andrea, A. D., Matulonis, U. A., and Konstantinopoulos, P. A. (2016). Association and prognostic significance of BRCA1/2-mutation status with neoantigen load, number of tumor-infiltrating lymphocytes and expression of PD-1/PD-L1 in high grade serous ovarian cancer. *Oncotarget*, **7**(12), 13587–13598.

Sutherland, G. R. (1977). Fragile sites on human chromosomes: demonstration of their dependence on the type of tissue culture medium. *Science*, **197**(4300), 265–6.

Suzuki-Takahashi, I., Kitagawa, M., Saijo, M., Higashi, H., Ogino, H., Matsumoto, H., Taya, Y., Nishimura, S., and Okuyama, A. (1995). The interactions of E2F with pRB and with p107 are regulated via the phosphorylation of pRB and p107 by a cyclin-dependent kinase. *Oncogene*, **10**(9), 1691–8.

Swaika, A., Crozier, J. A., and Joseph, R. W. (2014). Vemurafenib: an evidence-based review of its clinical utility in the treatment of metastatic melanoma. *Drug Design, Development and Therapy*, **8**, 775–87.

Szerlip, N. J., Pedraza, A., Chakravarty, D., Azim, M., McGuire, J., Fang, Y., Ozawa, T., Holland, E. C., Huse, J. T., Jhanwar, S., Leversha, M. A., Mikkelsen, T., and Brennan, C. W. (2012). Intratumoral heterogeneity of receptor tyrosine kinases EGFR and PDGFRA amplification in glioblastoma defines subpopulations with distinct growth factor response. *Proceedings of the National Academy of Sciences of the United States of America*, **109**(8), 3041–6.

Takai, H., Smogorzewska, A., and De Lange, T. (2003). DNA damage foci at dysfunctional telomeres. *Current Biology*, **13**(17), 1549–1556.

te Poele, R. H., Okorokov, A. L., Jardine, L., Cummings, J., and Joel, S. P. (2002). DNA damage is able to induce senescence in tumor cells in vitro and in vivo. *Cancer Research*, **62**(6), 1876–83.

Teitelman, G., Alpert, S., and Hanahan, D. (1988). Proliferation, senescence, and neoplastic progression of beta cells in hyperplasic pancreatic islets. *Cell*, **52**(1), 97–105.

Textor, B., Sator-Schmitt, M., Richter, K. H., Angel, P., and Schorpp-Kistner, M. (2006). c-Jun and JunB are essential for hypoglycemia-mediated VEGF induction. *Annals of the New York Academy of Sciences*, **1091**(1), 310–8.

Thomsen, M. K., Bakiri, L., Hasenfuss, S. C., Wu, H., Morente, M., and Wagner, E. F. (2015). Loss of JUNB/AP-1 promotes invasive prostate cancer. *Cell Death & Differentiation*, **22**(4), 574–82.

Topalian, S. L., Hodi, F. S., Brahmer, J. R., Gettinger, S. N., Smith, D. C., McDermott, D. F., Powderly, J. D., Carvajal, R. D., Sosman, J. A., Atkins, M. B., Leming, P. D., Spigel, D. R., Antonia, S. J., Horn, L., Drake, C. G., Pardoll, D. M., Chen, L., Sharfman, W. H., Anders, R. A., Taube, J. M., McMiller, T. L., Xu, H., Korman, A. J., Jure-Kunkel, M., Agrawal, S., McDonald, D., Kollia, G. D., Gupta, A., Wigginton, J. M., and Sznol, M. (2012). Safety, activity, and immune correlates of anti-PD-1 antibody in cancer. *New England Journal of Medicine*, **366**(26), 2443–2454.

Toshiyuki, M. and Reed, J. C. (1995). Tumor suppressor p53 is a direct transcriptional activator of the human bax gene. *Cell*, **80**(2), 293–299.

Tresini, M., Mawal-Dewan, M., Cristofalo, V. J., and Sell, C. (1998). A phosphatidylinositol 3-kinase inhibitor induces a senescent-like growth arrest in human diploid fibroblasts. *Cancer Research*, **58**(1), 1–4.

Vartanian, R., Masri, J., Martin, J., Cloninger, C., Holmes, B., Artinian, N., Funk, A., Ruegg, T., and Gera, J. (2011). AP-1 Regulates Cyclin D1 and c-MYC Transcription in an AKT-Dependent Manner in Response to mTOR Inhibition: Role of AIP4/Itch-Mediated JUNB Degradation. *Molecular Cancer Research*, **9**(1), 115–130.

Vibhakar, R., Juan, G., Traganos, F., Darzynkiewicz, Z., and Finger, L. R. (1997). Activation-induced expression of human programmed death-1 gene in T-lymphocytes. *Experimental Cell Research*, **232**(1), 25–8.

Vijayaraghavan, S., Karakas, C., Doostan, I., Chen, X., Bui, T., Yi, M., Raghavendra, A. S., Zhao, Y., Bashour, S. I., Ibrahim, N. K., Karuturi, M., Wang, J., Winkler, J. D., Amaravadi, R. K., Hunt, K. K., Tripathy, D., and Keyomarsi, K. (2017). CDK4/6 and autophagy inhibitors synergistically induce senescence in Rb positive cytoplasmic cyclin e negative cancers. *Nature Communications*, **8**, 15916.

Vila-del Sol, V., Punzón, C., and Fresno, M. (2008). IFN-gamma-induced TNF-alpha expression is regulated by interferon regulatory factors 1 and 8 in mouse macrophages. *The Journal of Immunology*, **181**(7), 4461–70.

Wang, C.-M., Wu, Z.-Q., Wang, Y., Guo, Y.-L., Dai, H.-R., Wang, X.-H., Li, X., Zhang, Y.-J., Zhang, W.-Y., Chen, M.-X., Zhang, Y., Feng, K.-C., Liu, Y., Li, S.-X., Yang, Q.-M., and Han, W.-D. (2017). Autologous T Cells Expressing CD30 Chimeric Antigen Receptors for Relapsed or Refractory Hodgkin Lymphoma: An Open-Label Phase I Trial. *Clinical Cancer Research*, **23**(5), 1156–1166.

Wang, X., Wong, S. C., Pan, J., Tsao, S. W., Fung, K. H., Kwong, D. L., Sham, J. S., and Nicholls, J. M. (1998). Evidence of cisplatin-induced senescent-like growth arrest in nasopharyngeal carcinoma cells. *Cancer Research*, **58**(22), 5019–22.

Wannemacher, M., Wenz, F., and Dubus, J. (2006). *Strahlentherapie*. Springer, Berlin.

Weinstock, M. and McDermott, D. (2015). Targeting PD-1/PD-L1 in the treatment of metastatic renal cell carcinoma. *Therapeutic Advances in Urology*, **7**(6), 365–377.

Wellbrock, C., Ogilvie, L., Hedley, D., Karasarides, M., Martin, J., Niculescu-Duvaz, D., Springer, C. J., and Marais, R. (2004). V599EB-RAF is an oncogene in melanocytes. *Cancer Research*, **64**(7), 2338–42.

Wieder, T., Eigentler, T., Brenner, E., and Röcken, M. (2018). Immune checkpoint blockade therapy. *The Journal of Allergy and Clinical Immunology*, **142**(5), 1403–1414.

Wilmott, J. S., Long, G. V., Howle, J. R., Haydu, L. E., Sharma, R. N., Thompson, J. F., Kefford, R. F., Hersey, P., and Scolyer, R. A. (2012). Selective BRAF inhibitors induce marked T-cell infiltration into human metastatic melanoma. *Clinical Cancer Research*, **18**(5), 1386–94.

Wu, D. and Prives, C. (2018). Relevance of the p53-MDM2 axis to aging. *Cell Death & Differentiation*, **25**(1), 169–179.

Yadav, S., Kalra, N., Ganju, L., and Singh, M. (2017). Activator protein-1 (AP-1): a bridge between life and death in lung epithelial (A549) cells under hypoxia. *Molecular and Cellular Biochemistry*, **436**(1-2), 99–110.

Yamazaki, T., Akiba, H., Iwai, H., Matsuda, H., Aoki, M., Tanno, Y., Shin, T., Tsuchiya, H., Pardoll, D. M., Okumura, K., Azuma, M., and Yagita, H. (2002). Expression of Programmed Death 1 Ligands by Murine T Cells and APC. *The Journal of Immunology*, **169**(10), 5538–5545.

Yilmaz, M. and Christofori, G. (2009). EMT, the cytoskeleton, and cancer cell invasion. *Cancer Metastasis Reviews*, **28**(1-2), 15–33.

Yin, Y., Wang, S., Sun, Y., Matt, Y., Colburn, N. H., Shu, Y., and Han, X. (2009). JNK/AP-1 pathway is involved in tumor necrosis factor-alpha induced expression of vascular endothelial growth factor in MCF7 cells. *Biomedicine & Pharmacotherapy*, **63**(6), 429–35.

Yogev, O., Anzi, S., Inoue, K., and Shaulian, E. (2006). Induction of transcriptionally active Jun proteins regulates drug-induced senescence. *The Journal of Biological Chemistry*, **281**(45), 34475–83.

Young, M. R., Li, J. J., Rincón, M., Flavell, R. A., Sathyanarayana, B. K., Hunziker, R., and Colburn, N. (1999). Transgenic mice demonstrate AP-1 (activator protein-1) transactivation is required for tumor promotion. *Proceedings of the National Academy of Sciences of the United States of America*, **96**(17), 9827–32.

Yunis, J. J., Soreng, A. L., and Bowe, A. E. (1987). Fragile sites are targets of diverse mutagens and carcinogens. *Oncogene*, **1**(1), 59–69.

Zenz, R., Scheuch, H., Martin, P., Frank, C., Eferl, R., Kenner, L., Sibilia, M., and Wagner, E. F. (2003). c-Jun regulates eyelid closure and skin tumor development through EGFR signaling. *Developmental Cell*, **4**(6), 879–89.

Zenz, R., Eferl, R., Kenner, L., Florin, L., Hummerich, L., Mehic, D., Scheuch, H., Angel, P., Tschachler, E., and Wagner, E. F. (2005). Psoriasis-like skin disease and arthritis caused by inducible epidermal deletion of Jun proteins. *Nature*, **437**(7057), 369–75.

Zglinicki, T. V., Saretzki, G., Ladhoff, J., Fagagna, F. D. D., and Jackson, S. P. (2005). Human cell senescence as a DNA damage response. In *Mechanisms of Ageing and Development*, volume 126, pages 111–117.

Zhang, W.-Y., Wang, Y., Guo, Y.-L., Dai, H.-R., Yang, Q.-M., Zhang, Y.-J., Zhang, Y., Chen, M.-X., Wang, C.-M., Feng, K.-C., Li, S.-X., Liu, Y., Shi, F.-X., Luo, C., and Han, W.-D. (2016). Treatment of CD20-directed Chimeric Antigen Receptor-modified T cells in patients with relapsed or refractory B-cell non-Hodgkin lymphoma: an early phase IIa trial report. *Signal Transduction and Targeted Therapy*, **1**, 16002.

Zhang, X., Jin, J. Y., Wu, J., Qin, X., Streilein, R., Hall, R. P., and Zhang, J. Y. (2015). RNA-Seq and ChIP-Seq reveal SQSTM1/p62 as a key mediator of JunB suppression of NF-κB-dependent inflammation. *The Journal of Investigative Dermatology*, **135**(4), 1016–1024.

Zhong, X., Tumang, J. R., Gao, W., Bai, C., Rothstein, T. L., and Rothstein, T. L. (2007). PD-L2 expression extends beyond dendritic cells/macrophages to B1 cells enriched for VH11/VH12 and phosphatidylcholine binding. *European Journal of Immunology*, **37**(9), 2405–2410.

Zhou, F. H., Foster, B. K., Zhou, X.-F., Cowin, A. J., and Xian, C. J. (2006). TNF-alpha mediates p38 MAP kinase activation and negatively regulates bone formation at the injured growth plate in rats. *Journal of Bone and Mineral Research*, **21**(7), 1075–88.

Zhu, J., Woods, D., McMahon, M., and Bishop, J. M. (1998). Senescence of human fibroblasts induced by oncogenic Raf. *Genes & Development*, **12**(19), 2997–3007.

Zou, L. and Elledge, S. J. (2003). Sensing DNA damage through ATRIP recognition of RPA-ssDNA complexes. *Science*, **300**(5625), 1542–8.

Erklärung zum Eigenanteil

Mouse genotyping was performed by Viola Galinat, Susanne Weidemann, and myself.

FACS experiments were performed by Cornelia Grimmel in the Flow Cytometry Core Facility of the university medical center Tübingen.

Mycoplasma testing was performed by the group of molecular mycology of the dermatology department of the university medical center Tübingen.

Subcutaneous injections of the RT2 cell line 3 in $CD8^+$-depleted C3HeB/FeJ mice were performed by Fatima Ahmetlić (Translational Molecular Immunology, HelmholzZentrum München). The growth arrest assays of the parental RT2 cell line 3, as well as the mSc tumors, were performed by Ellen Brenner (dermatology department of the university medical center Tübingen). Experiments according to Figure 3.1 were performed by Ellen Brenner.

All other experiments and statistical analysis presented in this thesis were performed by myself.

Eidesstattliche Erklärung

Ich erkläre hiermit, dass ich die zur Promotion eingereichte Arbeit mit dem Titel: „Tumor suppressor $p16^{INK4a}$ and its potential regulator JunB in cytokine-induced senescence“ selbständig verfasst, nur die angegebenen Quellen und Hilfsmittel benutzt und wörtlich oder inhaltlich übernommene Stellen als solche gekennzeichnet habe. Ich erkläre, dass die Richtlinien zur Sicherung guter wissenschaftlicher Praxis der Universität Tübingen (Beschluss des Senats vom 25.5.2000) beachtet wurden. Ich versichere an Eides statt, dass diese Angaben wahr sind und dass ich nichts verschwiegen habe. Mir ist bekannt, dass die falsche Abgabe einer Versicherung an Eides statt mit Freiheitsstrafe bis zu drei Jahren oder mit Geldstrafe bestraft wird.

Acknowledgments

I would like to take this opportunity to thank Prof. Dr. med. Jürgen Bauer for welcoming me into his laboratory, for the excellent supervision and for his support.

Furthermore, I would like to thank Prof. Dr. Hans-Georg Rammensee for taking over the second report, for the helpful comments and for the admission to the IRTG 685.

In addition, I would like to thank Prof. Dr. med. Martin Röcken for welcoming me in his research group, for financing and for his support in national and international scientific exchange.

My thanks also go to Prof. Dr. Thomas Wieder and Dr. Heidi Braumüller for their guidance in the laboratory.

I also thank my colleagues Ellen Brenner, Katharina Böhm, Britta Bauer, Maximilian Rentschler, Viola Galinat and Susanne Weidemann. Many thanks for your support, whether it was in introducing me to new methods or in executing large-scale experiments. Thank you for the scientific and non-scientific discussions during lunch, coffee breaks, or when meeting in the doctoral candidates' room. Thanks for the excellent working atmosphere and the great solidarity.

My thanks also go to Evelyn Mazcey. Together we have mastered the genetic research of AG Bauer!

Thanks also to all my colleagues who supported me in my work and accompanied me for a part of my way.

I would also like to thank my parents in particular, who supported me in all my decisions. Thank you for being there and for always supporting me!

Finally, I would like to thank my husband Mark Benedikt Boss. Thank you for supporting me every step of the way and for always believing in me. I look forward to our shared future.